HEFT

D3.1 Modular, high-efficient and cost-oriented 800V powertrain architecture

**Funded by
the European Union**

Call	HORIZON- CL5-2020-D5-01	
GA Number	101096306	
Deliverable No.	D3.1	
Deliverable Title	Modular, high-efficient and cost-oriented 800V powertrain architecture	
Deliverable Date	2024-04-26	
Contractual delivery	2023-11-30	
Deliverable Type	R	
Dissemination level	PU	
Status	V2.1	2024-04-26

Written By	Victor Manuel Lopez, Alejandro Fernandez, Amaia López de Heredia, Iñigo Aranburu	2024-02-27
Checked by	Fernando Garramiola	2024-03-11
Approved by	Javier Poza	2024-04-26

HORIZON CL5-2020-D5-01. HEFT 101096306 – Novel concept of a Low Cost, High Power Density and Highly Efficient Recyclable motor for next generation mass produced electric vehicles

GLOSSARY

Abbreviation/ acronym	Description
AC	Alternative Current
BEV	Battery Electric Vehicle
DC	Direct Current
DM	Differential Mode
CM	Common Mode
COP	Coefficient of Performance
EMC	Electro Magnetic Compatibility
EU	European Union
EV	Electric Vehicle
FFT	Fast Fourier Transforms
GBD	Grain Boundary Diffusion
HEV	Hybrid Electric Vehicle
HV	High Voltage
IGBT	Insulated Gate Bipolar Transistor
OBC	Onboard Charger
OEM	Original Equipment Manufacturer
PMSM	Permanent Magnet Synchronous Motor
PPE	Premium Platform Electric
Si	Silicon
SiC	Silicon Carbide
SOC	State Of Charge
V2G	Vehicle-to-grid
V2L	Vehicle-to-load
WP	Work Package

1 EXECUTIVE SUMMARY

Climate change has created an increased need for innovation in various sectors, including the automotive industry. Many corporations are striving to fulfil this need by developing and producing electric cars. However, the production process remains inefficient and environmentally harmful. The EU-funded HEFT project will reverse this trend by introducing a revolutionary synchronous motor for electric cars, which will be recyclable, cost-efficient and require fewer materials while producing fewer emissions and creating novel European circular economies.

HEFT Project proposes a set of innovation challenges on electric synchronous motor configuration based on SiC inverters (direct cooling of rotor and stator, advance insulation for high voltage, multibarrier rotor topology, wave windings) and advanced materials (advanced GBD magnets, epoxy for magnet fixation, composite for motor housing, insulation resin). These innovations will result in a high-efficient and low-cost solution that will be validated on 2 motor topologies.

- Motor topology type C: Motors for C-D-E vehicle segments.
- Motor topology type A: Motors for A-B vehicle segments.

In this document the work carried out in Task 3.1 of HEFT project has been summarized. a modular, high-efficient and cost-oriented 800V powertrain architecture is defined. Electrical, thermal, mechanical and control architectures will be analysed to deal with the challenges of increasing system voltage. Moreover, some simulations have been carried out to deal with high dv/dt effect due to SiC devices propagation models to avoid motor degradation, high switching frequency effect influence on EMC analysis, to comply with automotive standards, current versus voltage trade-offs: considering powertrain, batteries and recharge infrastructure optimization in order to improve EV range, advanced shared cooling in the powertrain, to reduce losses and improve EV range.

In this document the following issues will be covered:

1. A state of the art of 800V architecture EV.
2. Electrical, thermal, mechanical & control modular, high-efficient and cost-oriented architecture proposal.
3. High dv/dt motor degradation simulation model.
4. Influence on EMC analysis, to comply with automotive standards.
5. Current versus voltage trade-offs simulation to improve EV range.
6. Advanced shared cooling in the powertrain, to reduce losses and improve EV range.

2 DRIVE SPECIFICATIONS

In this section, drive specifications considered for this task will be described. On the one hand, there are two segments of vehicles considered (A+B and C+D+E), leading to two different motors. On the other hand, silicon carbide (SiC) inverter will be detailed.

Two different motors specifications are detailed in Table 1 and Table 2, resulted values come from a market analysis.

Table 1 Motor Specifications for A+B segment.

A + B Segment			
	Units	**Peak**	**Continuous**
Duration of operation point	S	30	1800
Shaft power	kW	110	55
Max Shaft torque - example	Nm	163	
Corner speed	rpm	6.444	
Maximum speed - example	rpm	20.000	
Maximum speed - market constraint	rpm	20.000	
Maximum overspeed	rpm	+10%	
Nominal DC Voltage	Vdc	650	
Maximum phase current	Arms	350	
Power Density - Continuous		~27,7kW/L (KPI3.2) & ~8,39kW/kg (KPI 4.1)	
Torque Density - Continuous - Option B		~55,87 Nm/L & ~35,84Nm/kg (KPI 4.2)	
Motor losses - Mean over WLTP	Wh/km		11,4
Maximum temperature on winding	°C	180	180
Maximum rotor temperature	°C	150	150

Table 2 Motor specifications for C+D+E Segment

C + D + E Segment			
	Units	Peak	Continuous
Duration of operation point	S	30	1800
Shaft power	kW	170	111
Max Shaft torque - example	Nm	260	
Corner speed	rpm	6.250	
Maximum speed - example	rpm	19.914	
Maximum speed - market constraint	rpm	20.000	
Maximum overspeed	rpm	+10%	
Nominal DC Voltage	Vdc	650	
Maximum phase current	Arms	350	
Power Density - Continuous		~28,1kW/L (KPI3.2) & ~7,07kW/kg (KPI 4.1)	
Torque Density - Continuous		~50,18 Nm/L & ~32,19Nm/kg (KPI 4.2)	
Motor losses - Mean over WLTP	Wh/km		TBD[1]
Maximum temperature on winding	°C	180	180
Maximum rotor temperature	°C	150	150

SiC inverter specifications are described in Table 3.

Table 3 SiC inverter specifications

SiC inverter			
dV/dt & Risetime (maxDCBus / (dU/dt) = risetime)	[kV/µs]	5 typical	10 stretch
Max Switching Frequency	[Hz]	20.000	
Fundamental Frequency max	[Hz]	~1000	
Number of phases	[-]	3	
max. DC-Bus-Voltage	Vdc	800	
PDIV Phase-Phase	Vpk-pk	3726	
PDIV Phase-Ground	Vpk-pk	2381	

Among these two vehicle segments, there are many design decisions regarding the powertrain architecture that can be reconfigured to be used in both cases. Therefore, the following section covers the different EV architectures that are found in the state of the art, finding out the most adequate for this project based on their advantages and disadvantages.

---

[1] Motor losses - Mean over WLTP. To Be Defined according to fulfil at least 20% reduction over baseline eMotor

3 800V POWERTRAIN ARCHITECTURE

Up until mid-2022 most of EV available in the market operate with 400V batteries. OEM already realised the advantages of moving towards 800V architecture: reduce charging time by half, reduce charging current and overheating, increase component efficiency, reduce power losses, etc. Thus, the transition towards 800V is expected to be quite fast. As is stated in [1], by 2027-2030 more than 90% of EV will probably have 800V battery system.

Some OEMs already sell 800V EVs: Hyundai, Audi, Porsche and Kia. Lucid motor has integrated a 900V battery into its vehicle model Lucid Air. Hyundai has promised to launch 23 EV models with 800V architecture by 2025 [1].

800V electrical architecture will be based on SiC technology. It is well known that SiC devices have lower losses, can reach higher temperatures, can switch much faster, reduce weight and volume, etc. As it said in [2], SiC technology will achieve cost effectiveness with low losses for mass production. As it can be seen in Figure 1, most 800V EV use SiC devices.
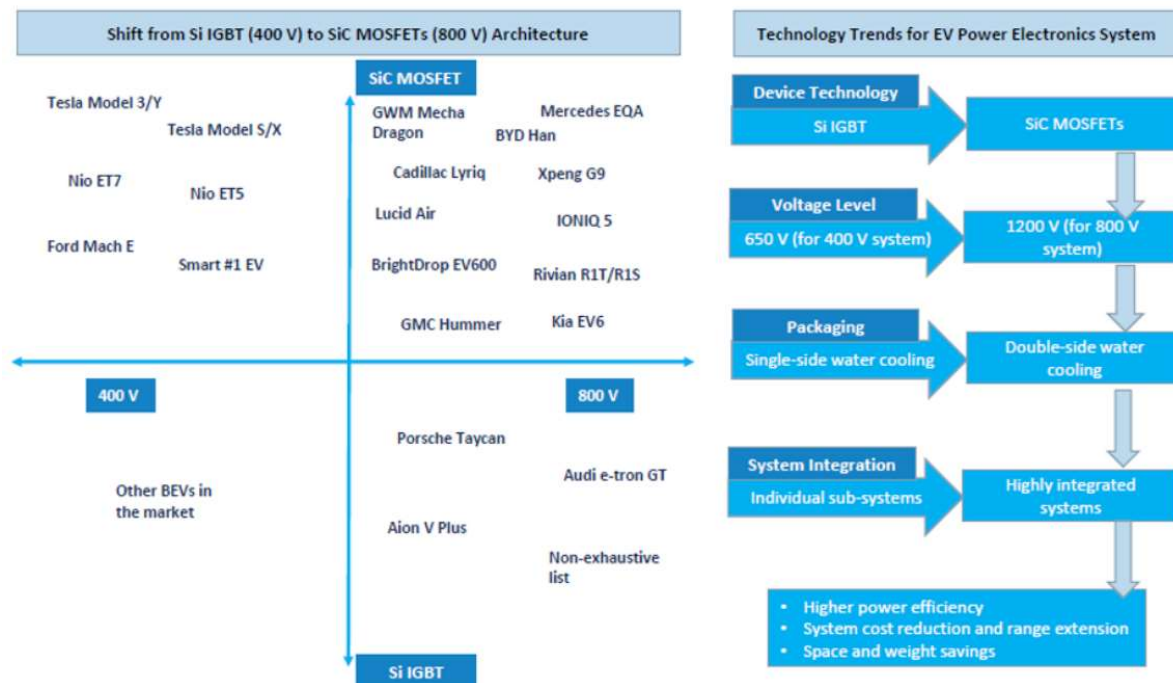
Figure 1. 400V to 800V architecture shift implies shift from Si IGBT to SiC Mosfets [2].

3.1 State of the Art of 800V EV

In this section 800V architecture EV characteristics will be analysed. Hyundai, Audi-Porsche and Lucid Air platforms have been analysed.

3.1.1 Hyundai: E-GMP platform

Hyundai 800V platform is called E-GMP (Electric-Global Modular Platform) and is also used by other OEM like Kia or Genesis.

Figure 2. Hyundai E-GMP 800V platform [3].

One of the main characteristics of E-GMP platform is that it is prepared to be used with two motors. One on the front and another one, more powerful, on the rear. The power devices of both inverters are different: front inverter uses Si IGBT power modules, and the rear inverter uses SiC MOSFET power modules [3].

Other important characteristic is that it is a multi-charging system. It supports both 800V and 400V charging. For 800V charging high voltage battery is directly connected. However, for 400V charging the drive is used to boost charger 400V to battery 800V, as it is shown in Figure 3.

Figure 3. Hyundai multi-charging system [3].

IONIQ 5 Hyundai EV 800V architecture is shown in Figure 4 [4]. As can be seen, it has two motors, one on the front (PMSM 70kW) and the other on the rear (PMSM, 155kW). Comparing with HEFT motors, the front motor could be Segment A+B motor and rear motor Segment C+D+E motor.
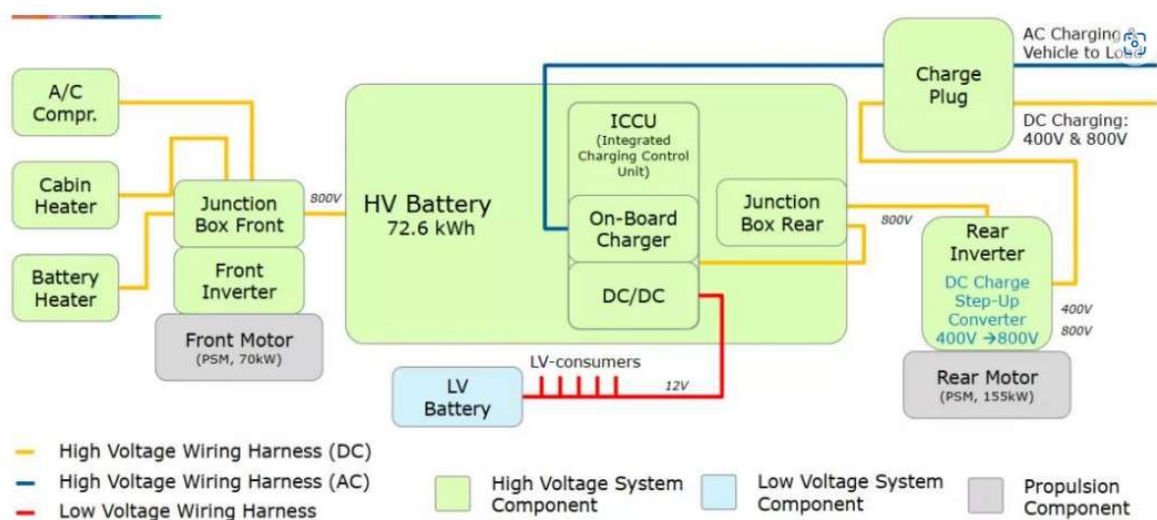
Figure 4. IONIQ 5 Hyundai EV 800V electrical architecture [4].

Moreover, with 800V charging system (250kW), battery charging from %10 of the State of Charge (SOC) up to 80% is achieved in 18min. One full charge offers a driving range of 500km. Battery capacity is 72.6kWh.

Regarding the OBC, it can be chosen between 11kW and 22kW. This car is also equipped with Vehicle-to-Load (V2L) technology. Thus, external devices can be supplied with the electricity stored in the EV battery.

Concerning the drive, in [3] it is stated that 93% of efficiency is achieved considering SiC inverter. Hyundai uses Vitesco SiC inverters, which improve the extended range by %5. Front drive adopts three -in-one (motor + inverter + differential) assembly and rear drive five-in-one (motor + inverter + differential + OBC+DC/DC converter), as shown in Figure 5. Both motors are PMSM and have hairpin windings and are oil spray cooled (oil is also used for lubrication).

Figure 5. IONIQ 5 Hyundai front (left) and rear (right) drives assembly [3].

Finally, Figure 6 shows IONIQ 5 800V EV thermal architecture. As can be seen, batteries are cooled on a different channel than the inverters and the motors.
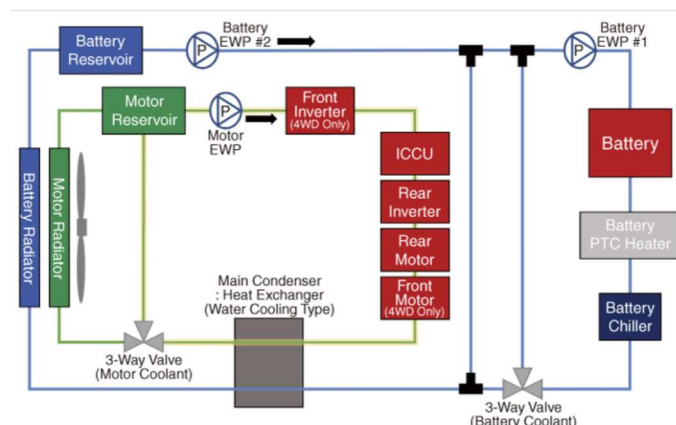
Figure 6. IONIQ 5 Hyundai EV 800V thermal architecture [4].

3.1.2   Porsche Audi PPE platform

In 2019 Volkswagen group presented the Premium Platform Electric (PPE) that is used in Audi, Porsche [5]. This flexible platform allows variable ground clearance, variable wheelbase and variable axle track, as it is shown in Figure 7. Thus, a wide range of models can be built using PPE between B and D segments.

Figure 7. Porsche -Audi PPE platform [5].

Audi A6 etron is the first 800V EV based on PPE platform. This EV has two motors, one on the front and the other on the rear. In total 350kW with a torque of 800Nm. Concerning the axle drive, 3 in 1 assembly and cost-oriented approach is considered. Reduced variance combined with flexibility in key components, highest efficiency and performances are achieved [5] (see Figure 8).
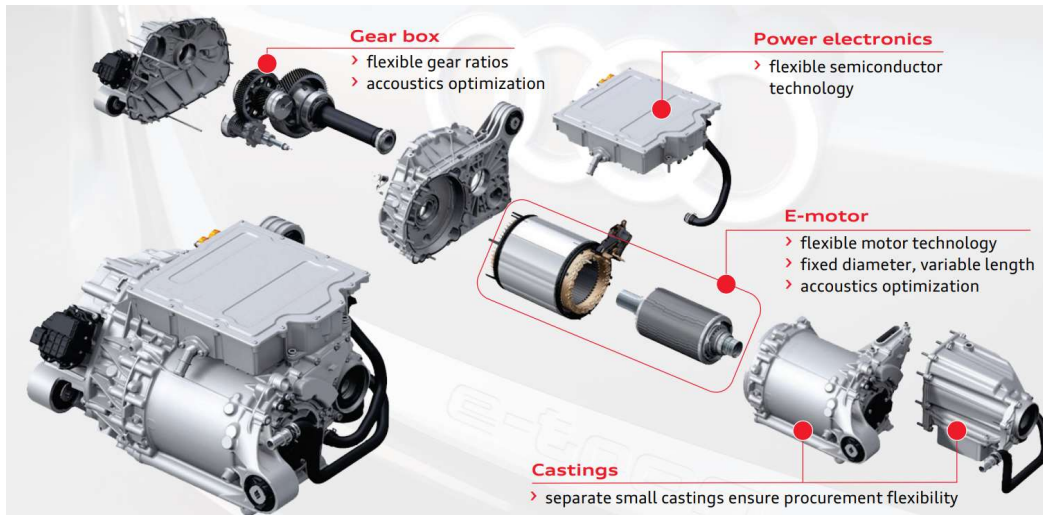
Figure 8. Cost-oriented PEE drive [5].

PPE drive component modularity is shown in Figure 9. Regarding the motor, 4 different options can be used, all of them with the same motor diameter: 200mm length PMSM motor, 150mm length PMSM motor, 100mm length PMSM and 100mm length asynchronous motor. Concerning the inverter, the same converter is used but devices can be either Si or SiC. Finally, at gearbox, 4 different gear ratios can be used via one reduction stage (from 8.5 up to 11).
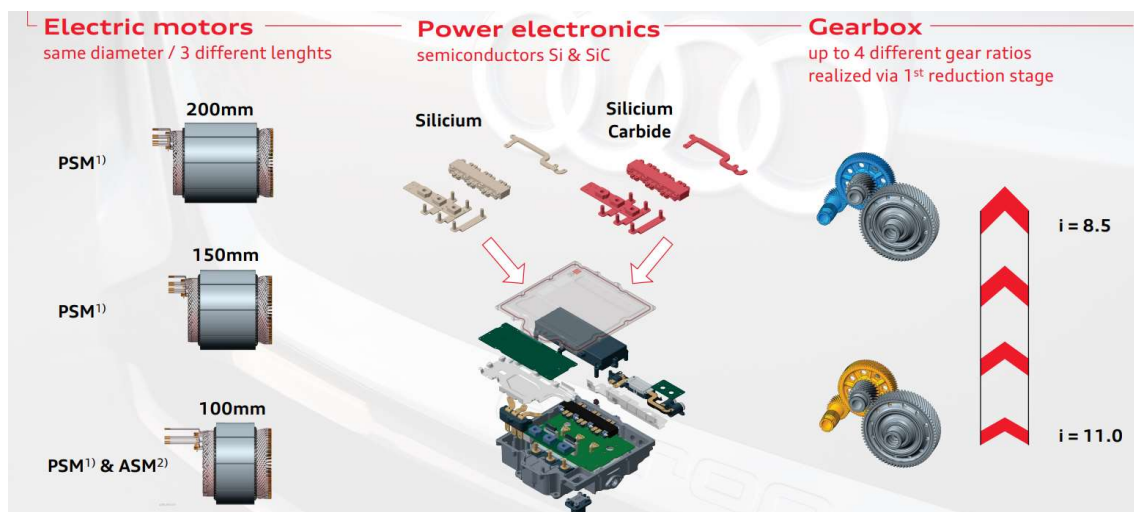
Figure 9. PPE drive modularity [5].

Motor and gearbox use oil systems with electric oil pump and dry sump lubrication, to reduce friction and improve efficiency. Stator and rotor direct oil cooling and hairpin windings are used to improve power density and the reduction of rare earths [5].

Comparing PPE drive with previous e-tron drive, motor dimensions are reduced 35%, drive weight has been reduced 20% and drive losses have decreased 50%. Overall system performance has increased 33% and drive costs have decreased 15% and energy consumption has decreased 30%.

Moreover, with 800V charging system (270kW), battery charging from %5 of the SOC up to 80% is achieved in less than 25min. In 10min charge a driving range of 300km is achieved. Battery capacity is 93kWh. OBC is 22kW and is located at the rear axle.

Porsche Taycan also uses 800V PPE platform. This EV is a sport car that can generate up to 560kW, using two liquid cooling PMSM motors (one on the front axle and other in the rear-axle). These drives modules have the highest power density (kW per litre) of all electric powertrain on the market today [6].

Both axles' inverters maximum current is 300A (in Taycan Turbo) and 600A (in Taycan Turbo S). Both inverters have very high efficiency, almost 98%. Concerning the gearbox, a single speed ratio 8:1 is used in the front axle. However, in the rear axle a double speed transmission (also ratio 8:1) system is used.

Regarding the fast charging capability, with 800V charging system (270kW), battery charging from 5% of the SOC up to 80% is charged in 22.5min. In 5min charge a driving range of 100km is achieved. Battery capacity is 93.4kWh. OBC is 11kW and is located at the rear axle.

Figure 10 shows the Porsche Taycan thermal architecture. As can be seen, two different loops are considered. One for the motor and the converters and the other for the battery system. Moreover, additional cooling via a radiator is proposed for high load [4].
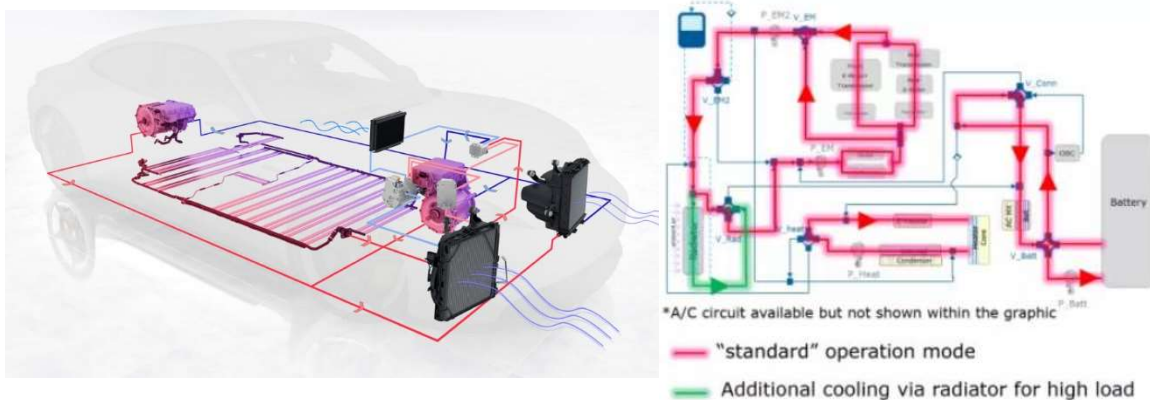
Figure 10. Porsche Taycan thermal architecture [4].

3.1.3 Lucid Air

Lucid Motor presented a 900Vdc Lucid Electric Advanced Platform (LEAP). Lucid Air is the luxury car based on this platform, which has three PMSM motors: one on the front and two on the rear, achieving 500kW, all of them have hairpin windings. 1200V/ 450A SiC devices are used in the inverters. Moreover, OBC is bidirectional, allowing Vehicle-to-Grid (V2G) operation [7].

Concerning the fast charging, 300kW can charge in 12 min a range of 320km. This EV has 88kWh battery system.
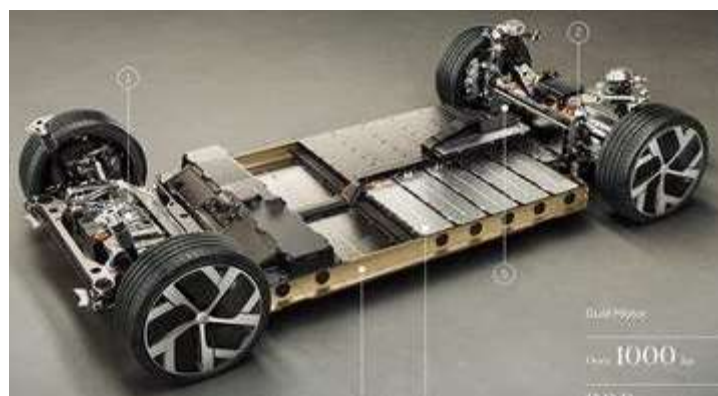
Figure 11. 900Vdc Lucid Electric Advanced Platform [7].

3.1.4 SoA conclusions

It can be concluded that 800V architecture is already a reality. There is a clear trend to move to higher voltage EV. There are also some new EU calls for 2024 dealing with this topic, "Integration and testing of next generation post-800V electric powertrains" [8]. Dedicated electric vehicle platforms are usually used and front and rear axles are the most common solution. PMSM motors and SiC based inverters are dominant at this moment, due to their best performances.

3.2 Global 800V architecture

The EV system architecture is divided into four different parts: electrical, thermal, mechanical and control. Nowadays, six different configurations (see Figure 12) are proposed for EVs, which impact on the sizing and configuration of the whole architecture.
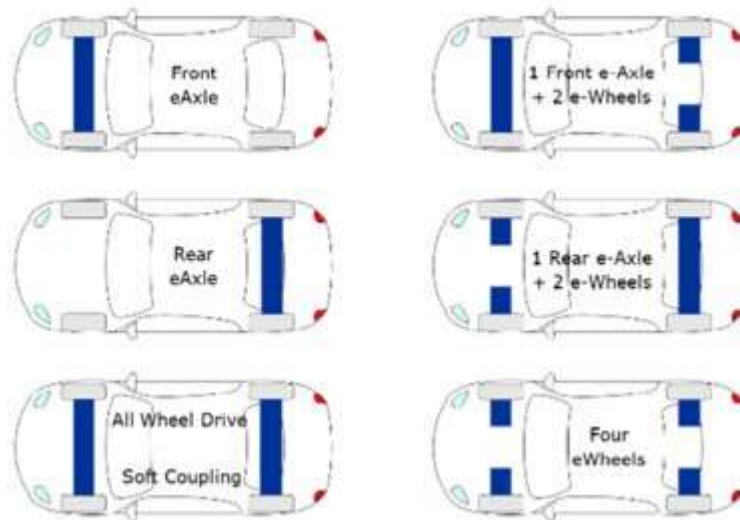
Figure 12 Configurations for EVs [9].

In this project, *front eAxle*, *rear eAxle* and *all-wheel drive* configurations have been selected based on the state of the art. In this context, different proposals of inverter and motor integration can be found in the literature and commercial products, where motor mounted or integrated solutions show to be the path to follow in future EVs architectures, although offset mounted solutions are the path to follow in present years (see Figure 13). The advantages of this offset solution are cost optimization (HV cables and connector eliminated, reduced radiated EMI and combining motor and inverter cooling) and design for manufacturing (compact design, motor-inverter becomes a single tested element). However, this offset solution has a challenge, as mechanical and thermal stress increase [9].

Figure 13 Different electro-mechanical integrations [9].

These solutions provide advantages regarding the elimination of HV wiring, electromagnetic compatibility (EMC) and integrated thermal solution for inverter and motor. An overview of the e-vehicle configuration selected for this project is given in Figure 14. In this case, there is an offset mounted motor and inverter, where both as well as the battery package are refrigerated with liquid

cooling systems. Furthermore, Compatible Connector Systems provide the possibility to charge the battery package from AC (slow charge) and DC (fast charge) grids.
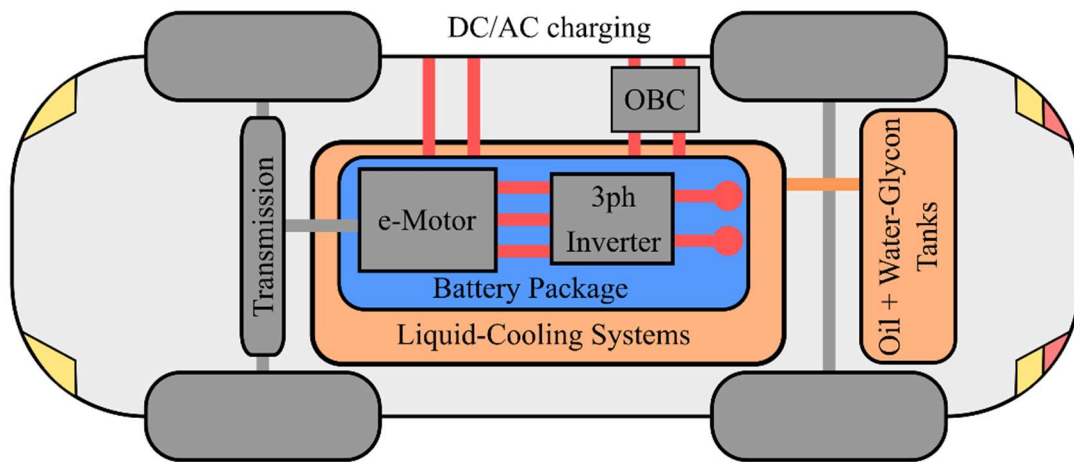
Figure 14 General overview of the e-vehicle architecture.

In following subsections, the global architecture of an e-vehicle is proposed, including the electrical, thermal, mechanical and control architectures. This architecture must be scalable and modular for the EV segments aimed in this project. Furthermore, cost is another parameter to be targeted in this document, since it will help to reach a competitive solution compared to market products.

3.3 Electrical architecture

The electrical architecture proposed is shown in Figure 15. A 650V battery system is connected to 11/22kW OBC. The DC link has three possibilities: a) one drive for Segment A+B EV, b) one more powerful drive for C+D+E segment and c) an all-wheel drive considering both motors, where Si devices could be a cost-oriented solution for the secondary drive.

Therefore, the electrical architecture of this application is mainly composed of a battery package, a three-phase inverter as the motor drive and an e-Motor, as presented in Figure 16. The battery package will provide the specified bus voltage, while the three-phase inverter feeds the required current to meet the e-motor specifications. Furthermore, the electrical system must include two sources (AC and DC) to charge the battery system. DC charging commonly comes from electrical stations, providing fast charging profiles. This case implies that a high-power converter is required, which is not included in the car due to the weight and volume impact. Nevertheless, AC/DC stage must be included inside the car to provide a slow-charging option. AC charging gives versatility to the final user, allowing them to charge their own car at home during the night. This AC charge is possible thanks to the On-Board Charger (OBC) included in the car. OBC is composed of an AC/DC rectifier and a DC/DC converter, providing isolation between battery system and grid.
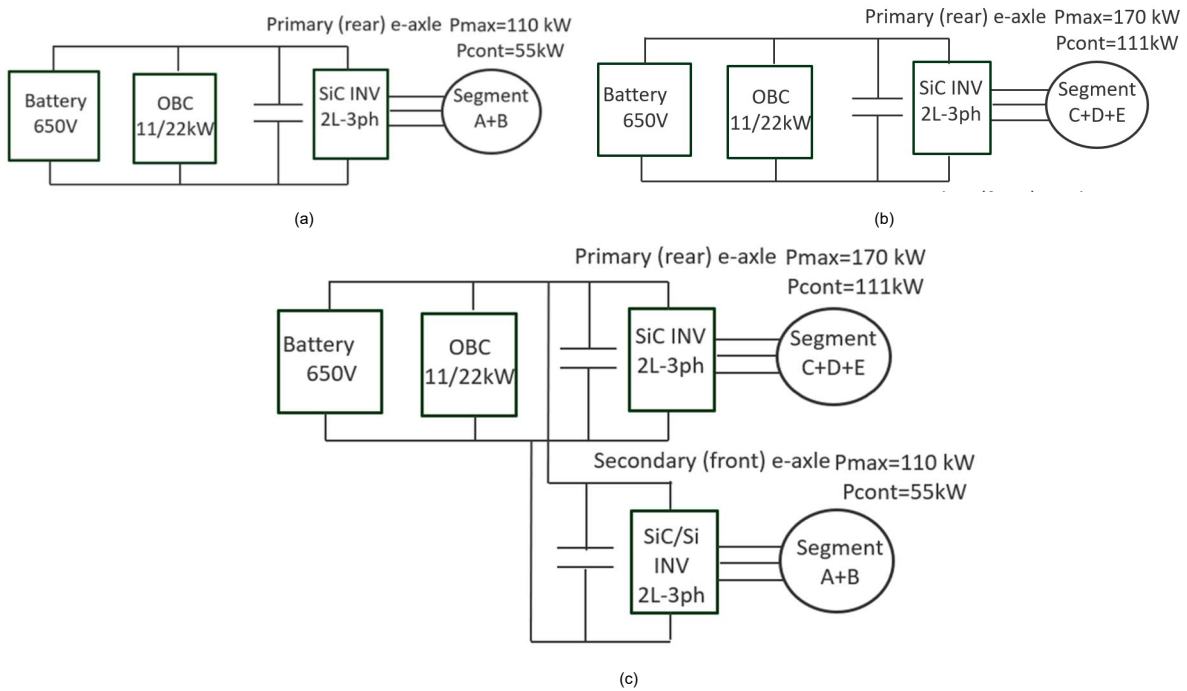
Figure 15 Electrical architecture proposal for Segment A+B EV (a), one more powerful drive for C+D+E segment (b) and an all-wheel drive considering both motors (c).
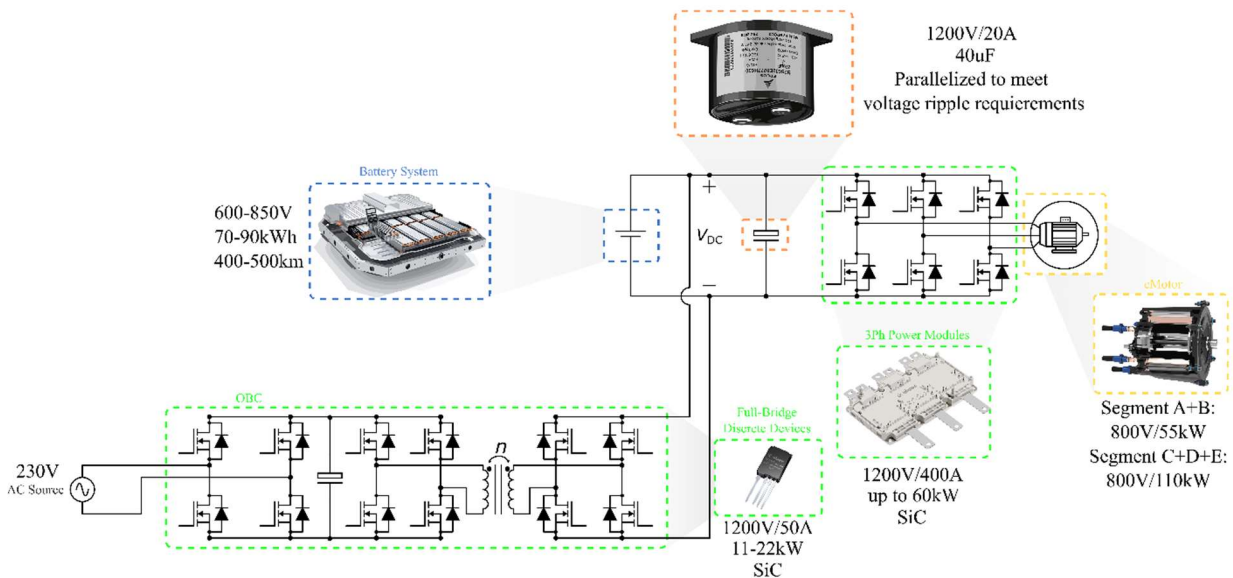
Figure 16 Power electronic schematic for EV electrical architecture.

The power devices selected for the OBC are SiC based, allowing switching at higher frequencies while improving system efficiency. Since the voltage level of the DC bus reaches up to 800V, 1200 SiC devices are considered due to their better performance when switching at higher frequencies. Depending on the power level, both discrete (low power) and power modules (high-power) are viable options to design these power electronic converters. Hereinafter, a cost evaluation of the different possible solutions is presented to select the most appropriate for each stage (OBC and motor drive). To give a fair comparison, Infineon semiconductors given in Table 4 are aimed for this analysis. The power modules (FS03MR12A6MA1LB and FF3MR20KM1H) are chosen since they are rated for the same voltage and current ratings in different module packages.

Table 4 Infineon Power Semiconductors. Cost analysis performed based on [10] prices.

Infineon Power Semiconductors					
Semiconductor	Type	Vds [V]	Id [A]	Rds [mΩ]	Price [€]
FS03MR12A6MA1LB	Three-Phase Module	1200	400	2.75	3325
FF3MR20KM1H	Half-Bridge Module	1200	375	2.6	1051
IMW120R007M1H	Discrete	1200	225	7	77

Discrete devices are a good choice for OBC power converter (see Figure 16) due to the power level managed (11-22kW). However, the number of discrete devices that would be required for three-phase inverter in comparison to power modules is huge, impacting on both efficiency and power density. This fact makes the system more complex, making it difficult to develop a modular architecture based on discrete devices. Therefore, half-bridge and three-phase modules are selected for this topology. Both have similar characteristics, but there is a trade-off between the price and on-board weight.

Considering the topology of each device, three half-bridge power modules are needed, while just one three-phase module is required for the motor drive. In this case, the total cost reduction (200€) by including 3 half-bridge modules is not enough to deal with the on-board weight and volume increment. Due to this fact, a three-phase module (FS03MR12A6MA1LB) is selected for the three-phase inverter. In the case of the OBC, the cost reduction obtained by parallelizing SiC discrete devices is large enough to consider these devices. In this converter, the total power is above 11-22kW, which can be obtained by parallelizing from 2-4 discrete devices. Nowadays, considering the market prices for both module and discrete devices, discrete seems to be the most cost optimal solution. Nevertheless, the price of power modules is decreasing as years go by, making them a suitable option for future EV OBCs.

The electrical architecture presented in this section is scalable for both motor segments aimed in HEFT project. In this context, modularization and low-cost solution have been aimed to reach a solution able to be utilized in both motors, considering the same thermal, mechanical and control architectures given in following subsections.

3.4 Thermal architecture

Thermal management in electric vehicles is one of the most important points in the design stages. Future motor integrated solutions include the thermal management system in a 4-1 solution. Then, the coolant circuit is implemented together with the battery system, three-phase inverter and eMotor. There are two coolant liquids considered for thermal management, which are glycol-water and oil. Nowadays, oil coolant motors are dominant in the market, meanwhile both water-glycol and oil are considered for the inverter stage. Due to the optimal operating temperature in each part of the system, the battery system is water-coil refrigerated. Both oil and water-glycol coolant liquids coexist in the thermal architecture, enabling them to interact to optimize the system efficiency. These solutions are depicted in Figure 17 and Figure 18, being a representation of a thermal system management example. The main drawback of water-glycol solutions in the inverter heatsink is its electrical conductivity, making the mechanical distribution more complex since it cannot be in contact with electrical components.

In a future context, full oil solutions are considered [11] (see Figure 19). These solutions seem to reduce the complexity of the thermal architecture, as well as the number of integrated components for the cooling systems, while maintaining the operating temperature on desirable values. This fact not only reduces the complexity of the system but also improves its safety and flexibility. However, battery, inverter and motor oil cooling is a trend research topic and industrial implementation is seen as a long-term solution, as there are still a lot of challenges.
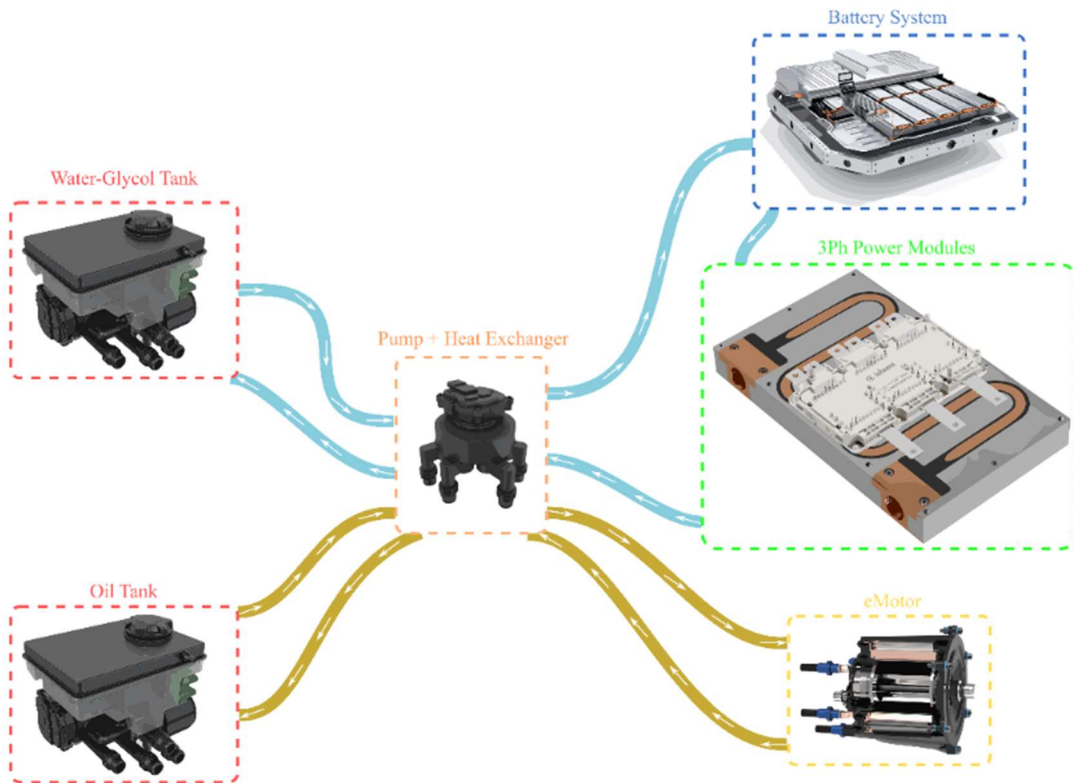
Figure 17 Cooling system concept: motor oil cooling, inverter and battery water glycol cooled, solution 1.
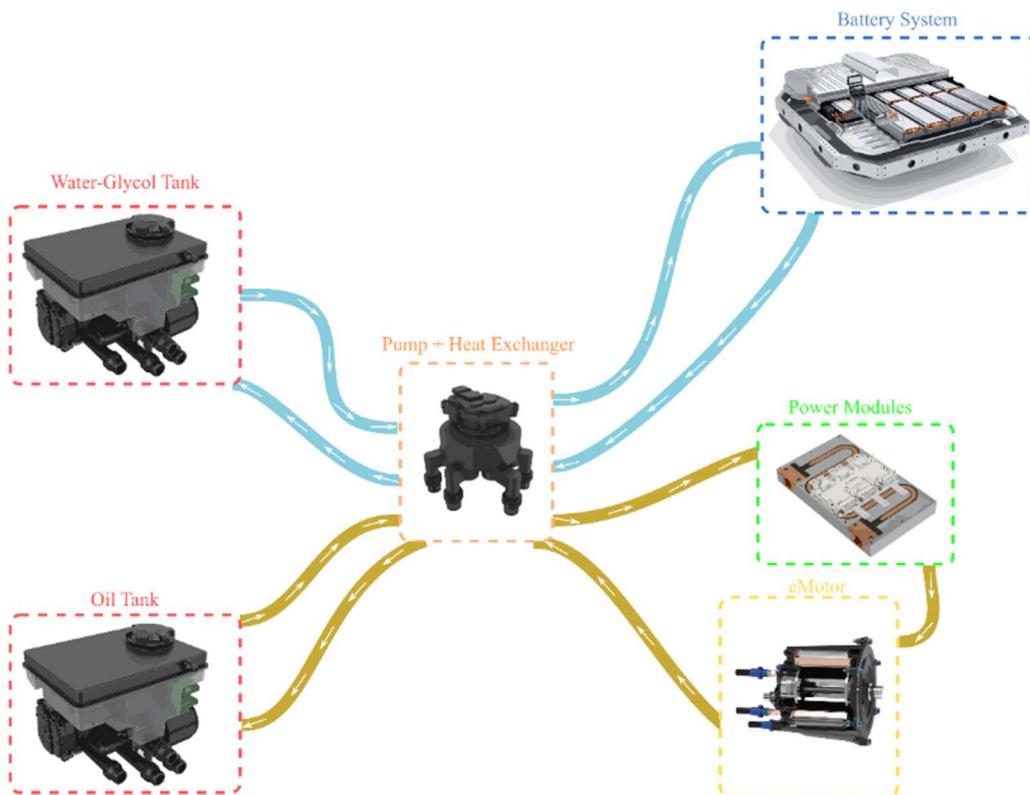
Figure 18 Cooling system concept: motor and inverter oil cooling and battery water glycol cooled, solution 2.
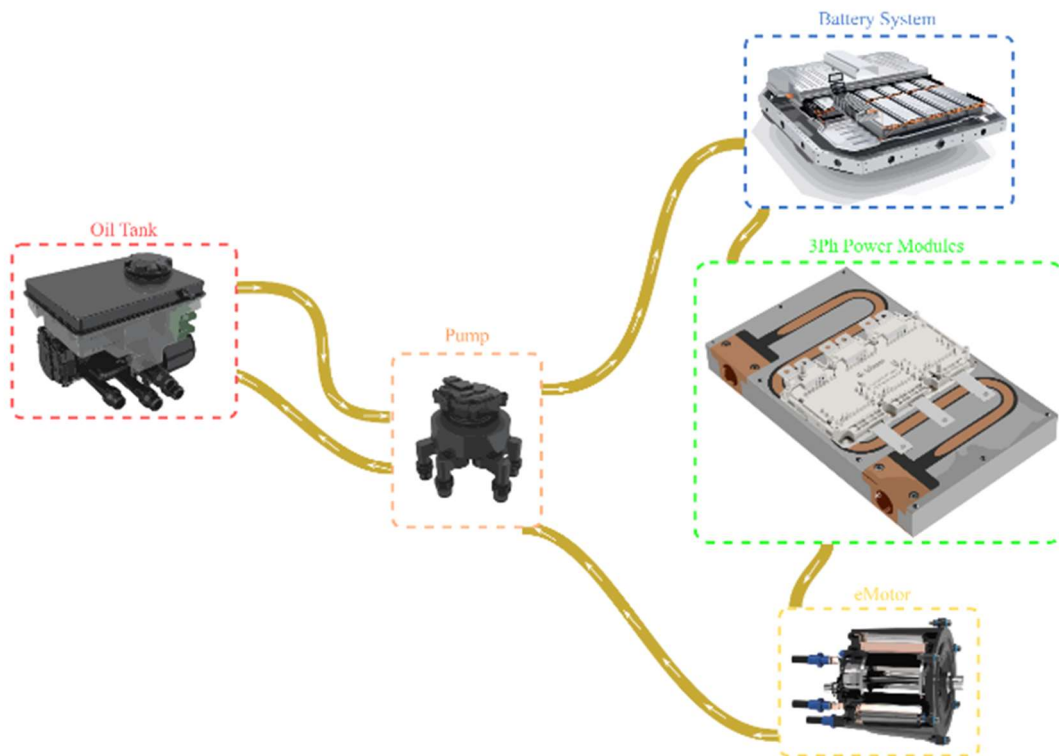
Figure 19 Cooling system concept: motor, inverter and battery oil cooling, solution 3.

An example of these configurations is the integrated Thermal Management Module developed by Marelli [12]. The system they propose allows to combine the different circuits into one single component, reducing the system complexity while improving safety and flexibility. This idea is also taken by other manufacturers such as Bosch since it also provides a considerable cost reduction regarding classical thermal architectures [13].

3.5 Mechanical architecture

Regarding mechanical architecture, most OEMs already have dedicated electric vehicle platforms for 400V architecture. In Figure 20, an example of Volkswagen mechanical architecture is shown, the battery system is located in the bottom center of the EV, and at the front and the rear the axle drives.

Figure 20 Mechanical distribution concept of Volkswagen EV [3].

Most of the surface is occupied by the battery system, which is also linked to the wheel axis. Each wheel axis is composed of a 3 in 1 motor, inverter and gearbox connected to the side shaft, as seen in Figure 21.
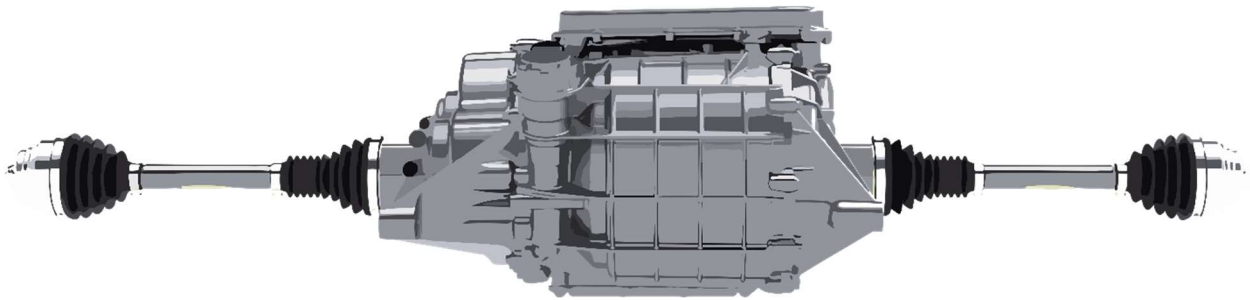
Figure 21 GKN's eaxle drive [14].

Where the motor, inverter and cooling systems are integrated in the axis center as shown in Figure 22.
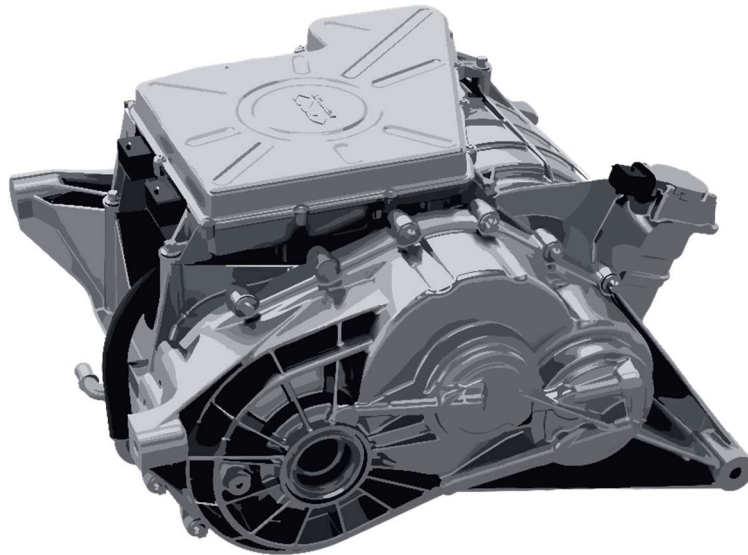
Figure 22 GKN's 3 in 1 integrated system with Inverter, motor and gearbox [14].

3.6   Control architecture

There are no differences from 400V control architecture. EV powertrain is composed of different control units: one for the OBC, another for the drive and another for the Battery Management System, and there is a higher-level control unit to manage all of them.

Regarding communications, CAN communication is usually used between the different control units. However, there is a new trend at research level to use Ethercat communication to achieve a faster communication between the battery and the EV control unit, as it can be seen in 2024 EU call [15], where one of the scope deals with "enhanced communication between battery and vehicle control units for a more efficient battery operation by synchronizing ECUs of the BMS and the EV".

3.7 800V architecture conclusions

Regarding 800V **electrical architecture**, multiple powertrain configurations are possible, axle drive being the most promising solution at present. There is a tendency to have a primary axle drive (in the rear) and some EV also have a secondary axle drive (in the front). Moreover, using SiC based inverters drive's efficiency is improved considerably. These SiC devices have less losses, reducing inverter losses, and have higher switching frequency, that can be used by the control to reduce motor harmonics and thus, to reduce motor losses. Modularity is achieved by the possibility to use different battery packs or OBC. The architecture is scalable to achieve different power level using different motor lengths but same rotor diameter, using the same inverter and paralleling devices, using different gear ratios, etc. Finally, cost oriented solution can be achieved by using Si devices for the secondary axle drive, where less powerful systems are usually required.

Concerning 800V **thermal architecture**, there is a tendency to use oil cooling, not only for the motor but also for the inverter and even for the battery system. However, this is long term research and for HEFT drive oil cooling will be considered for motor and, inverter and battery system will be cooled using water-glycol.

800V **mechanical architecture** and control architecture are quite similar to 400V architectures. No differences have been found.

4 800V SIC-BASED EV DRIVE SIMULATION & ANALYSIS

In this section different 800V SiC based EV drive simulations and analysis have been done to study the following aspects:

- SiC device high dv/dt effect propagation model simulation.
- High switching frequency influence on EMC to comply with automotive standards analysis.
- 400V-800V EV performance comparison simulation.
- Advanced shared cooling in the powertrain analysis and simulation

4.1 High dv/dt effect propagation models

4.1.1 Introduction

With the aim to illustrate the dynamics of the expected waveforms in an 800V SiC based driver train, a dynamic characterization of a suitable 1200V SiC module is presented in Figure 23 under a 600V and 800V DC bus voltage, with a current of 300A.
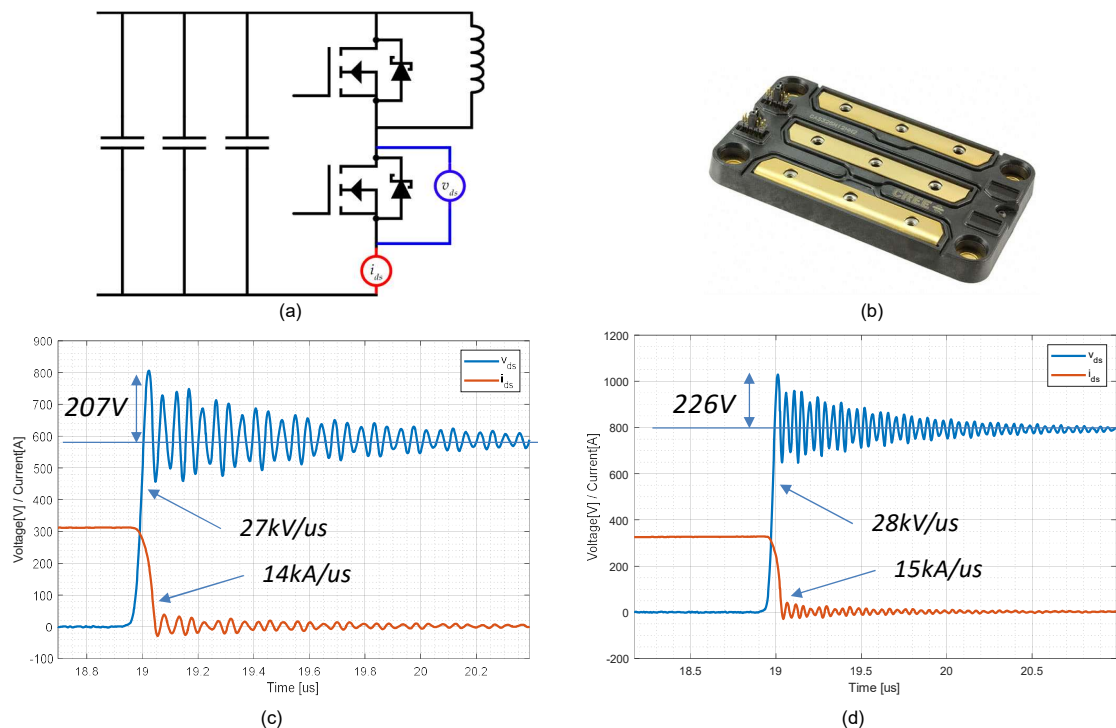
Figure 23. Experimental waveforms obtained with a 1200V Wolfspeed SiC module. (a) Double-pulse schematic, with the variables measured: drain-to-source voltage, v_{ds}; and drain-to-source MOSFET current, i_{ds}. (b) Wolfspeed module used for the test: CAS325M12HM2. (c) voltage and current waveform at 600V DC bus voltage, and 300A. (d) voltage and current waveform at 800V DC bus voltage, and 300A.

The FFT of the voltage waveform is plotted on Figure 24 for the 800V case (Figure 23.d). This waveform corresponds with the voltage generated by the converter (phase to -DC terminal voltage). And this is the "perturbation" seen by all the elements connected to the converter (i.e. cables/copper bars, motor, etc…). The voltage harmonics have a high bandwidth (up to 27MHz, that corresponds with the ringing frequency).
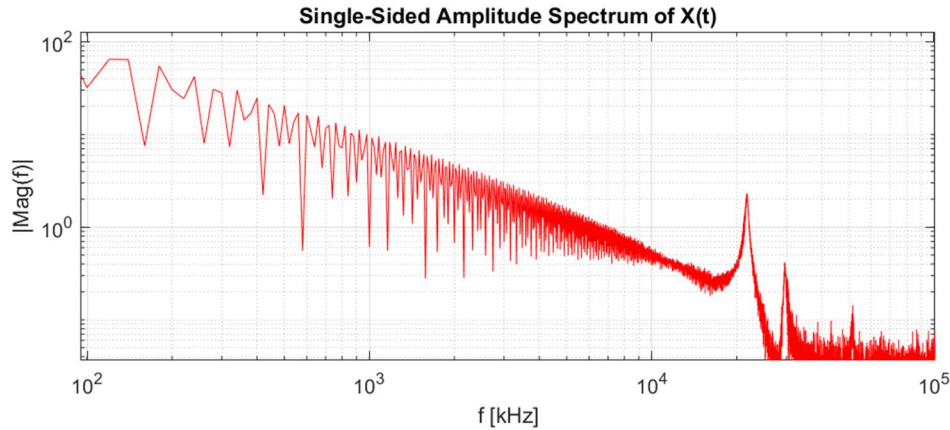
Figure 24. FFT of the 800V voltage waveform

This FFT of the "systems perturbation" is the responsible of the current and voltage oscillations that are going to appear on the drive-train, and are totally dependent of the voltage rise-a and fall-time, as can be seen on Figure 25.

The fall- and rise-times achieved with the 1200V SiC devices used as example here, are creating important frequency harmonics up to 30MHz, so this is the bandwidth that is going to be considered in the main of the simulations presented in this document, that corresponds with the main frequency ranges considered in EMC topics.

In addition, the dv/dt that will be seen by the motor terminals will be, at least, around the values achieved in the converter (27 and 28 kV/us), that have a direct impact in the isolation requirements of the motor. These aspects are deeply analyzed in the next sections of the document.
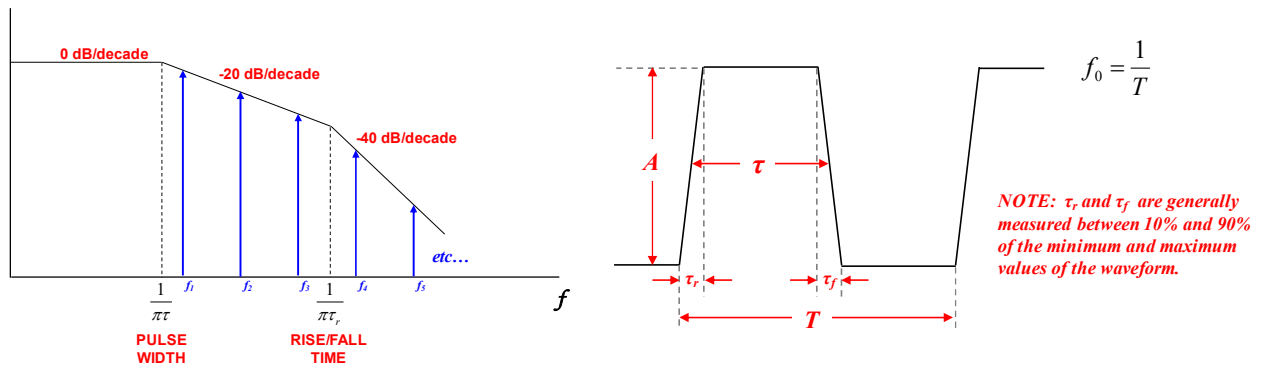
Figure 25. (a)FFT of a (b) trapezoidal waveform as function of the rise & fall time.

The electrical architecture involves large complexity since electromagnetic compatibility (EMC) must be analyzed in detail. In this context, the connection between the three-phase inverter and motor, as well as the returning path between motor and inverter must be characterized to ensure that no large common-mode currents are originated.

In last years, SiC power devices have set in the market as one of the most popular choices when aiming high-voltage applications due to their large breakdown voltage and good switching performance. The switching behavior enables achievement of higher switching frequencies. Nevertheless, there is a main drawback when considering EV applications, which falls on the larger dV/dtthanlassic silicon (Si) based power converters. This fact has a huge impact on the DM and CM noise, and thus in the motor degradation.

In this context, there are two factors that play an important role, which are the connections between each phase of the inverter and the motor, as well as between the motor housing and the ground reference of the system.

4.1.2 Frequency domain modelling

First, the frequency domain modelling is divided into common mode and differential mode. In this way, the models will provide the components that have larger impact on the converter behavior. In Table 5, the main parameter values that are employed in the simulations are listed. The bode diagrams obtained in this section help to determine not only the resonant frequencies that arise from the implementation of these systems, but also to explore which current paths create them.

Table 5 Reference parameter values utilized in EV.

Converter Parameters	Description	Value	Units
V_{dc}	DC voltage source	800	V
f_{sw}	Switching frequency	20	kHz
f_{red}	Fundamental frequency	1	kHz
C_{cm}	Common mode capacitors	50	nF
Winding Parameters	**Description**	**Value**	**Units**
L_w/C_w	Wiring parasitics	[290/90] *Length	nH/pF
$Length$	Wire length	0.1	m
Motor Parameters	**Description**	**Value**	**Units**
L_m	Motor inductance	40	µH
R_e	Motor parallel resistance	1100	Ω
Parasitic Parameters	**Description**	**Value**	**Units**
C_{hs}	Heatsink capacitance	0.1	nF
R_{hs}	Heatsink-source resistance	20	mΩ
L_{hs}	Heatsink-source wiring inductance	1	µH
$\square\square$	Motor-chassis capacitance	4	nF
C_{m2}	Phase-chassis capacitance	2	nF
L	Chassis-heatsink wiring inductance	100	nH

It is important to note that some parameters, i.e., V_{dc}, $f_{sw}V_{dc}f_{red}$ f_{sw} are only considered for time domain modeling since they do not impact on the frequency domain. Here in after, both models are presented together with the simulation results.

4.1.2.1 Common mode:

The simulation model developed for common mode characterization is presented in Figure 26. It is composed of a common mode voltage source that feeds the wiring of the converter as well as the three-phase motor. Furthermore, a returning path is included, which consists of the parasitic capacitors between the motor (C_m and C_{m2}) and the chassis, as well as the parasitic inductance of the wire, that connects the motor chassis with the heatsink/cold plate (cooling element for the SiC semiconductors). Moreover, the cold plate is connected to the negative terminal of the common mode voltage source, where the parasitic inductance, resistance of the wire and common mode bus capacitances are considered.
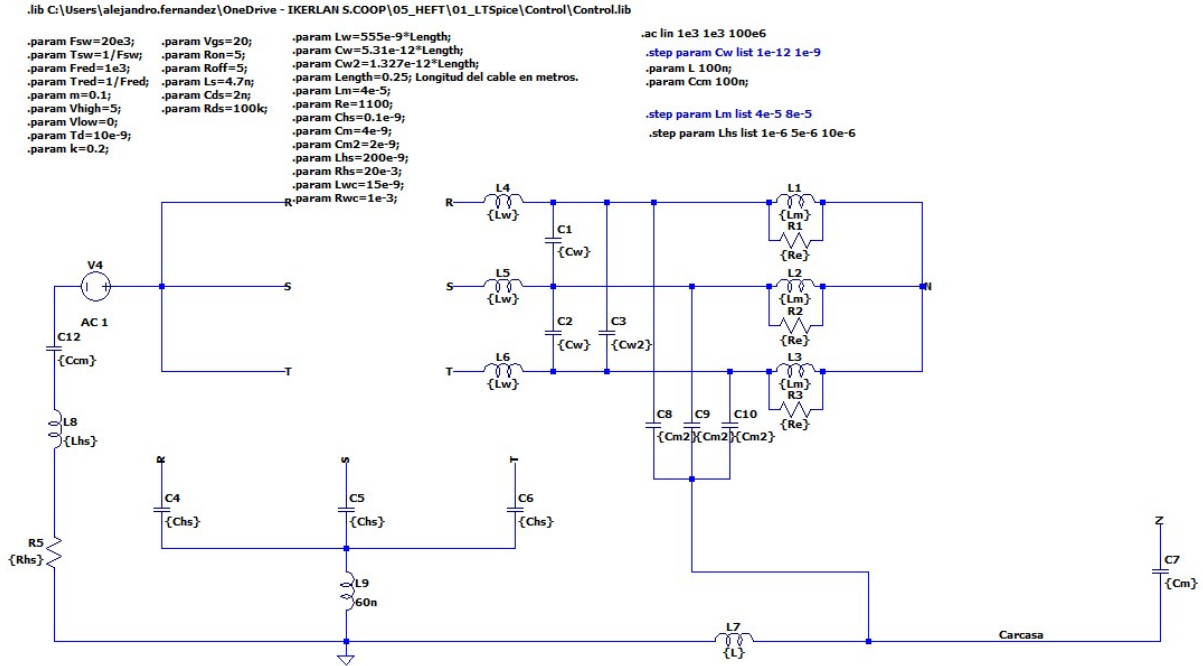
Figure 26 Common model schematic in LTSpice for EV application.

First parameter to be sweep is the length of the wiring between the three-phase inverter and the motor. The resulting bode diagrams of the common-mode current and phase-chassis voltage when varying the wiring length are presented in Figure 27 and Figure 28.

Analyzing these diagrams, we can see the resonant frequencies that are present when considering the parameters listed in Table 5 over green figure. The value of these frequencies lies at 0.67, 3.6 and 26.7 MHz, which will be referred to as A, B and C respectively. These frequencies will be repeated in every picture on the green plot, which is a reference to determine the impact of each parameter on converter performance.

The variation of the wiring length modifies the values of the $L\omega$ and $C\omega$ parasitic elements, Figure 27and Figure 28. These parameters have almost no impact on the resonance A, while B and C move to lower frequencies. Considering that this frequency is lower as higher is the wiring length set this parameter as one of the most critical on the system. Aiming to move B and C resonant frequencies to larger values, the wiring between three-phase inverter and motor must be as compact as possible.
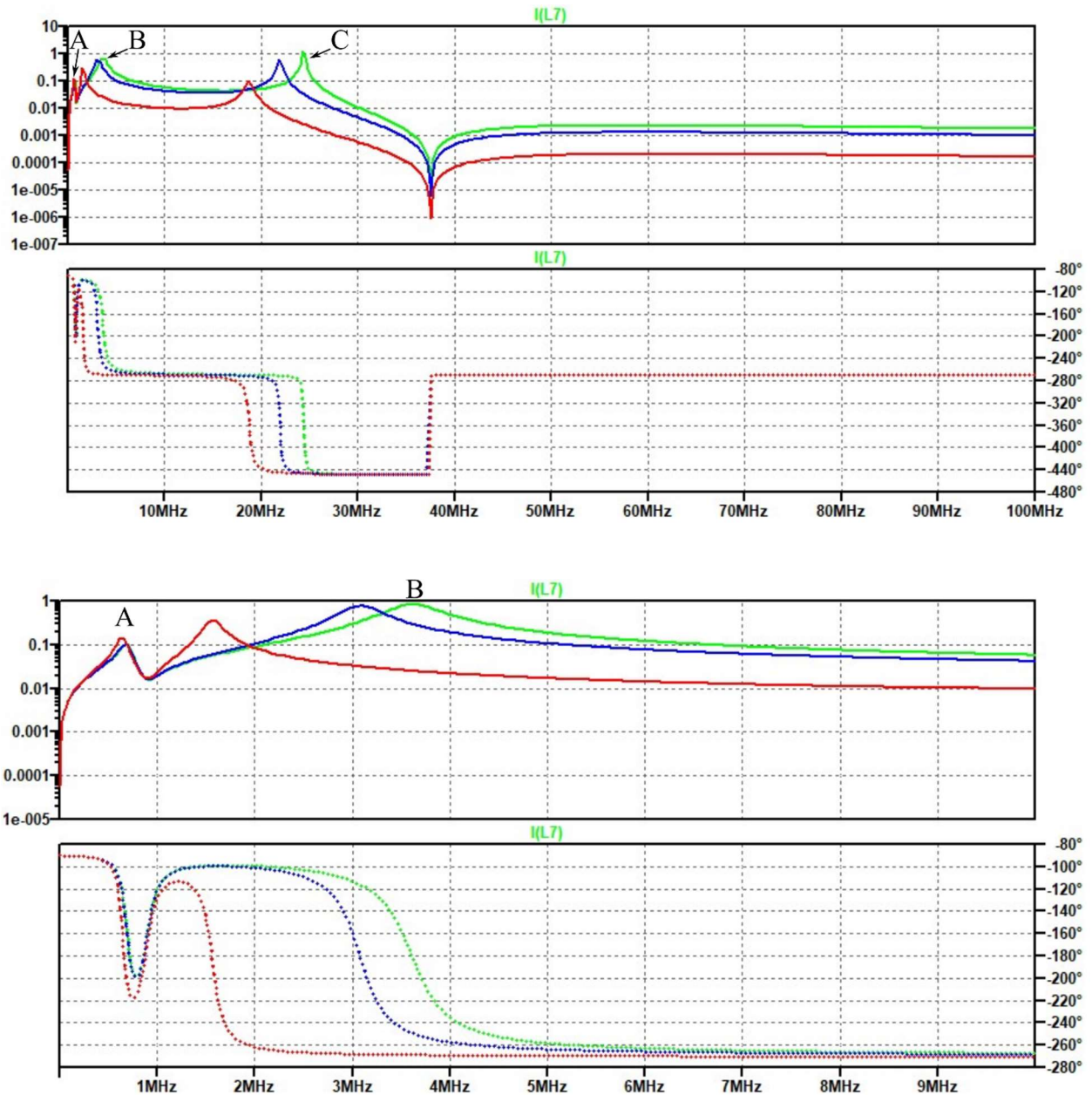
Figure 27 Bode diagram of the common mode current when varying the wiring length. Top: 1kHz-100MHz and Bot: 1kHz-10MHz. Length=0.25m (green), 1m (blue) and 10m (red).
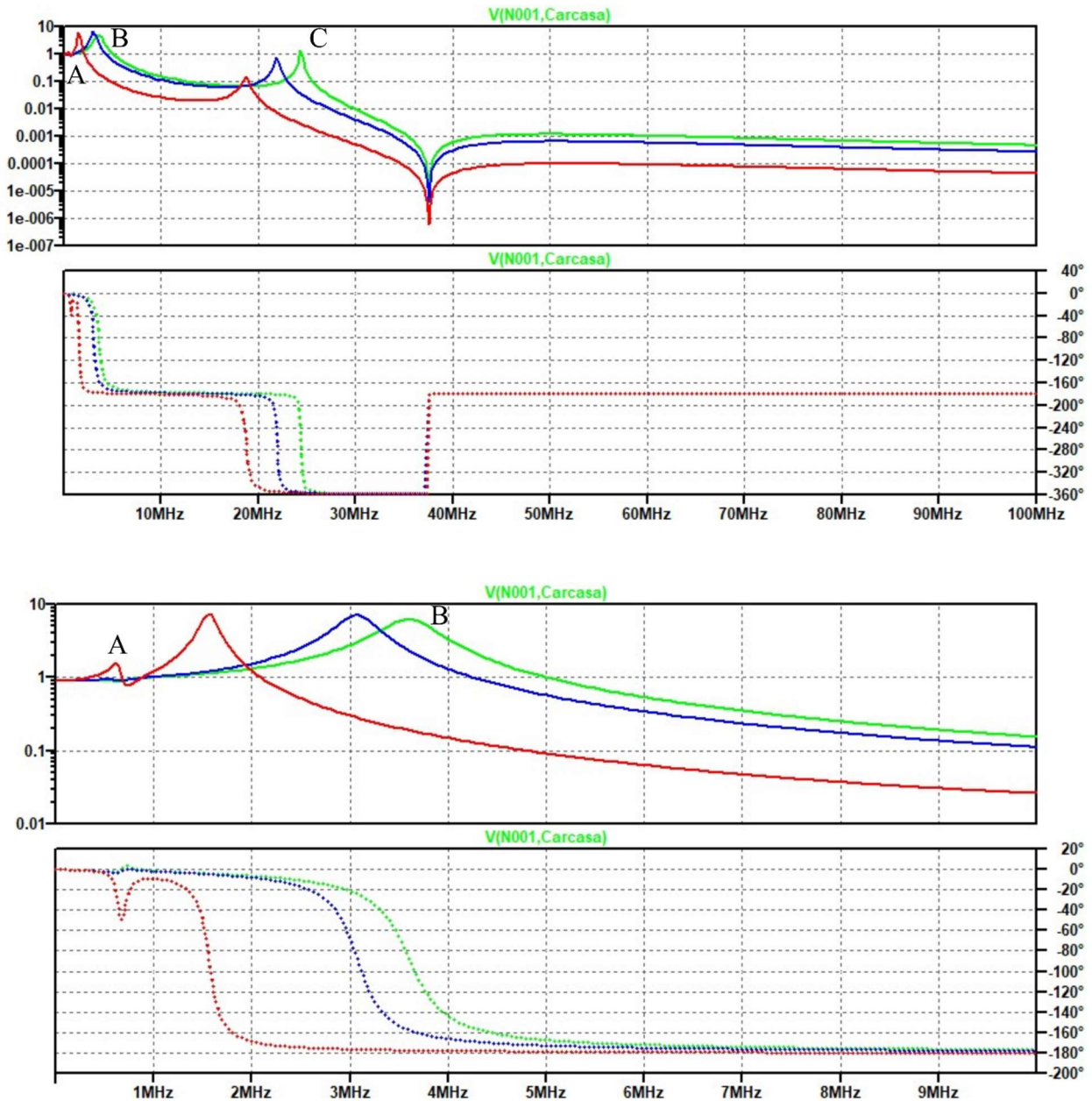
Figure 28 Bode diagram of the phase voltage when varying the wiring length. Top: 1kHz-100MHz and Bot: 1kHz-10MHz. Length=0.25m (green), 1m (blue) and 10m (red).

In Figure 29 and Figure 30, we have varied the motor inductance. It can be seen that this parameter does affect the lowest resonant frequency (A) of the common mode current. The amplitude of this resonance becomes insignificant as larger is the motor inductance. However, this parameter does not play an important role on the phase-chassis voltage, since the bode diagram in each step is almost identical.
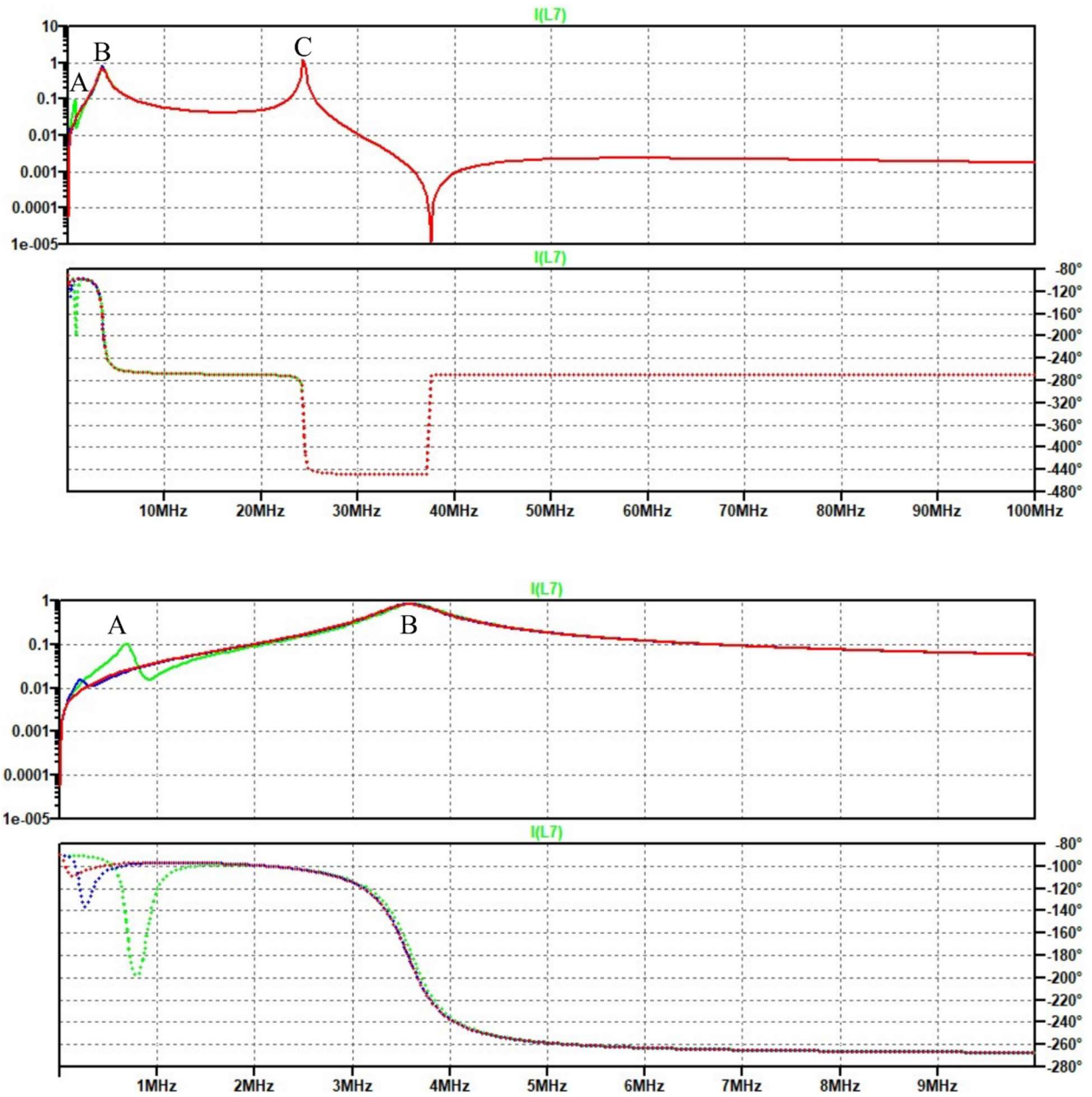
Figure 29 Bode diagram of the common mode current when varying the motor inductance. Top: 1kHz-100MHz and Bot: 1kHz-10MHz. Lm= 40μH (green), 400μH (blue) and 4mH (red).
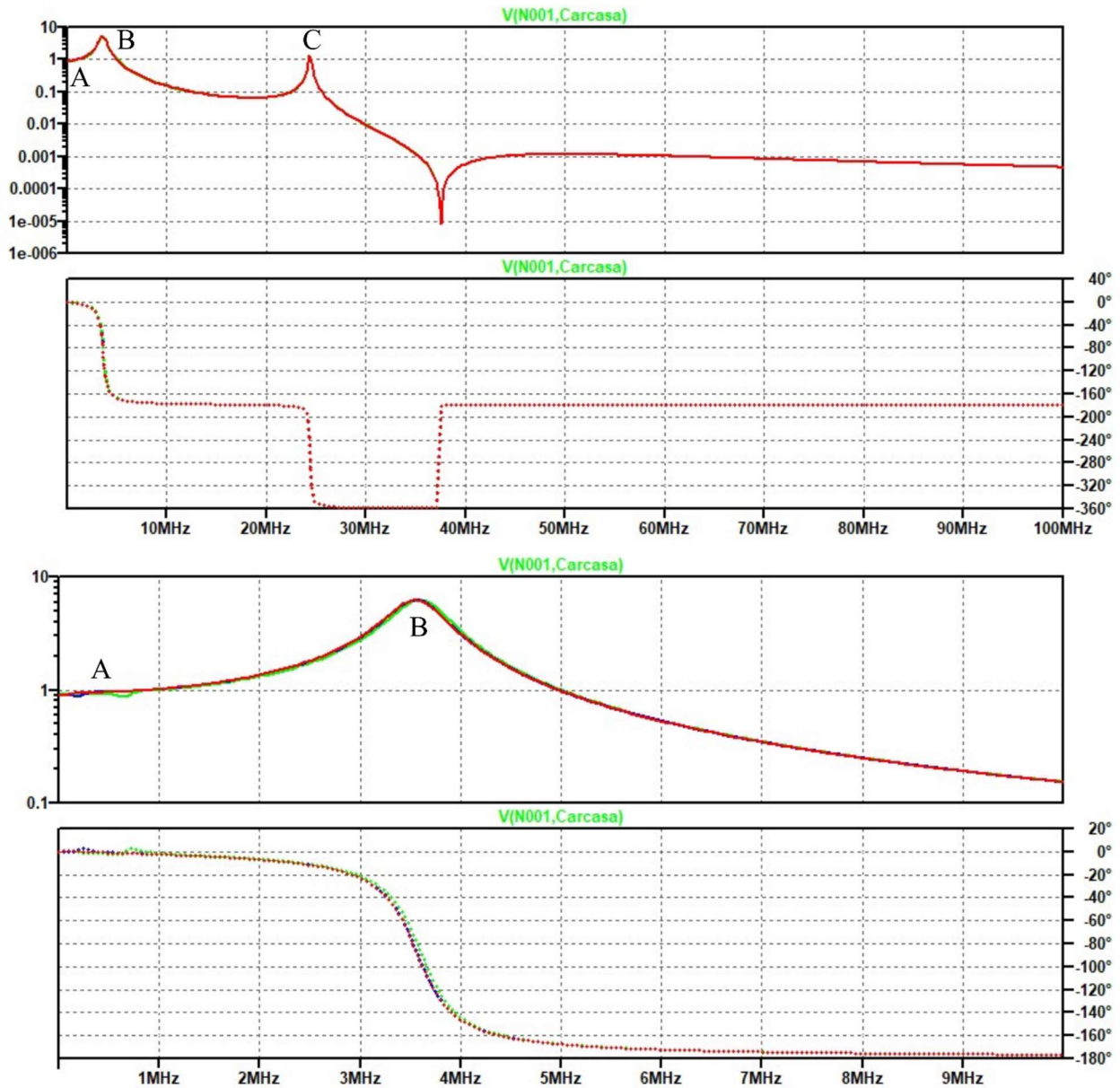
Figure 30 Bode diagram of the phase voltage when varying the motor inductance. Top: 1kHz-100MHz and Bot: 1kHz-10MHz. Lm= 40μH (green), 400μH (blue) and 4mH (red).

Same conclusions are extracted in the case of the parasitic capacitance between the motor neutral point and its chassis (see Figure 31 and Figure 32). The variation of this capacitance just impacts on the lowest resonant frequency (A) of the common mode current bode diagram. Nevertheless, it is important to note that the amplitude of this frequency becomes slightly larger. In the phase-chassis voltage diagram there is not a significant difference between each case.
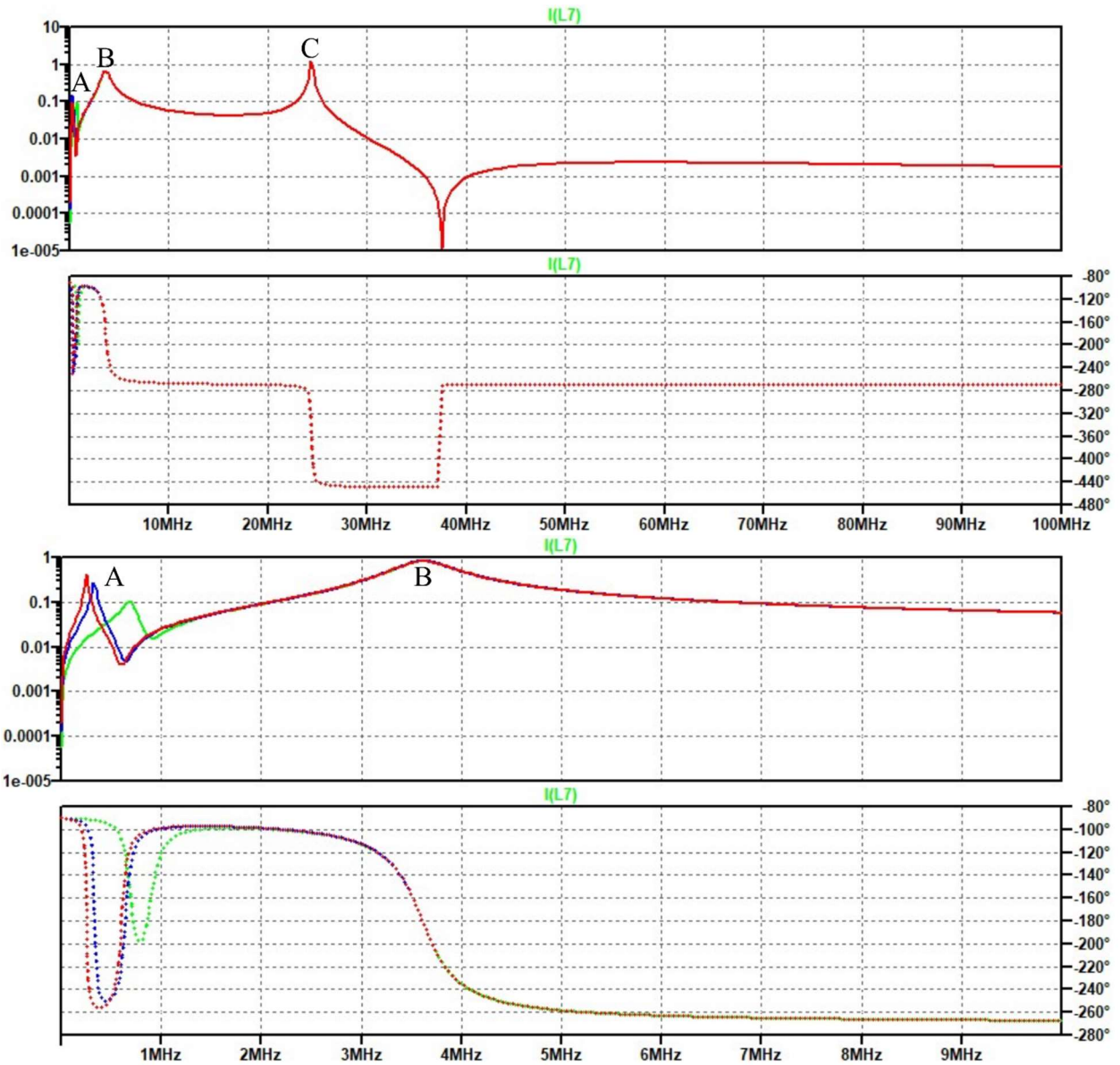
Figure 31 Bode diagram of the common mode current when varying the motor-chassis capacitance. Top: 1kHz-100MHz and Bot: 1kHz-10MHz.Cm=4nF(green), 20nF (blue) and 40nF (red).
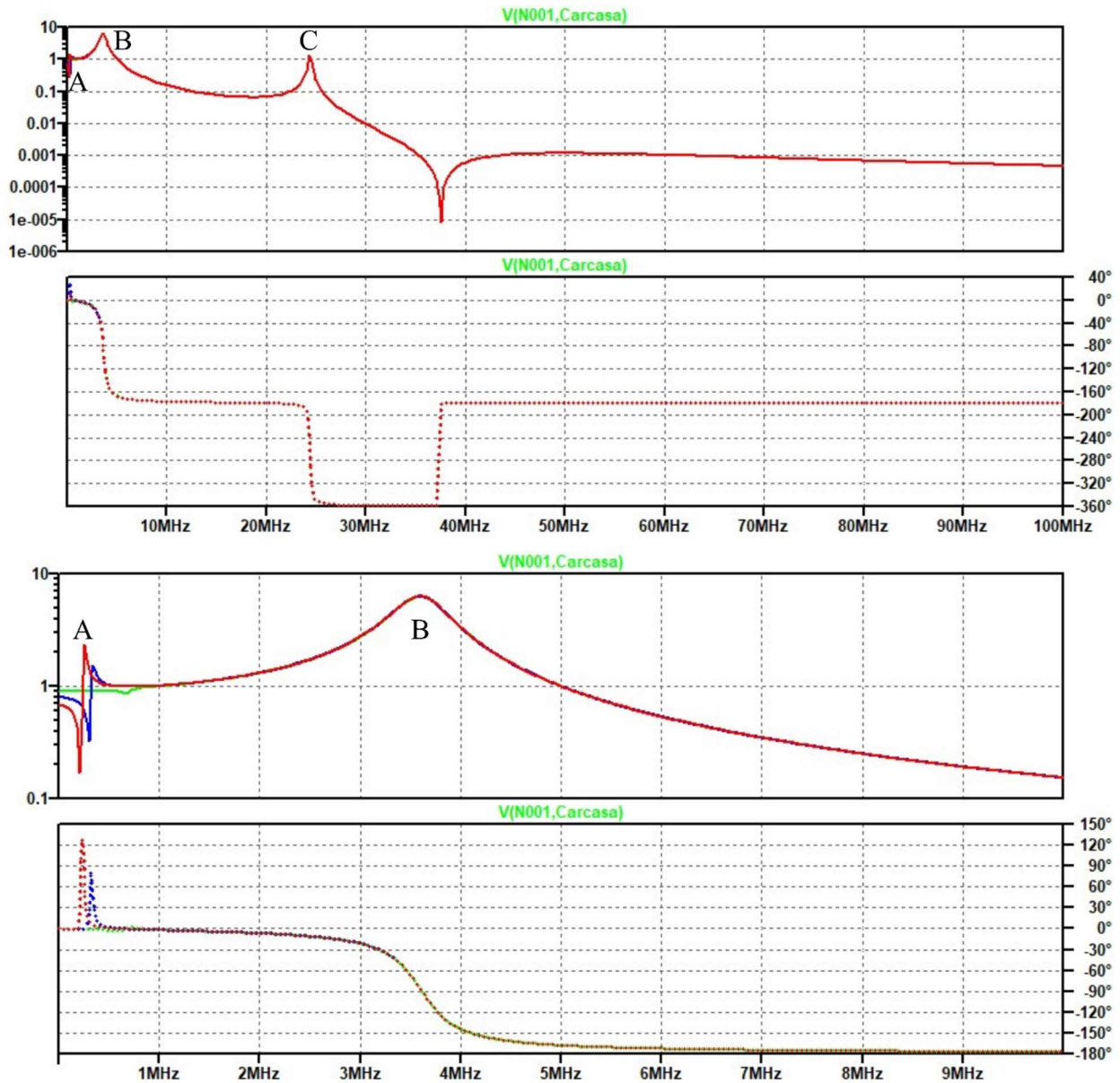
Figure 32 Bode diagram of the phase voltage when varying the motor-chassis capacitance. Top: 1kHz-100MHz and Bot: 1kHz-10MHz. Cm=4nF(green), 20nF (blue) and 40nF (red).

However, there are also three additional parasitic capacitances between each phase of the motor and its chassis, whose bode diagrams are presented in Figure 33 and Figure 34. This capacitance mostly modifies A and B resonant frequencies. In both common mode current and phase voltage bode diagrams, it is especially noticeable that B resonant frequency moves to lower values, which may be a problem depending on the rising and falling times of the power devices (see 4.1.3). Up to this point, it is concluded that design and parasitic parameters of the motor do not modify C resonant frequency but can determine whether A or B lies at.
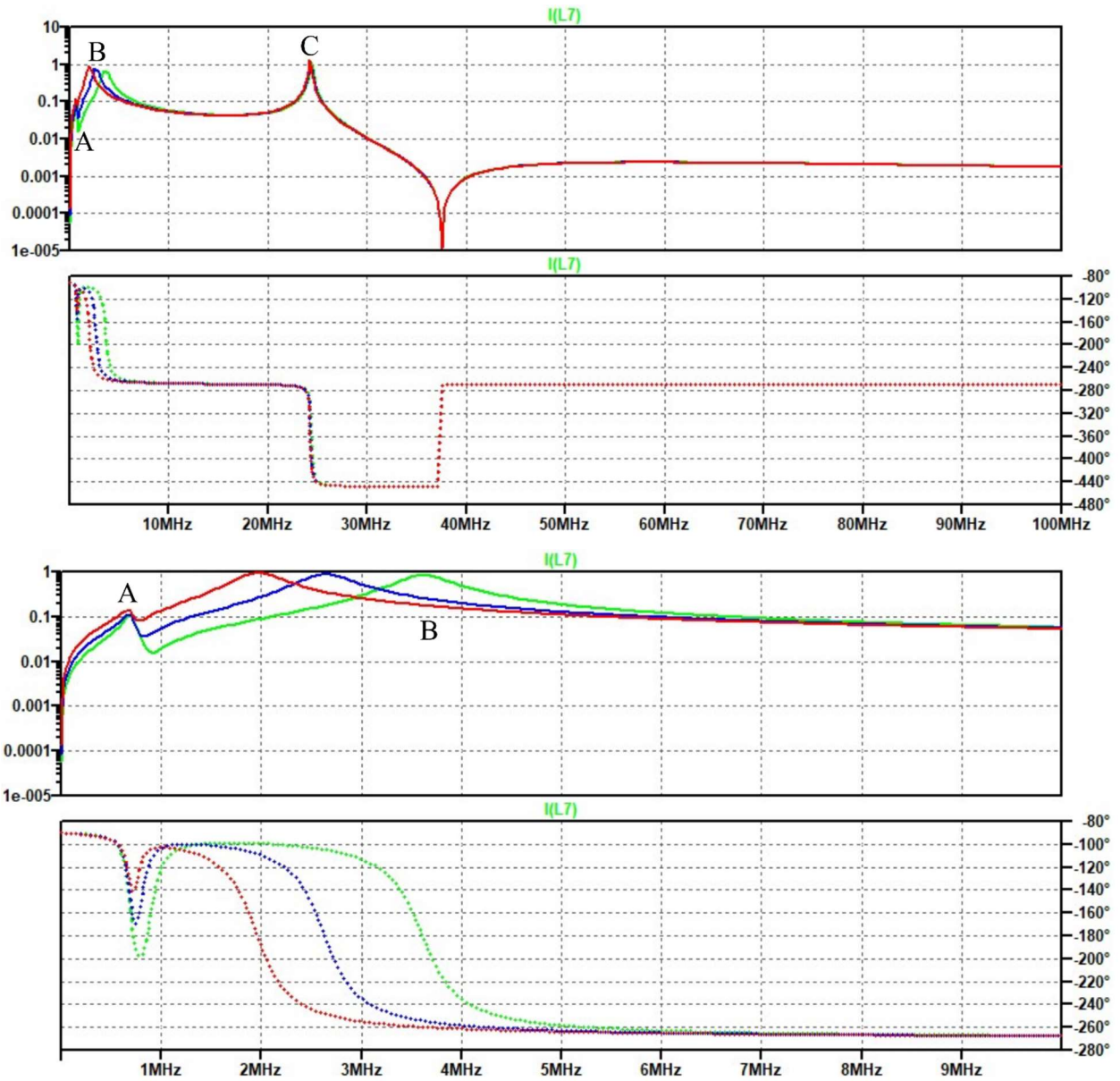
Figure 33 Bode diagram of the common mode current when varying the phase-chassis capacitance. Top: 1kHz-100MHz and Bot: 1kHz-10MHz. Cm2= 4nF (green), 20nF (blue) and 40nF (red).
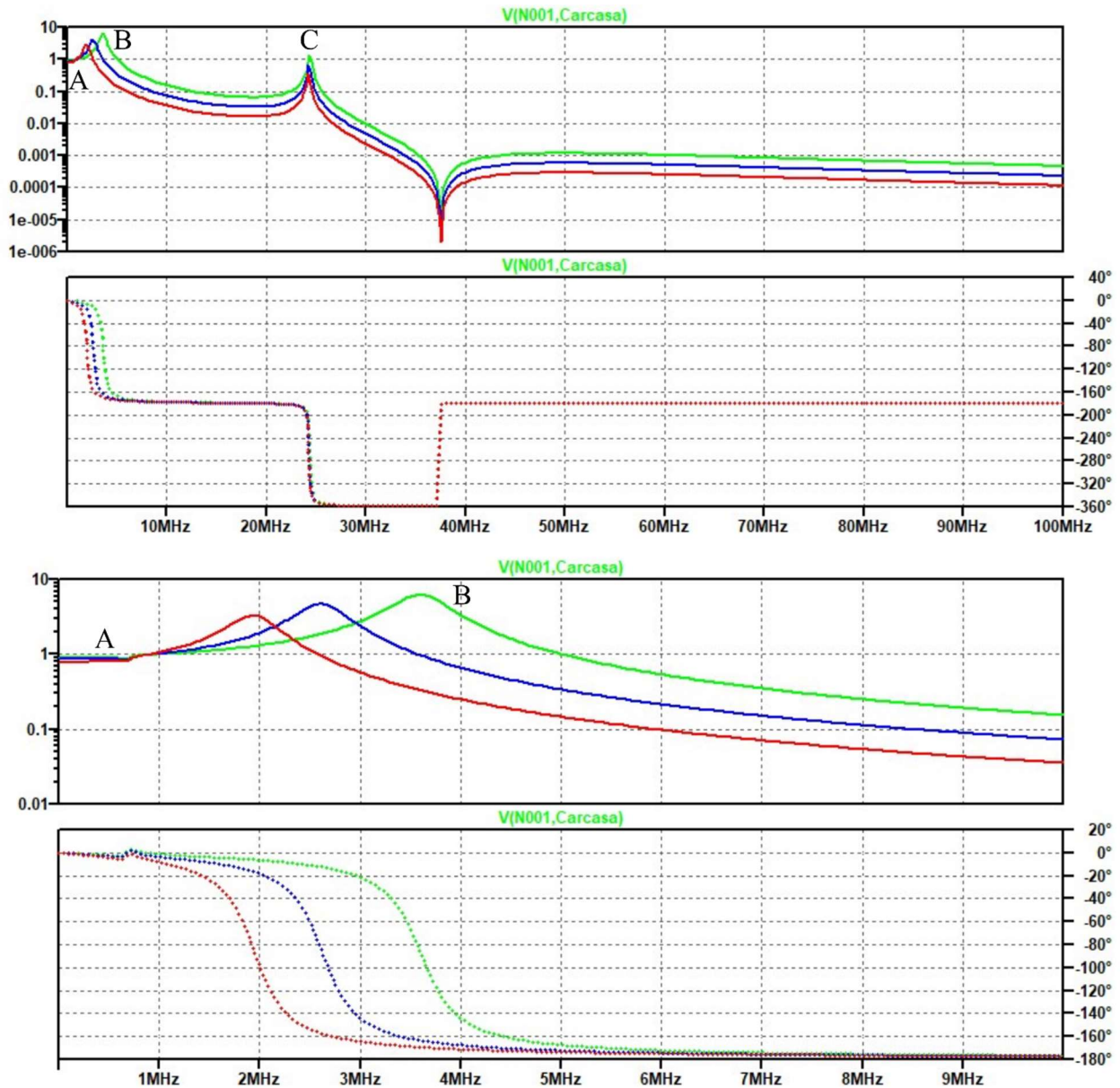
Figure 34 Bode diagram of the phase voltage when varying the phase-chassis capacitance. Top: 1kHz-100MHz and Bot: 1kHz-10MHz.Cm2= 4nF (green), 20nF (blue) and 40nF (red).

Other parameters to be swept (see Figure 35 and Figure 36) are the capacitances between the semiconductor case and the heatsink (C_{hs}). These parasitic capacitances must be carefully determined in the design steps, since they modify B resonant frequency which, as we will see in time domain modelling simulations, may have a huge impact on the resulting dv/dt.
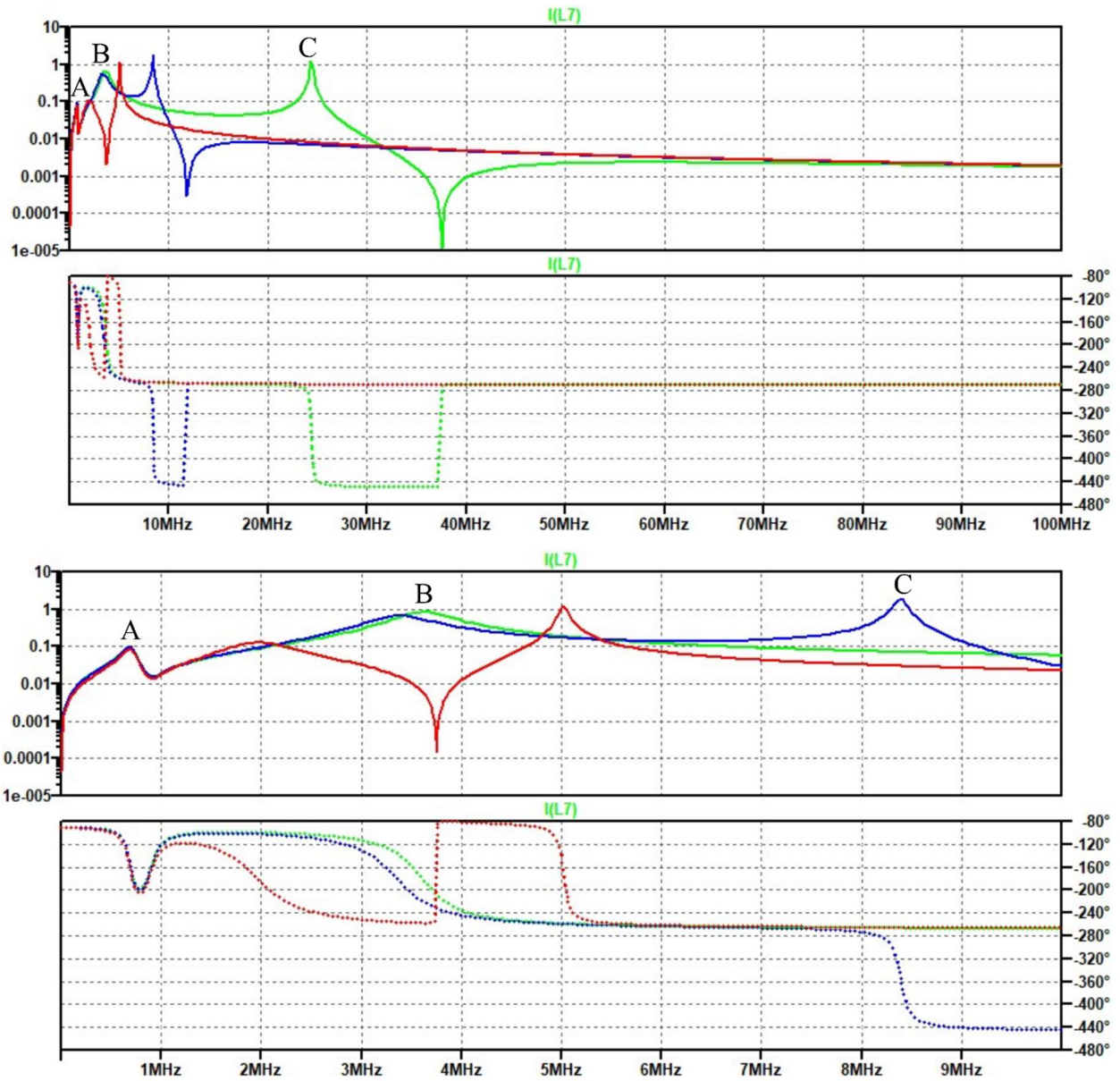
Figure 35 Bode diagram of the common mode current when varying the power device-heatsink parasitic capacitance.
Top: 1kHz-100MHz and Bot: 1kHz-10MHz. C_{hs}= 0.1nF (green), 1nF (blue) and 10nF (red).
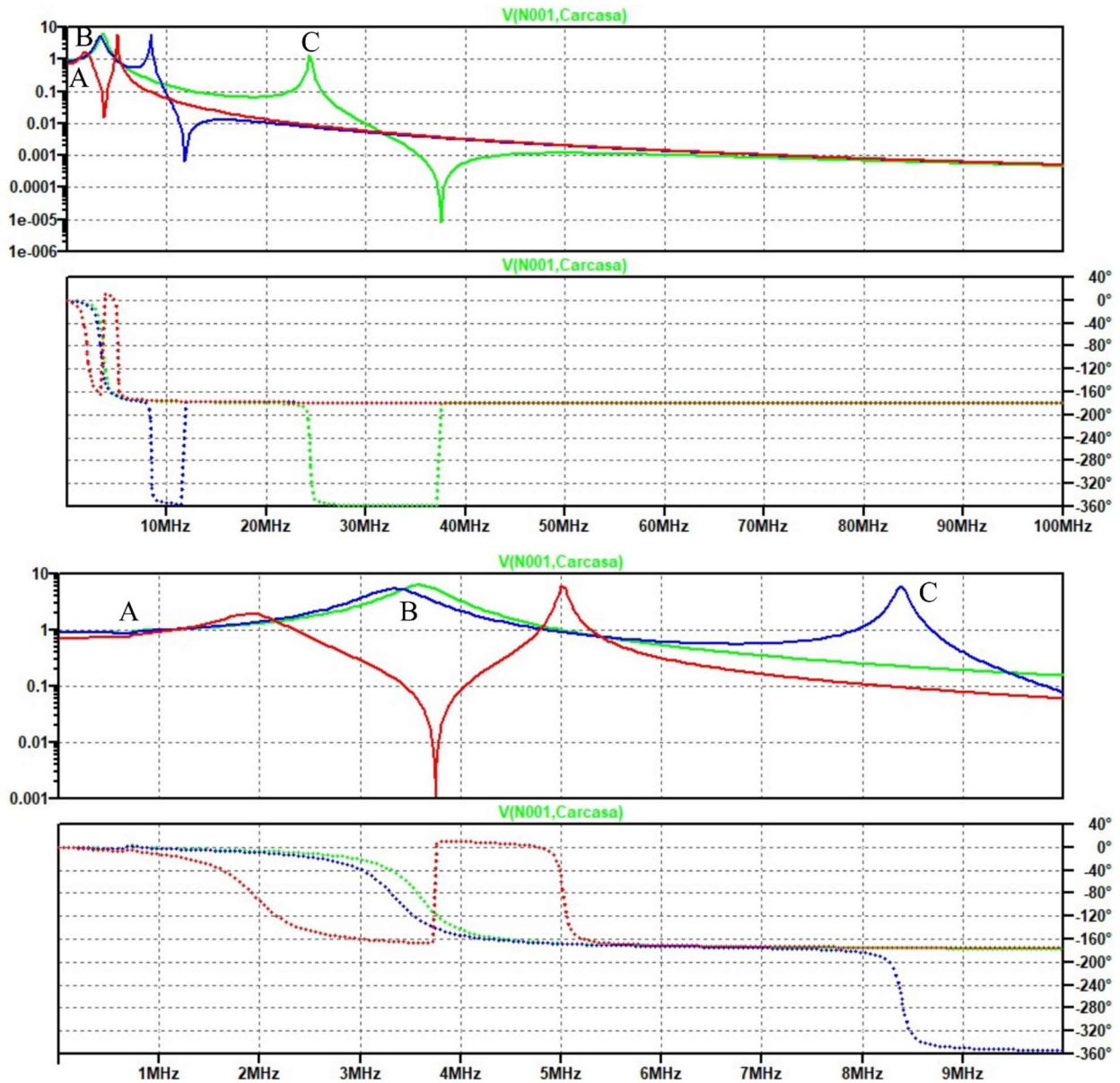
Figure 36 Bode diagram of the phase voltage when varying the power device-heatsink parasitic capacitance. Top: 1kHz-100MHz and Bot: 1kHz-10MHz. C_{hs}= 0.1nF (green), 1nF (blue) and 10nF (red).

The resulting bode when varying the parasitic inductance between the source DC bus and the heatsink is presented in Figure 37 and Figure 38. As with the heatsink parasitic capacitance, this variation modifies C resonant frequency, although the impact on that frequency is lower than modifying the parasitic capacitance of the heatsink. However, it also slightly modifies the value of B resonant frequency. Even though the impact seems not to be large, it is important to reduce the parasitic inductance of the connection between the heatsink and the source negative point.
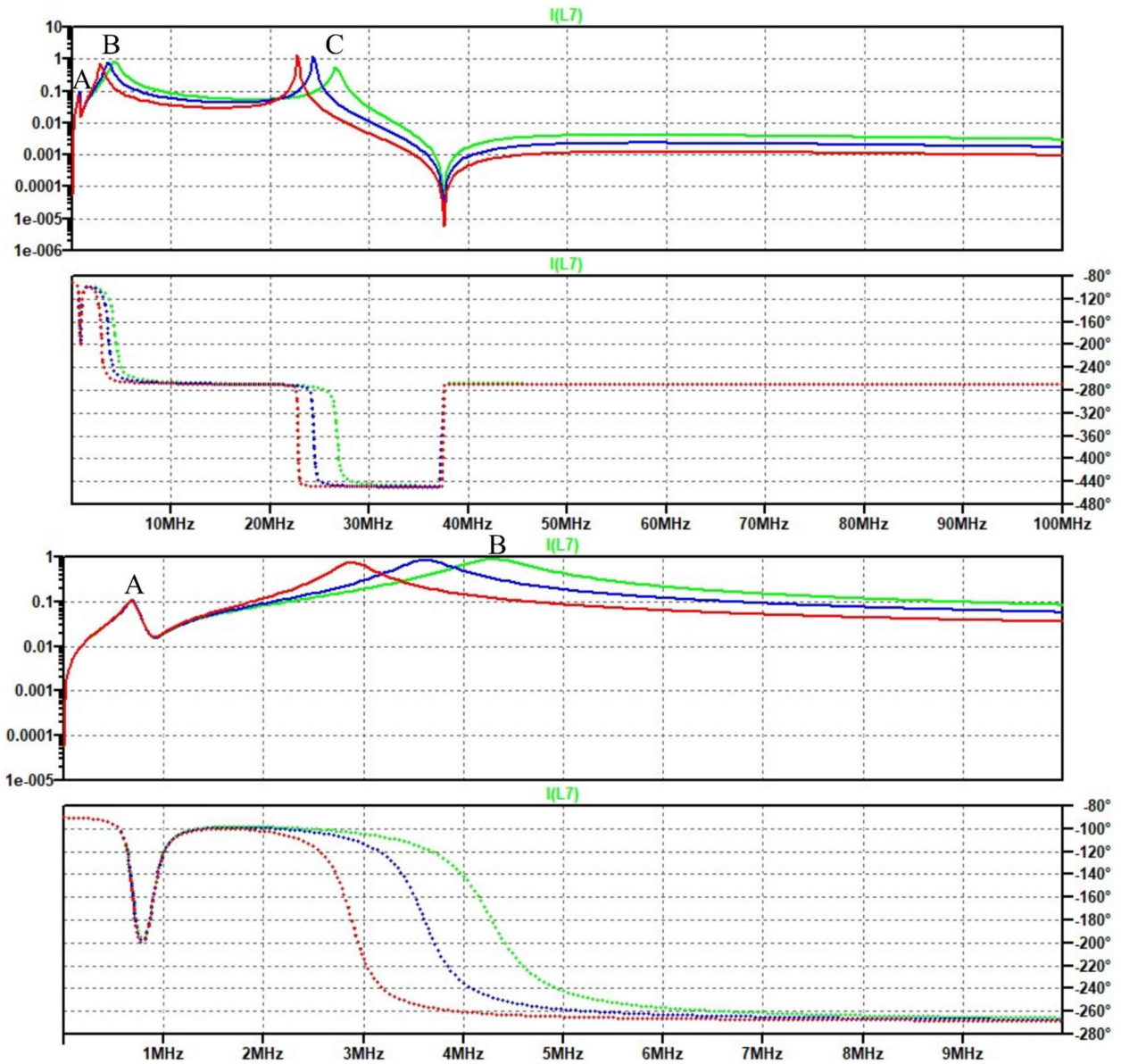
Figure 37 Bode diagram of the common mode current when varying the heatsink-source parasitic inductance. Top: 1kHz-100MHz and Bot: 1kHz-10MHz. L_{hs}= 100nH (green), 200nH (blue) and 400nH (red).
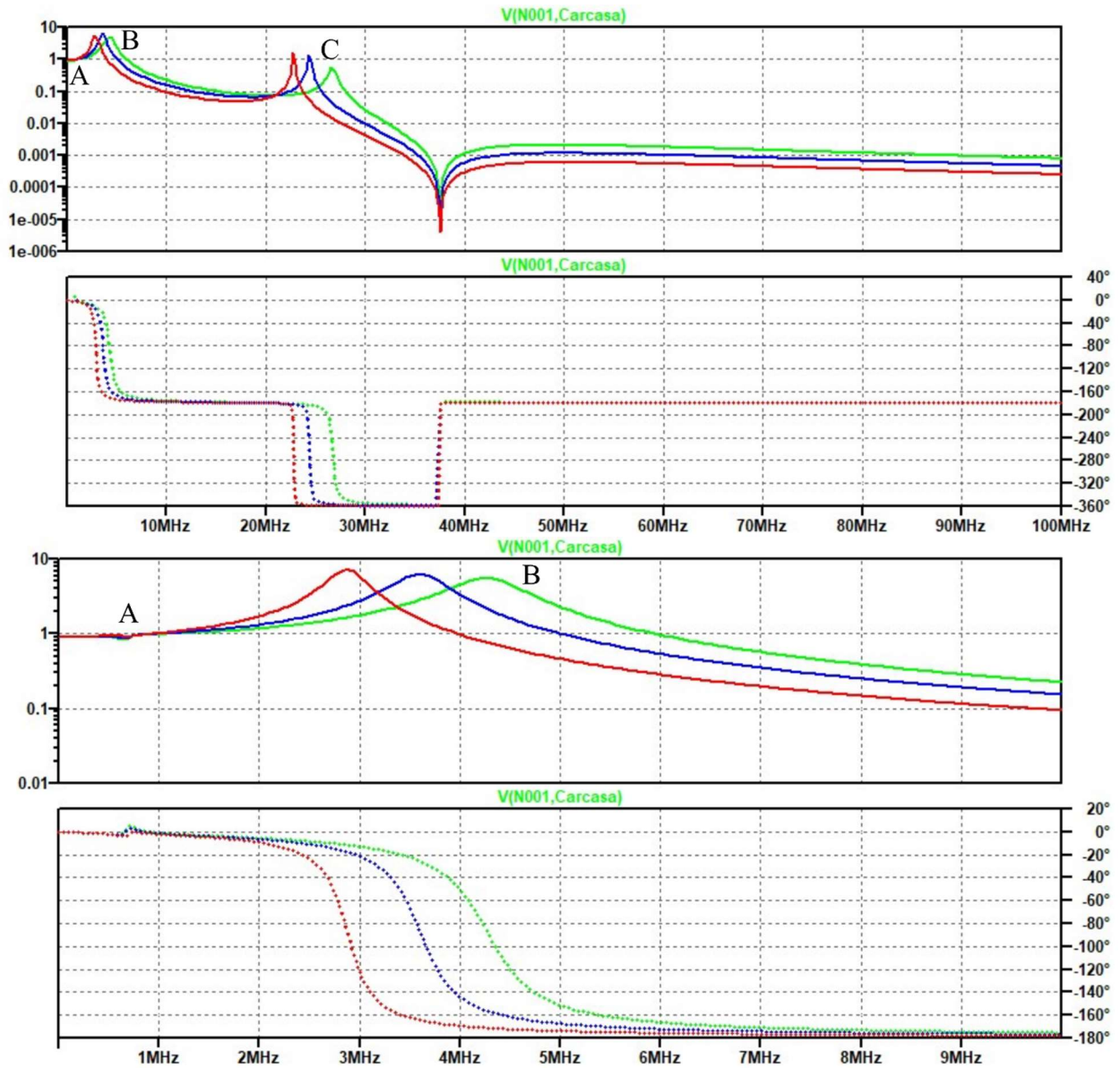
Figure 38 Bode diagram of the phase voltage when varying the heatsink-source parasitic inductance. Top: 1kHz-100MHz and Bot: 1kHz-10MHz. L_{hs}= 100nH (green), 200nH (blue) and 400nH (red).

Finally, the DC bus capacitance included to improve the common mode behavior of the system is analyzed. In this case, we can see in Figure 39 and Figure 40 that the impact of varying this capacitance is not large, although a minor variation is observed in B resonant frequency in both common mode current and phase voltage.
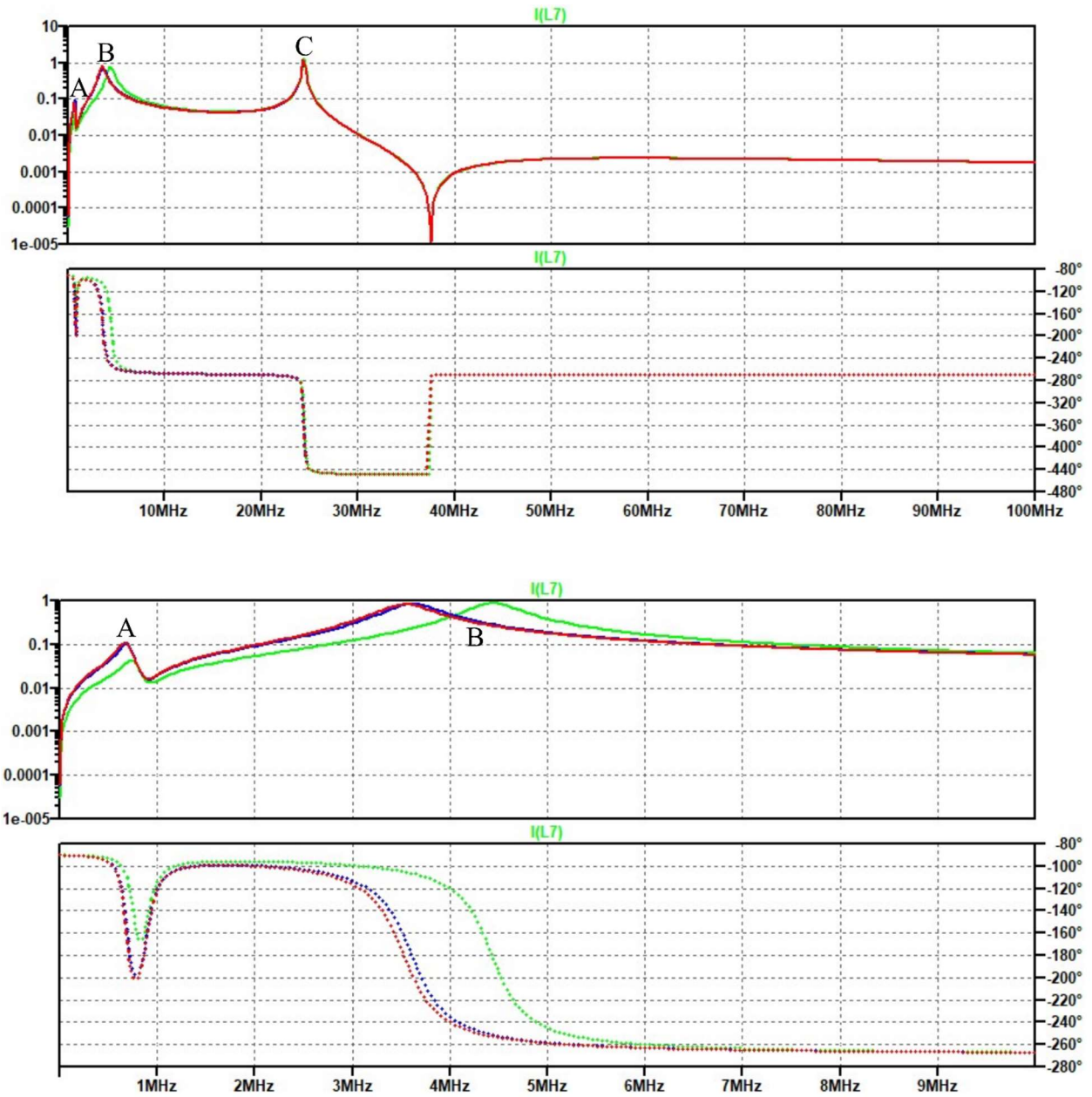
Figure 39 Bode diagram of the common mode current when varying the heatsink-source capacitors. Top: 1kHz-100MHz and Bot: 1kHz-10MHz. C_{cm} = 10nH (green), 100nH (blue) and 500nH (red).
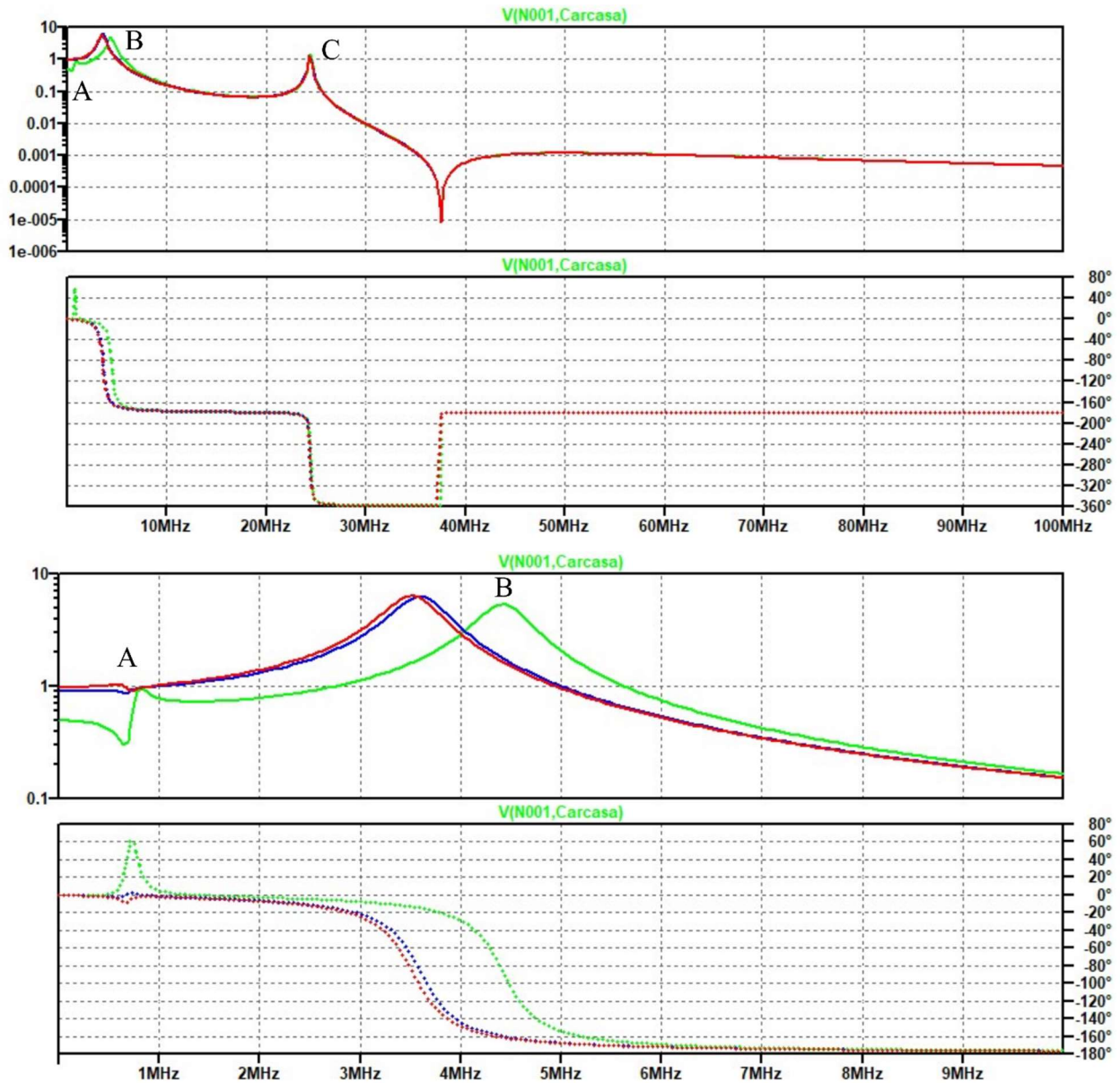
Figure 40 Bode diagram of the phase voltage when varying the heatsink-source capacitors. Top: 1kHz-100MHz and Bot: 1kHz-10MHz. C_{cm}= 10nH (green), 100nH (blue) and 500nH (red).

Along this subsection, we have provided the common mode resonances that arise from the connection of a three-phase inverter with a motor. Furthermore, the resonant frequencies that are present in this converter have been characterized, as well as which parameters, parasitic and non-parasitic, modify the resonant values.

4.1.2.2 Differential mode:

The simulation model utilized for differential mode characterization is presented in Figure 41. It is formed by a single differential mode voltage source that feeds one phase of the system, the wiring equivalent inductance and capacitance, the motor model and the heatsink parasitic capacitances. In this case, a return path is not included since it does not have any affection this model.

Since the parameter variation mainly influences the phase-to-phase voltage, the bode of this electrical variable is presented for different parameter variation. The bode diagram when varying the wiring length is given in Figure 42. First, it is noticed that the differential mode resonant frequencies lie at 9 and 32 MHz, which are named as A and B hereinafter.

.lib C:\Users\alejandro.fernandez\OneDrive - IKERLAN S.COOP\05_HEFT\01_LTSpice\Control\Control.lib

```
.param Fsw=20e3;        .param Vgs=20;        .param Lw=555e-9*Length;
.param Tsw=1/Fsw;       .param Ron=5;         .param Cw=5.31e-12*Length;
.param Fred=1e3;        .param Roff=5;        .param Cw2=1.32e-12*Length;
.param Tred=1/Fred;     .param Ls=4.7n;       .param Length=20; Longitud del cable en metros.
.param m=0.1;          .param Cds=2n;        .param Lm=4e-5;
.param Vhigh=5;        .param Rds=100k;      .param Re=1100;
.param Vlow=0;                               .param Chs=1e-9;
.param Td=10e-9;                             .param Cm=4e-9;
.param k=0.2;                                .param L 100n
```

.ac lin 1e3 1e3 100e6
.step param Chs list 0.1e-9 1e-9 10e-9

Figure 41 Frequency domain model of three-phase inverter differential mode in LTSpice.
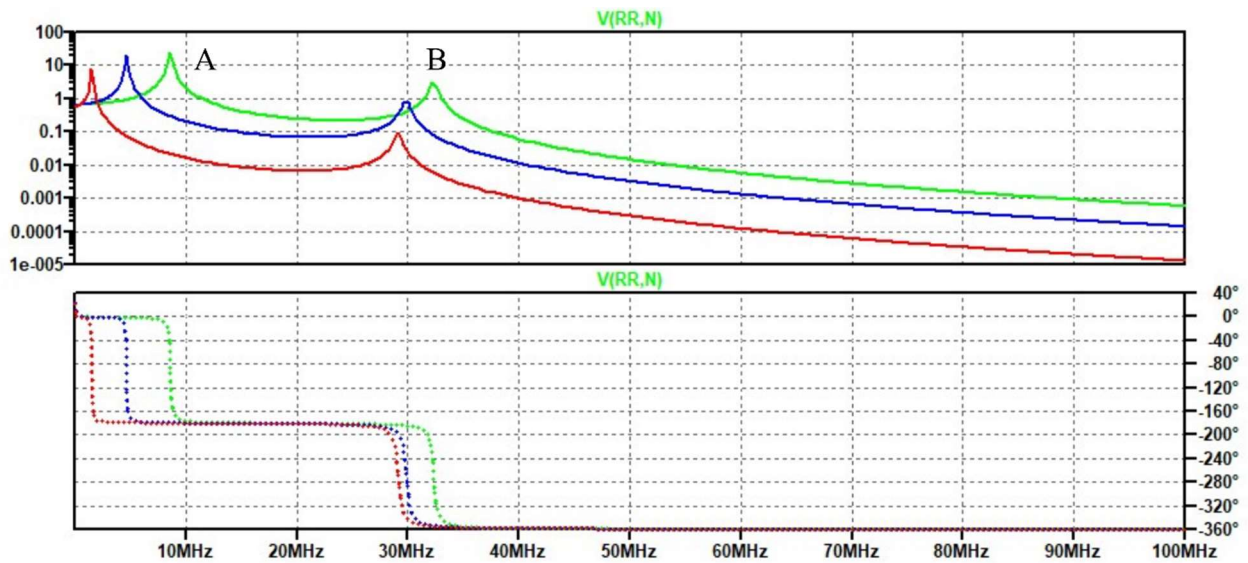
Figure 42 Bode diagram of the phase-to-phase voltage when varying the wiring length. $Length$= 0.25, 1 and 10 m.

As can be seen, as the wiring length increases, B resonant frequency is slightly modified. However, the impact on A is larger considering that this frequency lies to 1.5 MHz when the length is set to 10m. This fact implies that the harmonic content up to this frequency will considerably increase.

However, there is no variation on the bode diagram when modifying the motor inductance, as shown in Figure 43. This is because this parameter is not involved on the resonant frequency that is presented on the system behavior in differential mode.
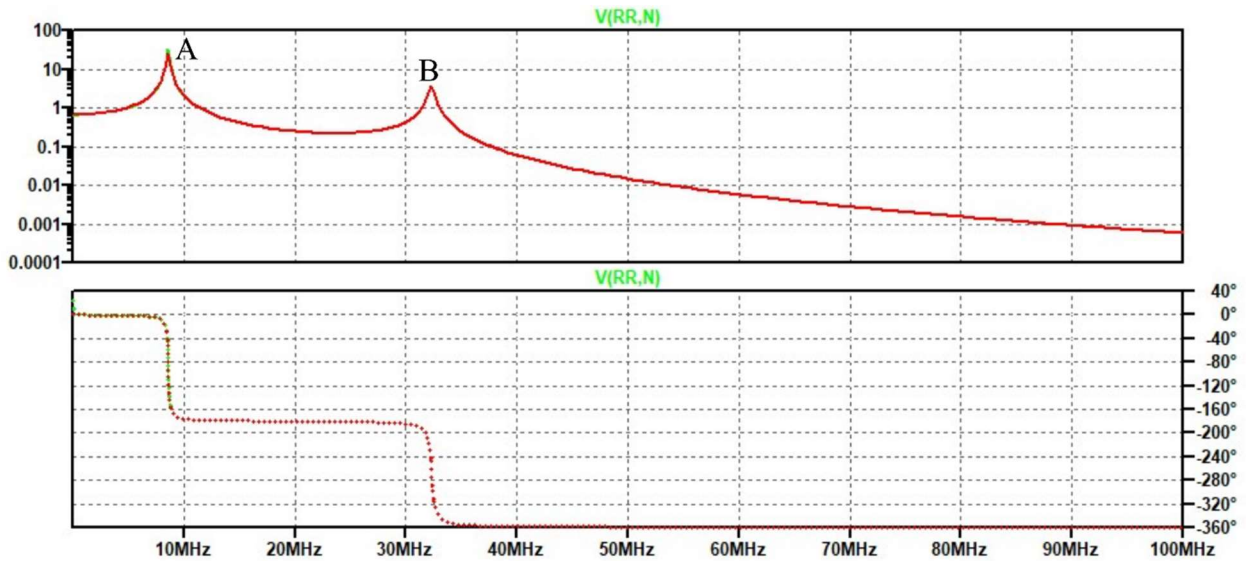
Figure 43 Bode diagram of the phase-to-phase voltage when varying the motor inductance. L_m = 40 μH, 400 μH and 4 mH.

The bode diagram of the phase-to-phase voltage when varying the heatsink capacitance is depicted in Figure 44. In this case, this parameter mainly modifies the high-frequency resonance (B), which is lower when the capacitance value increases. Since the value of this capacitance also increases the amplitude of the resonance, it is important to maintain this value as low as possible since the impact on the system may become problematic for large values.
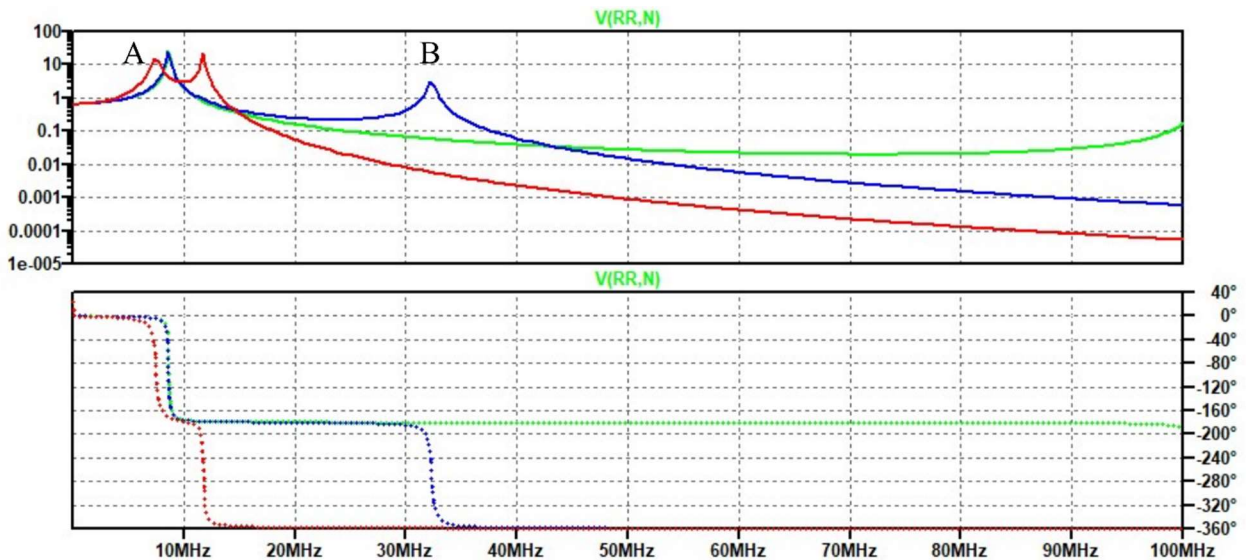
Figure 44 Bode diagram of the phase-to-phase voltage when varying the heatsink capacitance. C_{hs} = 0.1, 1 and 10 nF.

Finally, the impact of the phase-to-chassis capacitance (C_{cm2}) is given in Figure 45. It can be seen that this capacitance has a huge effect on A resonant frequency. To enhance the converter behavior, it is important to maintain this capacitance as low as possible, which must be analyzed during the motor design.
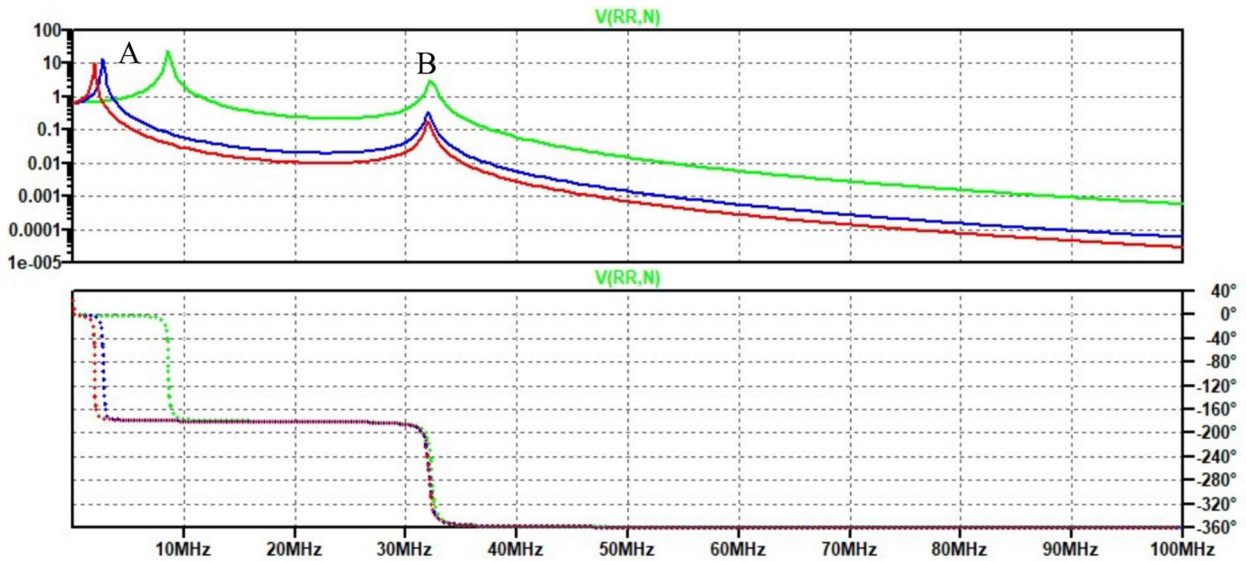
Figure 45 Bode diagram of the phase voltage when varying the phase-chassis capacitance. C_{m2}= 4nF (green), 20nF (blue) and 40nF (red).

4.1.3 Time domain modelling

Once the bode diagrams of the system give us the idea of the system behavior, a time domain model of a three-phase inverter for a motor drive application has been developed (see Figure 46). This model is useful since it enables the analysis of the resulting Fast Fourier Transforms (FFT).
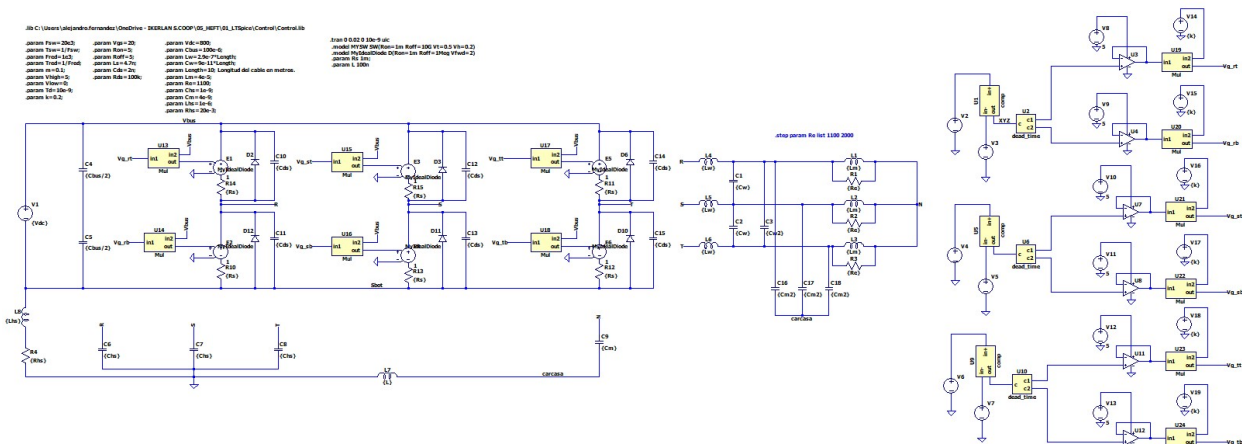
Figure 46 LTSpice model for time domain simulations.

The realization of this analysis helps to correlate the resonant frequencies given in previous subsections with the FFT of the real waveform. Furthermore, the importance of the rising and falling times of the power devices in the turn-on and off transitions is analyzed, since it is the main problem that arises from the implementation of SiC power devices.

In Figure 47 the phase-to-chassis temporal waveforms are presented when varying the rising and falling times. As detailed in the beginning of this section, faster switching transitions lead to higher-frequencies present in the voltage and current waveforms due to the resulting bode (see Figure 25). These voltage waveforms correspond to the rising times listed in Table 6, showing that large rising times lead to low cutting frequencies, and thus to smaller oscillations on the voltage waveforms. This can be seen in the FFT presented in Figure 48 for each waveform, where the attenuation over voltage waveforms with large rising times starts at lower frequencies.

Table 6 Rising times and corresponding cutting frequencies.

Converter Parameters	$T_r\,[ns]$	$f\,[MHz]$
Red	30	10.610
Blue	265	1.201
Green	1000	0.318
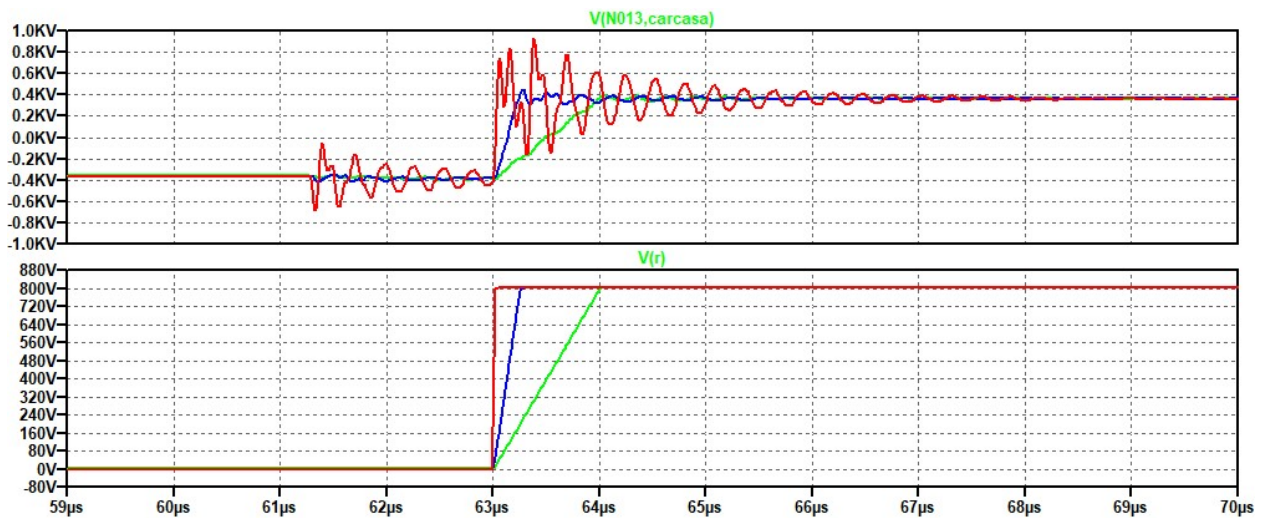
Figure 47 Phase-chassis voltage (top) and drain-source voltage in power devices (bottom).
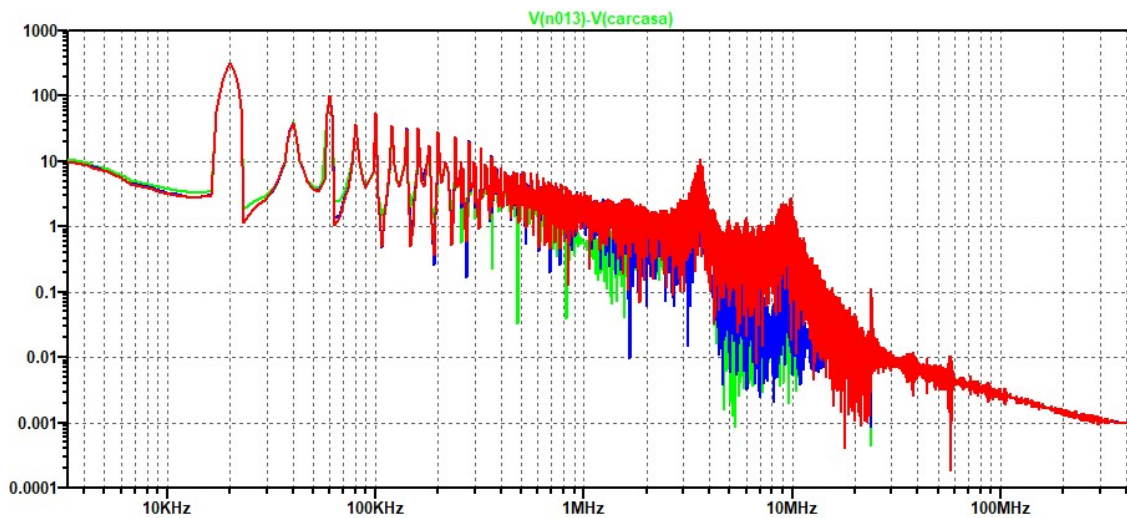
Figure 48 FFT of the phase-chassis voltage.

Finally, the frequencies found in the bode diagrams previously presented are matched with the FFT voltage waveform when considering a rising time of 100 ns. In this figure, the CM and DM resonant frequencies, which are at 3.5, 9, 26 and 33 MHz are present, which reflects that the simulation model presented is useful for the determination of the most important frequencies of the system when considering an electrical model close to the reality.
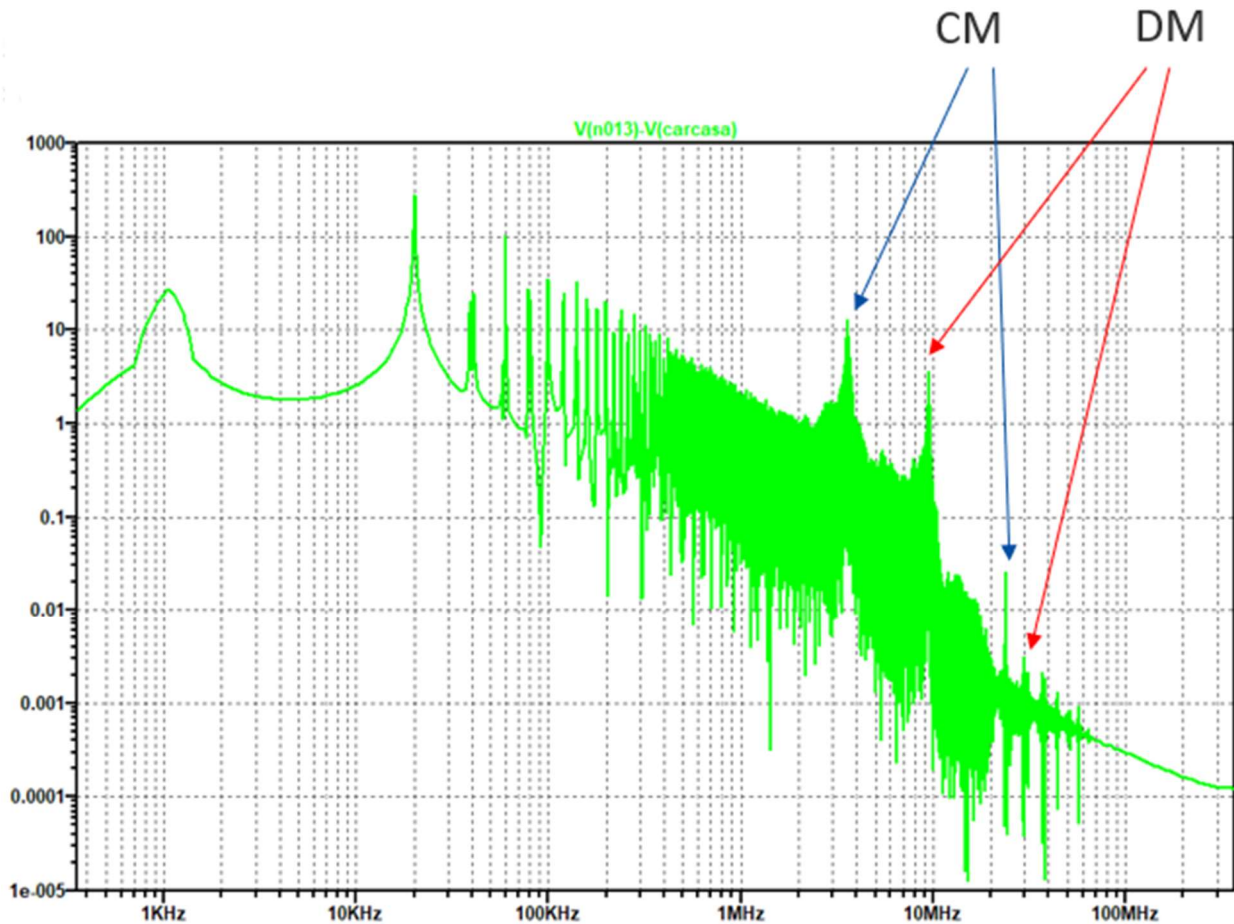
Figure 49 FFT of the phase-to-chassis waveform for t_r=100ns.

4.1.4 Conclusions

The conclusions obtained after this dv/dt model developed in this section are:

- The dv/dt are affected by common mode and differential mode perturbations.
- The main contribution is due to differential model perturbations (higher gain), however the common model paths and their resonances cannot be neglected.
- In the time domain, the model developed makes possible the change the rise & fall time of the inverter's output waveforms, to evaluate the whole harmonic content of the variables.
- The influence of the main variables (wiring length and parasitic components) is evaluated in the AC domain, to see the frequency range affected by each parameter.
- The influence of the main variables (wiring length and parasitic components) can be also evaluated in the time domain model, to see the frequency range affected by each parameter.

4.2 High switching frequency influence on EMC to comply with automotive standards.

The new 800V standard (doubles the 400V typical HV rating for EVs) is possible with the use of new SiC modules with high-switching speeds.

As has been commented before in this deliverable, the use of high dv/dt switches represents an increment on the dv/dt seen by the motor terminals. High-voltage EMC Standards/regulations for the EV powertrain modules are not focused on the dv/dt seen by the motor because the standards are focus on, for example:

- RF Conducted & radiated emission and immunity.
- Electric and magnetic field generation.
- HV transient emissions and immunity.
- Human exposition to magnetic field.
- …

Despite that, it must be considered by the designer that although it is not directly related, the resonance frequencies that appear on the motor voltage correspond also with frequencies seen previously in the model and simulation sections.

Three reference standards have been considered in the deliverable as the most connected with the dv/dt model depicted in this deliverable [16]:

Standard	Title
ISO/TS 7637-4	Road Vehicles — Electrical disturbance by conduction and coupling — Part 4: Electrical transient conduction along shielded high voltage supply lines only
CISPR 25	Limits and methods of measurement of radio disturbance characteristics for the protection of receivers used on board vehicles
CISPR 36	Electric and hybrid electric road vehicles – Radio disturbance characteristics – Limits and methods of measurement for the protection of off-board receivers below 30 MHz

4.2.1 ISO/TS 7637-4 [17]:

This standard exposes the test methods and procedures to ensure the compatibility to conducted electrical transients along shielded high voltage supply lines of equipment installed on electrical vehicles with voltages higher than 60Vdc and lower than 1500Vdc and a power supply isolated from the vehicle body. It describes bench tests for both, injection and measurement of transients. It is applicable to all types of electrical independent driven, road vehicles (e.g. battery electrical vehicle (BEV) or hybrid electrical vehicle (HEV), plugin hybrid electric vehicle (PHEV)).
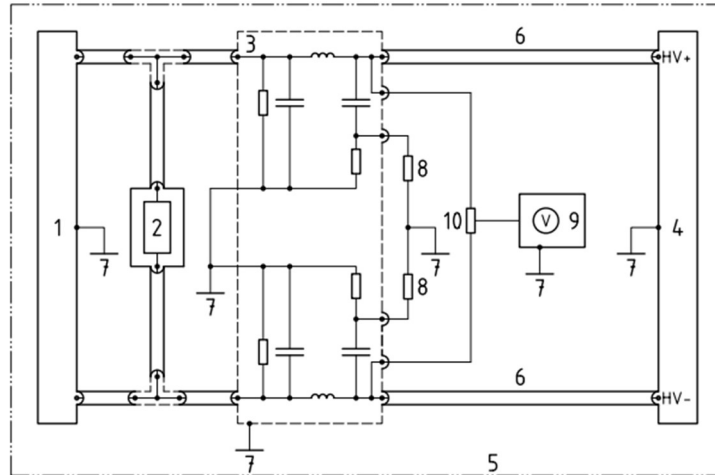
*Figure 50. ISO/TS 7637-4: Transient **emission** test set-up to measure voltage ripple along high voltage supply lines. 1-high voltage power supply (optional: shielded and / or filtered). 2-load for high voltage battery. 3-high voltage artificial network (HV-AN). 4-Device under test. 5-ground plane. 6-high voltage supply line. 7-ground connection. 8-50 Ω termination. 9-oscilloscope or waveform acquisition equipment. 10-high voltage differential probe.*

Therefore, this standard specifies, with the diagram presented on Figure 50 how the disturbances emitted are measured between HV+ and HV-. During this test, the voltage measurement seen on the oscilloscope/acquisition equipment (element 9 in Figure 50) is affected by frequency harmonics around the resonances presented previously on Section 4.1.2 defined by the parasitic components.

4.2.2   CISPR 25 [18]:

This standard defines the limits and procedures for measurement for radio disturbances in the frequency range of 150kHz to 1GHz, and applies to any electrical or electronic component to be used in vehicles.

The testing and limits are split into two separate types of emissions: conducted and radiated. Conducted emissions are coupled onto supply lines directly through conductors (such as traces or wires), and radiated emissions are emitted as EM waves and can be picked up by intentional and unintentional antennas on other systems.

Considering the frequency range of the disturbances generated by the converter, the limits to be considered are presented in the CISPR 25 Standard.

4.2.2.1 Conducted emissions

SERVICE OR BRAND	FREQUENCY (MHz)	LEVELS IN dV (µV)									
		CLASS 1		CLASS 2		CLASS 3		CLASS 4		Class 5	
		PEAK	QUASI PEAK	PEAK	QUASI PEAK	PEAK	QUASI PEAK	PEAK	QUASI PEAK	PEAK	QUASI PEAK
Broadcast											
LW	0.15 to 0.30	110	97	100	87	90	77	80	67	70	57
MW	0.53 to 1.8	86	73	78	65	70	57	62	49	54	41
SW	5.9 to 6.2	77	64	71	58	65	52	59	46	53	40
FM	76 to 108	62	49	56	43	50	37	44	31	38	25
TV Band 1	41 to 88	58		52		46		40		34	
TV Band 3	174 to 230	Conducted emission. Voltage method is not applicable.									
DAB 3	171 to 245										
TV Band 4 and 5	468 to 944										
DTTV	470 to 770										
DAB L Band	1447 to 1494										
SDARS	2320 to 2345										
Mobile services											
CB	26 to 28	68	55	62	49	56	43	50	37	44	31
VHF	30 to 54	68	56	62	49	56	43	50	37	44	31
VHF	68 to 87	62	49	56	43	50	37	44	31	38	25

Figure 51.CISPR 25. Peak and quasi-peak limits [18].

SERVICE OR BAND	FREQUENCY (MHz)	LEVELS IN dV (µV)				
		CLASS 1	CLASS 2	CLASS 3	CLASS 4	CLASS 5
		AVERAGE	AVERAGE	AVERAGE	AVERAGE	AVERAGE
Broadcast						
LW	0.15 to 0.30	90	80	70	60	50
MW	0.53 to 1.8	66	58	50	42	34
SW	5.9 to 6.2	57	51	45	39	33
FM	76 to 108	42	36	30	24	18
TV Band 1	41 to 88	48	42	36	30	24
TV Band 3	174 to 230	Conducted emission. Voltage method is not applicable.				
DAB 3	171 to 245					
TV Band 4 and 5	468 to 944					
DTTV	470 to 770					
DAB L Band	1447 to 1494					
SDARS	2320 to 2345					
Mobile services						
CB	26 to 28	48	42	36	30	24
VHF	30 to 54	48	42	36	30	24
VHF	68 to 87	42	36	30	24	18

Figure 52. CISPR 25. Average limits [18].

4.2.2.2 Radiated emissions

SERVICE OR BAND	FREQUENCY (MHz)	CLASS 1		CLASS 2		CLASS 3		CLASS 4		CLASS 5	
		PEAK	QUASI PEAK	PEAK	QUASI PEAK	PEAK	QUASI PEAK	PEAK	QUASI PEAK	PEAK	QUASI PEAK
Broadcast											
LW	0.15 to 0.30	86	73	76	63	66	53	56	43	46	33
MW	0.53 to 1.8	72	59	64	51	56	43	48	35	40	27
SW	5.9 to 6.2	64	51	58	45	52	39	46	33	40	27
FM	76 to 108	62	49	56	43	50	37	44	31	38	25
TV Band 1	41 to 88	52		46		40		34		28	
TV Band 3	174 to 230	56		50		44		38		32	
DAB 3	171 to 245	50		44		38		32		26	
TV Band 4 and 5	468 to 944	65		59		53		47		41	
DTTV	470 to 770	69		63		57		51		45	
DAB L Band	1447 to 1494	52		46		40		34		28	
SDARS	2320 to 2345	58		52		46		40		34	
Mobile services											
CB	26 to 28	64	51	58	45	52	39	46	33	40	27
VHF	30 to 54	64	51	58	45	52	39	46	33	40	27
VHF	68 to 87	59	46	53	40	47	34	41	28	35	22
VHF	142 to 175	59	46	53	40	47	34	41	28	35	22
Analog UHF	380 to 512	62	49	56	43	50	37	44	31	38	25
RKE	300 to 330	56		50		44		38		32	
RKE	420 to 450	56		50		44		38		32	
Analog UHF	820 to 960	68	55	62	49	56	43	50	37	44	31
GSM 800	860 to 895	68		62		56		50		44	
EGSM and GSM 900	925 to 960	68		62		56		50		44	
GPS L1 civil	1567 to 1583										
GSM 1800 (PCN)	1803 to 1882	68		62		56		50		44	
GSM 1900	1850 to 1990	68		62		56		50		44	
3G and IMT 2000	1900 to 1992	68		62		56		50		44	
3G and IMT 2000	2010 to 2025	68		62		56		50		44	
3G and IMT 2000	2108 to 2172	68		62		56		50		44	
Bluetooth and 802.11	2400 to 2500	68		62		56		50		44	

Figure 53. CISPR 25. Peak and Quasi-Peak Limits for Radiated Emissions Testing [18]

SERVICE OR BAND	FREQUENCY (MHz)	LEVELS IN dV (µV per m)				
		CLASS 1	CLASS 2	CLASS 3	CLASS 4	CLASS 5
		AVERAGE	AVERAGE	AVERAGE	AVERAGE	AVERAGE
Broadcast						
LW	0.15 to 0.30	66	56	46	36	26
MW	0.53 to 1.8	52	44	36	28	20
SW	5.9 to 6.2	44	38	32	26	20
FM	76 to 108	42	36	30	24	18
TV Band 1	41 to 88	42	36	30	24	18
TV Band 3	174 to 230	46	40	34	28	22
DAB 3	171 to 245	40	34	28	22	16
TV Band 4 and 5	468 to 944	55	49	43	37	31
DTTV	470 to 770	59	53	47	41	35
DAB L Band	1447 to 1494	42	36	30	24	18
SDARS	2320 to 2345	48	42	36	30	24
Mobile services						
CB	26 to 28	44	38	32	26	20
VHF	30 to 54	44	38	32	26	20
VHF	68 to 87	39	33	27	21	15
VHF	142 to 175	39	33	27	21	15
Analog UHF	380 to 512	42	36	30	24	18
RKE	300 to 330	42	36	30	24	18
RKE	420 to 450	42	36	30	24	18
Analog UHF	820 to 960	48	42	36	30	24
GSM 800	860 to 895	48	42	36	30	24
EGSM and GSM 900	925 to 960	48	42	36	30	24
GPS L1 civil	1567 to 1583	34	28	22	16	10
GSM 1800 (PCN)	1803 to 1882	48	42	36	30	24
GSM 1900	1850 to 1990	48	42	36	30	24
3G and IMT 2000	1900 to 1992	48	42	36	30	24
3G and IMT 2000	2010 to 2025	48	42	36	30	24
3G and IMT 2000	2108 to 2172	48	42	36	30	24
Bluetooth and 802.11	2400 to 2500	48	42	36	30	24

Figure 54. CISPR 25. Average Limits for Radiated Emissions Testing [18].

The test procedures and limits are different for both types of emissions: conducted and radiated. In both cases the device under test is placed in an isolated room or chamber and set up in a well-defined, reproducible-electrical setup.

All other possible emitters are removed from the chamber and the system is turned on. The system is powered through an artificial network (LISN) and loaded through its normal operation. A spectrum analyzer is used to measure the emissions across different frequencies (through the LISN or from an antenna) and compares the emissions against the CISPR 25 limits.

4.2.3   CISPR 36 [19]:

This standard defines the limits for 3 m measurement distance and methods of measurement that are designed to provide protection for off-board receivers (at 10 m distance) in the frequency range of 150 kHz to 30 MHz when used in the residential environment.

This standard applies to the emission of electromagnetic energy which might cause interference to radio reception, and which is emitted from electric and hybrid-electric vehicles propelled by an internal traction battery when operated on the road.

This document applies to vehicles that have a traction battery voltage between 100V and 1000V.

The standard presents the limits of the quasi-peak detector magnetic field strength when the converter is driving the motor (in "Propulsion" mode).

The test is an outdoor test with a loop antenna to measure the magnetic field, placed at 3 m distance from the car, following Figure 55.
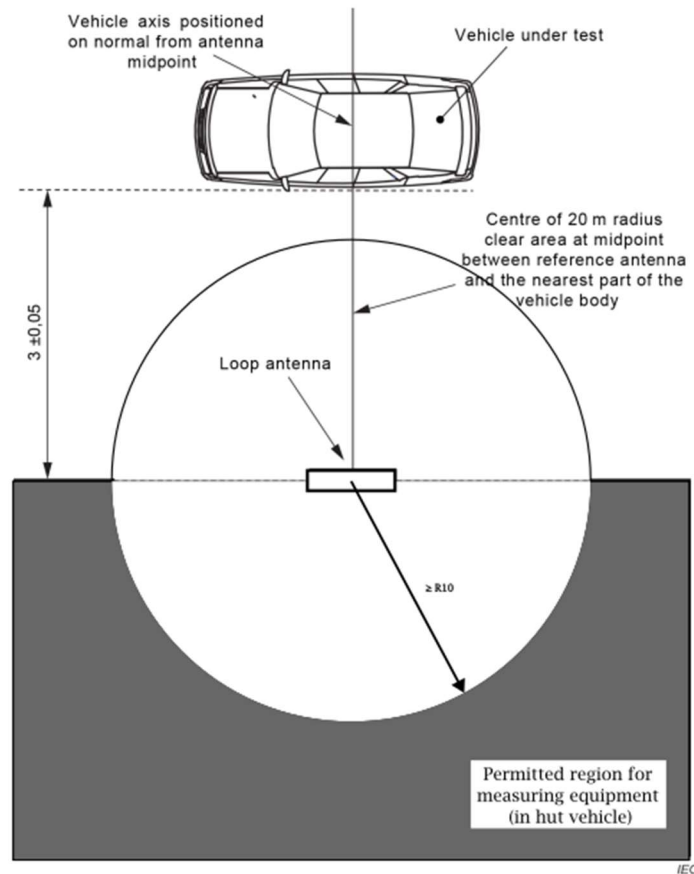
Figure 55. CISPR36: Measuring outdoor test site (OTS) for vehicles [19].

The limits of the emission are presented in Figure 56. It must be highlighted that the frequency range of the limits are between 100kHz and 30MHz. This range corresponds with the range influenced by the converter and motor parasitic explained and simulated in Section 4.1.2. Due to that, having a representative model of the EV power train, with a good definition of the resonance frequencies is mandatory to anticipate the EMC magnetic field frequencies.
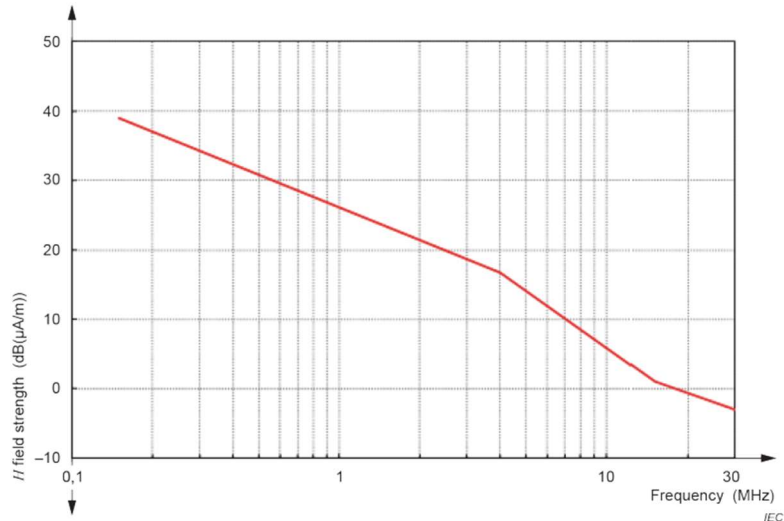
Figure 56. CISPR 36: Limit of magnetic field disturbance (quasi-peak detector) at 3 m antenna distance [19].

4.2.4   Conclusions

This section explains the connection between voltage frequency harmonics obtained in simulation models and the frequency ranges and amplitudes defined in the standards. This is a crucial step in understanding the potential electromagnetic interference (EMI) issues and ensuring compliance with EMC standards.

By correlating the voltage frequency harmonics from the simulation model with the frequency ranges and amplitudes outlined in EMC standards, it is possible to assess the potential impact of dv/dt on electromagnetic emissions and susceptibility. This understanding allows the anticipation of any EMI problems and take appropriate measures to mitigate them, such as implementing filtering techniques or optimizing the motor drive system design.

4.3 Current versus voltage trade-offs to improve EV range

A simulation in Matlab/Simulink has been developed to compare 400V and 800V architecture characteristics: charging time and range (see Figure 57). Starting from a defined driving cycle and considering vehicle dynamics, electric motor power is calculated. Then inverter and auxiliary power are considered. Based on these power needs and considering the battery module characteristic, battery SOC is calculated.
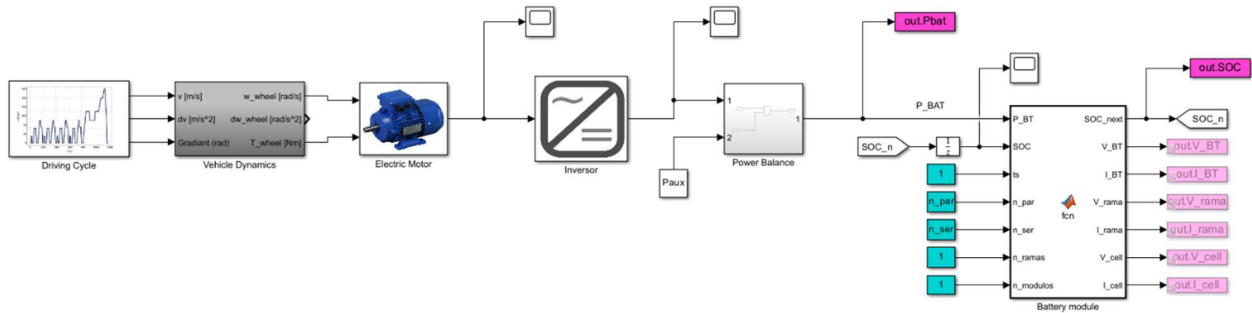
Figure 57. Matlab/Simulink model for obtain range and charging time comparing different EV architectures 400V-800V.

It is important to notice that battery system energy is based on Vdc voltage and battery capacity. If Vdc is doubled, from 400V to 800V and battery capacity is maintained (installing more batteries), stored energy and thus, EV range is doubled. However, another option can be to use 800V architecture but maintain battery system energy (connecting more cells in series but less in parallel), reducing battery system capacity. In this case, no changes in range and charging time from 400V to 800V would be achieved. For this study, it has been considered that not only DC bus voltage, but also battery capacity is increased with 800V technology, as it is a trend shown during the state of the art.

Three different cases have been analyzed. Firstly, 400V project baseline Fiat 500e has been considered with a battery system of 37.3kWh. Secondly 800V Segment A+B EV has been considered, assuming a battery system of 72.6kWh. Finally, 800V Segment C+D+E EV with a battery system of 93.4kWh has been proposed. Moreover, two different driving cycles: UDDS and WTLP and three different charger powers: 50kW, 150kW and 250kW have been considered for this study.

Figure 58 shows UDDS driving cycle speed time profile considered in this study.
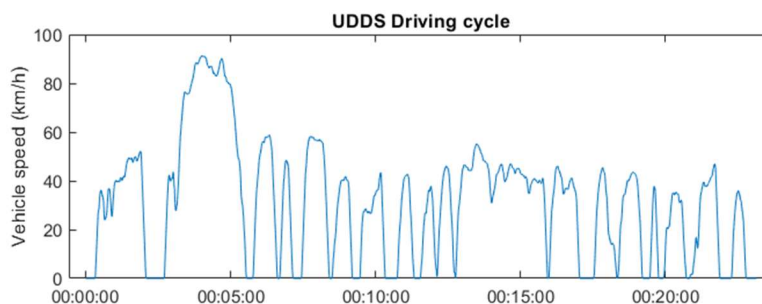
Figure 58. UDDS driving cycle speed time profile.

Figure 59 shows the range and the charging time of the three cases considering the three charging options. As it is known, more range is achieved with 800V architecture VE (as more battery capacity is integrated) and charging time decreases if higher power charger is used.

UDDS Driving cycle

	Range [km]	Charging time (50 kW)	Charging time (150 kW)	Charging time (250 kW)
400V Baseline (Fiat 500e)	194.25	"00:37:46"	"00:13:23"	"00:08:27"
800V Segment A+B	378.84	"01:14:16"	"00:25:35"	"00:15:50"
800V Segment C+D+E	460.79	"01:32:30"	"00:31:41"	"00:19:30"

Figure 59. Range and charging time considering different powers with UDDS driving cycle.

Regarding the discharge, from 90% up to 5% discharged has been simulated considering UDDC driving profile for three different cases. see Figure 60. 400V baseline EV needs more than six hours, 800V segment A+B case 12 hours and 800V segment C+D+E almost fifteen hours.
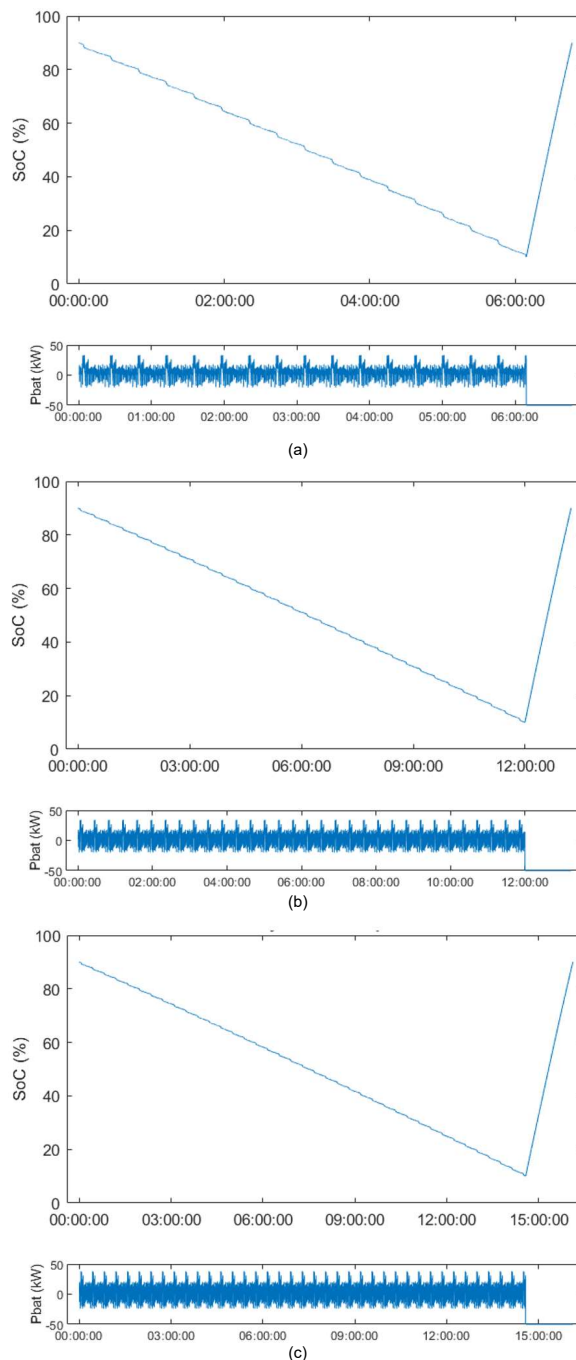
Figure 60. SOC and battery power for baseline at 400V (a), 800V Segment A+B (b) and 800V Segment C+D+E (c) for UDDS driving cycle.

On the other hand, Figure 61 shows WLTP driving cycle speed time profile considered in this study.
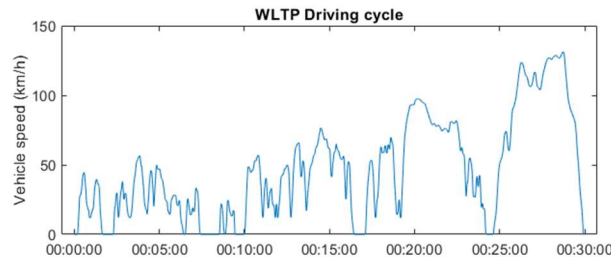
Figure 61. WLTP driving cycle speed time profile.

Figure 62 shows the range and the charging time of the three cases considering the three charging options. As can be seen, the same charging time as in the previous case has been achieved, as charges do not depend on the profile (as no regenerative charging has been considered in this study). As it is known, more range is achieved with 800V architecture EV (as more battery capacity is integrated) and charging time decreases if higher power charger is used.

WLTP Driving cycle				
	Range [km]	Charging time (50 kW)	Charging time (150 kW)	Charging time (250 kW)
400V Baseline (Fiat 500e)	133.66	"00:37:46"	"00:13:23"	"00:08:27"
800V Segment A+B	259.5	"01:14:16"	"00:25:35"	"00:15:50"
800V Segment C+D+E	320.13	"01:32:30"	"00:31:41"	"00:19:30"
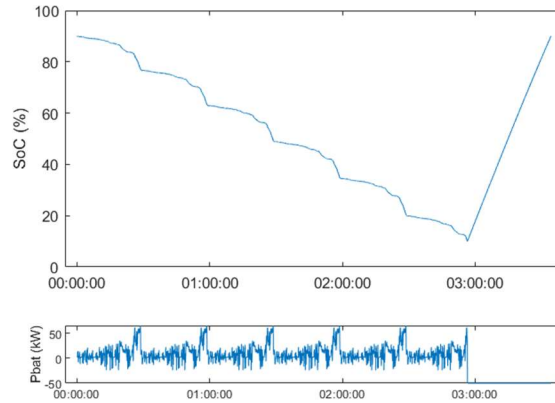
Figure 62. Range and charging time considering different powers with WLTP driving cycle.
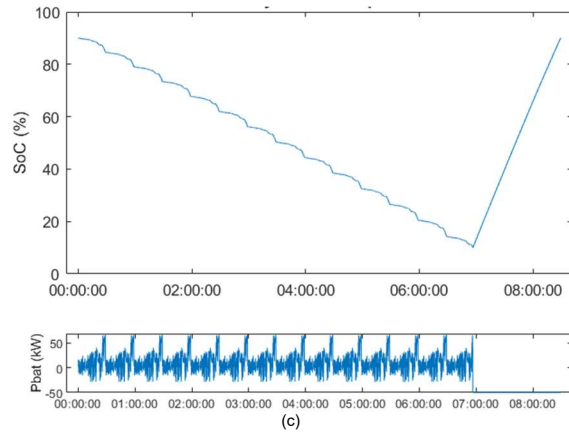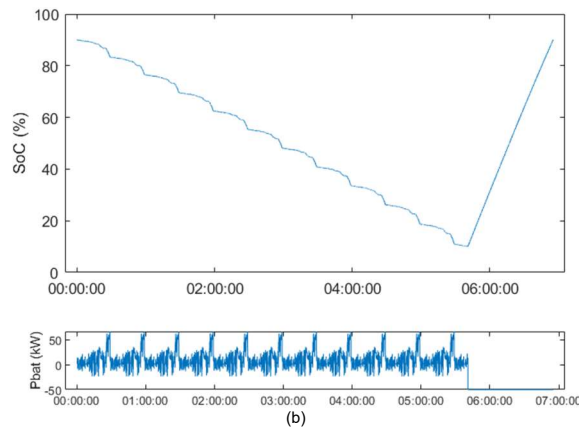
Figure 63. SOC and battery power for baseline at 400V (a), 800V Segment A+B (b) and 800V Segment C+D+E (c) for WLTP driving cycle.

From this study, it can be concluded that, increasing voltage, as it is related with increase battery capacity, extends EV range. Moreover, 800V fast chargers (250kW) allow a considerably decrease in charging times.

4.4 Advanced shared cooling to reduce losses and improve EV range

Efficiency improvement means that wasted thermal energy is reused at maximum, sharing heating and cooling among different elements of the systems (such as passenger cabin, inverter, motors and battery pack) depending on the operation conditions. That means the coolant loops that go through the elements can be linked or separated to combine the thermal energy sources and sinks depending on operation conditions of each element to take profit of the maximum available waste energy in each situation. The efficiency of the overall thermal management system of EV implies many operation modes with different boundary conditions; many combinations for sharing heating and cooling; and many options for transferring heat from/to different elements of the systems [20].

The scope of this study is limited to shared cooling in the powertrain (motor, inverter and also considering the battery pack) and the re-use of their waste-heat to heat the passenger's cabin to reduce the losses and improve EV range. The sharing of heating at the passenger's cabin, as element that also requires thermal management, is out of the scope of this analysis, even if the heating of the cabin is an important element in the overall EV thermal management system as it is described later.

After this introduction, an EV thermal management system state of the art has been carried out to obtain the components technical requirements and the operating conditions to be used later in the simulation model. Finally, two different case studies simulation results are shown, and conclusions are highlighted.

4.4.1 STATE OF ART OF EV THERMAL MANAGEMENT SYSTEM

Even if an air-cooled system was used for long time in Renault Zoe, most EV manufactures use liquid cooled system for the thermal management. Both systems are getting old fashioned respect to the efficiency that is being achieved in the most innovative EV thermal management systems.

Concerning liquid cooling, modern EV thermal management system has two independent circuits: a coolant circuit that runs through the powertrain elements (engine, inverters, converters and battery pack), and a coolant circuit of a vapour compression system used to cool the passenger compartment and the battery pack. In this refrigerant circuit there are two evaporators: one is for cooling the cabin and the second is for cooling the battery pack. The last one, also called chiller, thermally connects the coolant circuit and the refrigerant circuit.

The modes of operation are closely related to the ambient conditions:

- At mild ambient temperatures (also called "cool condition"), the coolant circulates in one unique circuit through all the powertrain elements (motor, inverters, and battery pack). The waste heat of all of them is dissipated to the ambient by a radiator-fan system located in the coolant loop. The battery pack keeps its optimal temperature being heated by the motor and inverters waste heat; or heated by an auxiliary electrical resistance in case it is necessary.
- At hot ambient temperatures ("hot condition"), the coolant circulates through two separate loops. One loop cools the motor, the inverters and the on-board charging system, and their waste heat is dissipated to the ambient by the radiator-fan system located in the coolant loop. The second loop cools the battery pack by the above-mentioned chiller that thermally links the coolant loop with the refrigerant circuit of the air conditioning system.
- At cold conditions (winter mode), there is also a closed coolant loop that goes through the battery pack (the rest of elements do not require heating) and that is heated by the auxiliary electrical resistance (see Figure 64) .
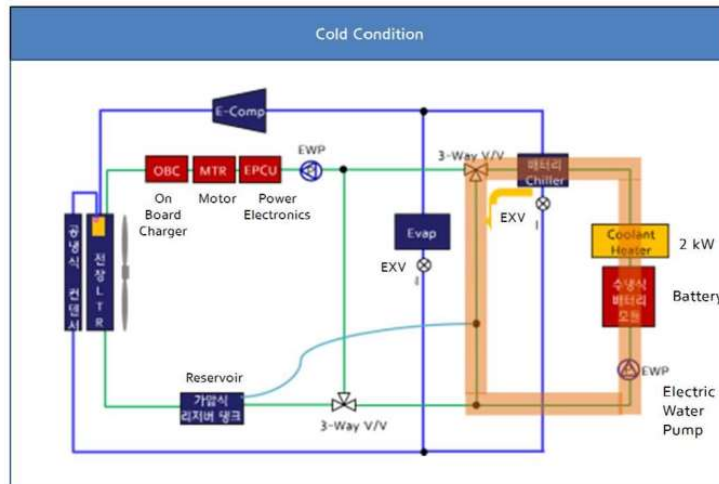
Figure 64. Winter mode operation (cold condition)

Main handicap of the EV thermal management and heat pump

While the waste heat available for heating the cabin is high in a combustion engine vehicle, the waste heat available in an EV is much lower because the efficiency of the powertrain elements is much higher (approximately around of 95%) than a combustion engine (approximately around of 30%). In an EV the rest of the required heating energy is fed by the battery pack and, therefore, the thermal management has a direct impact in the driving range of the EV.

Most of the EVs are provided by an air conditioning system to cool down the cabin and by electrical heaters to heat it (PTC heaters, positive temperature coefficient heating element) as the available waste heat is not enough to meet the heating needs of the cabin. The Norwegian Automobile Federation (NAF) recently compared 20 EVs in cold and warm weather conditions to identify models with the most consistent driving range and charging performance. The test monitored each vehicle's performance deviation in cold weather conditions compared to the manufacturer's cited figures. The Kona Electric took first place, covering 405 km in bitter cold, compared to the 449 km cited in WLTP combined cycle test conditions (23°C). In severe cold weather conditions, the electric Kona offered 91 percent of its WLTP combined-cycle range, deviating only 9 percent from its all-electric driving range [21]. As can be seen in Figure 65, Hyundai Kona and Kia Niro EV, that have a heat pump system for heating, consume much lower battery energy than other EV at cold weather conditions.
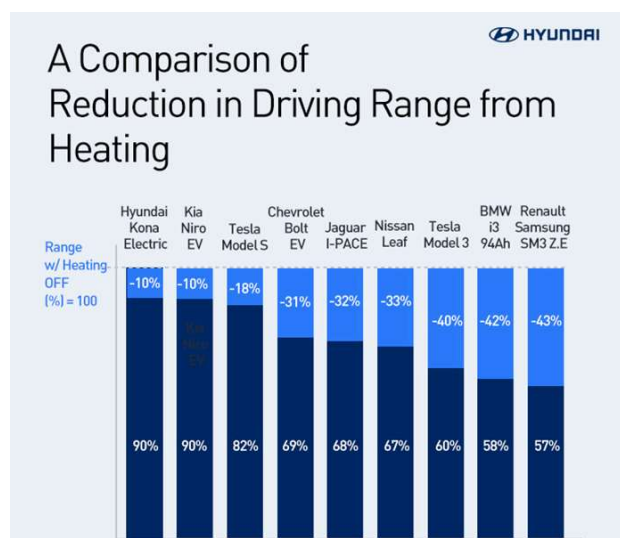
Figure 65. EV driving range reduction at cold weather [20].

One solution to this problem that most of EV manufacturers are adopting, is to replace the heating resistance (and even the heating resistance of the battery) with a heat pump system. The Coefficient of Performance (COP), defined as the ratio of cooling capacity to consumed electricity power, of a heat pump is higher than one (COP>1) and higher than electric heaters efficiency (COP = 1 maximum). However, the minimum operation temperature of heat pumps is limited (around -4ºC, although there are being many improvements and some heat pumps could operate even at -20ºC) and its efficiency decreases if temperature goes down. Hence, the heating system needs an auxiliary heater too. In addition, heat pump is a more complex system than an electrical resistance.

Nevertheless, manufacturers of several EVs currently available in the market (for example, BMW i3, Nissan Leaf, Jaguar I-Pace, Audi E-tron, Toyota Prius Prime, Volkswagen e-Golf, etc.) indicate that 20-30% driving range increase can be obtained using heat pump heating.

Advanced thermal management solutions

All EV manufacturers aim to maximise their driving range, and the first step for that is the liquid cooling system. Most of EV manufacturers have adopted liquid cooling (instead of air cooling) for battery thermal management. Liquid cooling makes possible the increase of battery pack capacity (and the driving range of the EV) without increasing the physical dimensions of the battery pack. Liquid cooling channels take less space than air cooling channels and allow increasing battery density by up to 35%.

The heat pump is also a technology that improves the EV's range. In addition to its higher efficiency (COP>1), the capture and reuse of waste heat from different elements (engine, inverter, on-board charging) to heat the passenger compartment reduces the temperature differential between which the heat pump works, to further improve the COP.

The heat management assisted by a heat pump enables significant improvements in energy efficiency and EV range. It is a complex but interesting technology. The heat pump is an innovation that is being gradually introduced throughout the EV sector. Introduced more than 10 years ago by Hyundai/Kia, it is currently being expanded to the entire EV market.

Hyundai Kona. Heat pump Technology.

The last Hyundai heat pump system collects waste heat from a wider variety of components to heat the cabin more efficiently. Previous models collected waste heat from motor, inverter and on-board charging; and the newest model, collects heat also from the battery pack. Figure 66 shows the scheme of the system in Heating mode operation and Figure 67 shows a 3D representation of the heat pump system.
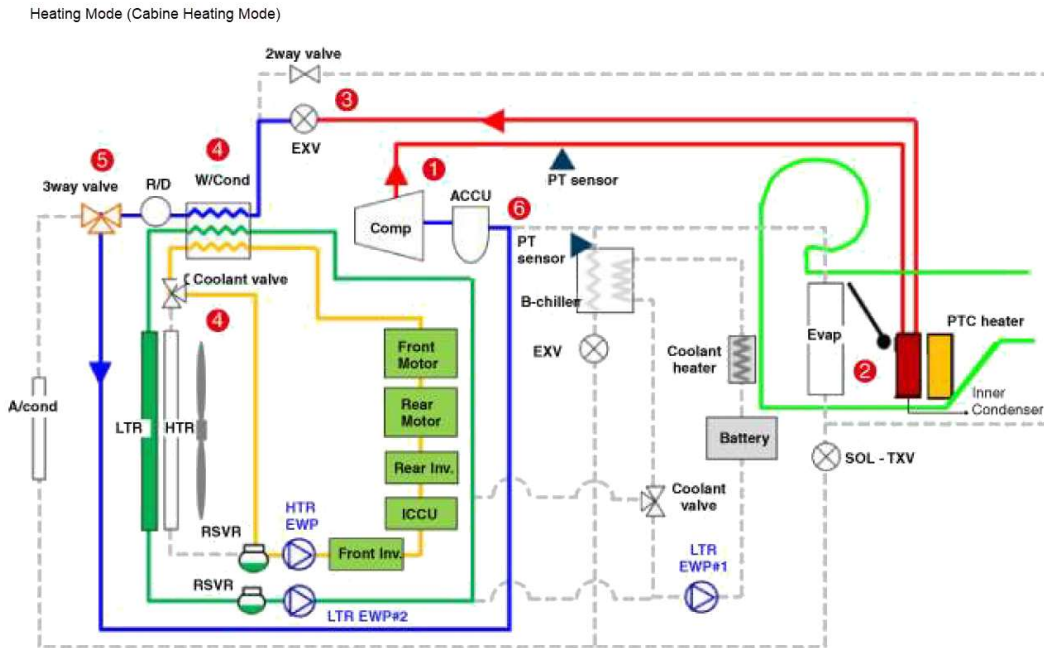
Figure 66. Hyundai heat pump. Cabin heating mode re-using motor and inverter heat [22].

Figure 66 shows the following components:

1. **Electric air conditioner compressor**: It is operated by an electric motor and converts the gas refrigerant of low-temperature/low-pressure into the gas of high-temperature/high-pressure and sends it to the indoor condenser.
2. **Evaporator**: It cools air by using the vaporizing effect of the refrigerant
3. **EXV**: In heating mode, it converts the liquid refrigerant of high-temperature/high-pressure into the low-temperature/low-pressure to facilitate phase change.
4. **R/D water-cooled condenser**: It expands the liquid refrigerant of low-temperature/low-pressure into the gaseous refrigerant of low-temperature/low-pressure.
5. **3-way valve**: It controls the refrigerant to move it to the accumulator.
6. **Accumulator**: It separates the gas/liquid of the refrigerant so that only the gaseous refrigerant can flow into the compressor.

Figure 67 Photo Hyundai Kona EN and 3D of its heat pump system [22].

Tesla Y

Model 3, Model S and Model X of Tesla had an electric resistance for cabin heating. The Model Y was the first Tesla model equipped with a heat pump. Shortly after, Tesla started to provide heat pump in all of their vehicles. Today, all of Tesla new EVs are equipped with heat pump as standard, which makes a huge difference in efficiency and driving range at cold weather conditions.

Like Kona, Tesla collects waste heat from many components (there are up to 12 heating operation modes). However, Tesla's system stands out for its compact mechanical design and a smaller number of components (see Figure 68) that enables to reduce ductwork, simplify the assembly, and increase reliability.

Figure 68. Tesla Y thermal management system [23].

Tesla's heat pump incorporates two main innovations that characterize it, such as the "supermanifold" and the "octovalve" (two four-way valves coupled), which help to increase the efficiency and the integration of the heat pump system (see Figure 69).

Figure 69. Tesla supermanifold; Octovalve and overall assembly set containing several elements: supermanifol, octovalve. liquid condenser, evaporator, expansion tank etc. [24]

The Tesla thermal management system has up to 16 different operation modes. Figure 70 shows two of the 12 heating operation modes.
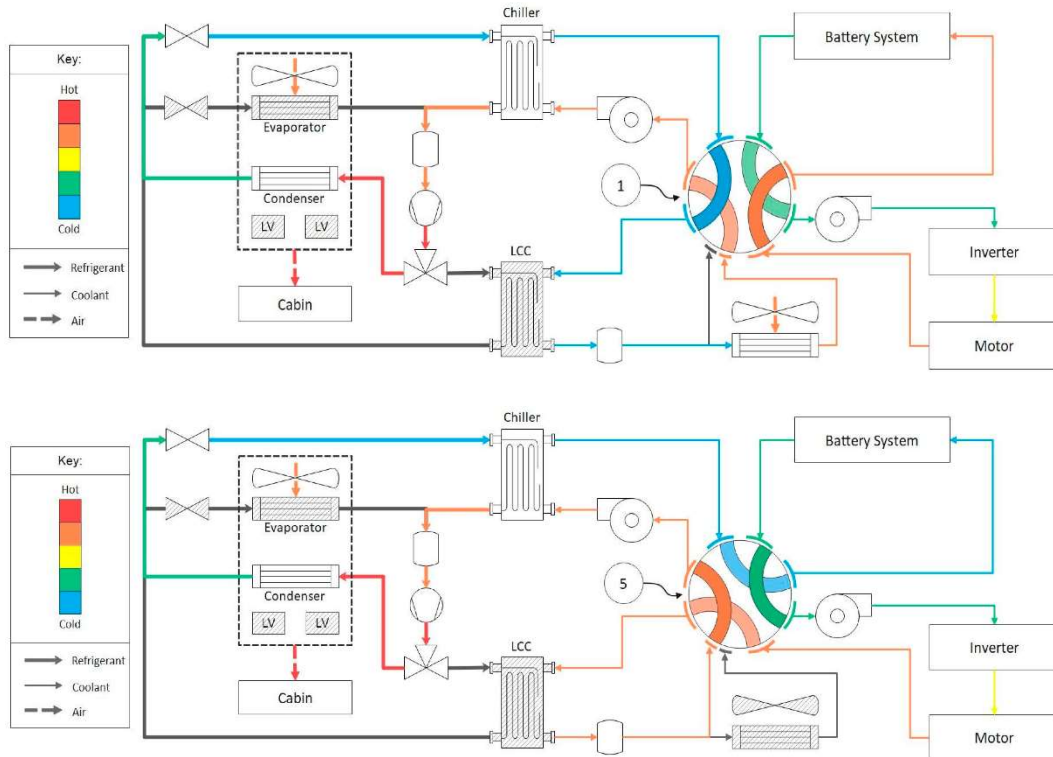
Figure 70. Two cabin heating modes schemes of Tesla [23].

Heating mode 1a and 1b: Thermal circuit diagram with relative fluid temperatures Mode 1 is the most efficient cabin heating mode operating in a COP >> 1 state (pure heat pump).

In this mode, energy is sourced by either the ambient air or the battery system/drive unit (considered to be 'free' from a cycle efficiency perspective) shown in the top figure. The heat pump compressor operates in an efficient mode to maximise vehicle range. Heat can be sourced from the ambient air if the atmospheric temperature is above −10 °C (coolant thermal energy is greater than the refrigerant and the chiller). However, the closer to −10 °C, the less effective the system becomes.

If the drivetrain is above ambient or the battery requires cooling, it is more effective to source energy from these components as shown in bottom figure. In both instances, the 3-way valve routing fluid to the LCC is closed, EXV to the cabin evaporator is fully closed, and the chiller and cabin condenser are active. On the coolant side, the octovalve is set to position 1 for ambient sourcing and 5 for drivetrain sourcing. In both cases, heat from the coolant side is transferred to the chiller refrigerant to be rejected at the cabin condenser.

Volkswagen. CO 2 Heat pump

Volkswagen's new ID.5 model (2022) has a CO2 heat pump. According to the manufacturer, the energy requirement to heat the cabin at outdoor temperatures below 0°C is up to 40% lower than in an EV without an energy-efficient heat pump.

The climate impact of the refrigerant R744 (CO2) used in the heat pump is lower than other fluorinated refrigerants (Global Warning Potential =1; Ozone Warning Potential = 0; very low warming risk).

The lower power demand reduces the energy consumption and thus increases battery capacity, which has a positive effect on the vehicle driving range.

State of the art conclusions

Heat pumps are a good option for EVs because, unlike a combustion engine vehicle, the propulsion components of an EV do not produce enough waste heat to properly heat the cabin during the winter, and it needs auxiliary heaters. Therefore, **obtaining heat from a heat pump gives an improvement in the driving range compared to EVs without a heat pump.**

The heat pump is not a specific component but a set of several components that, together, make the heat pump "system" capable of heating or cooling the cabin. The complexity increases because to make it more efficient **at low temperatures**, manufacturers **take advantage of the waste heat from other power components** (inverters, motors, DC/DC converters, and AC/DC converters) and from the high-voltage battery. This **drastically reduces the energy consumption of the battery and increases the driving range of** the vehicle**.**

4.4.2   TECHNICAL REQUIREMENTS & DEFINED OPERATION CONDITIONS

The temperature requirements and the expected efficiency of the main powertrain elements and battery pack used in this work are given in [27].

Table 7. Powertrain and battery pack thermal technical requirements.

Element	Operation temperature limits		Efficiency
Motor		<180ºC	98%
Inverter [25]		<85ºC	98.5%
Battery Pack	>15ºC	<35ºC	95%

The motor and inverter have only cooling needs to keep them below the maximum operation temperature. However, the battery pack needs to be cooled or heated to keep it above the minimum operation temperature and below the maximum operation temperature.

Inertia and thermal losses

In the developed simulation models (described in a later section), the definition of the thermal performance of the elements is given by an inertia (mass and Cp) and by the thermal losses or gains. The motor, the inverter and the battery pack are liquid cooled. Coolant goes through specific channels of the motor, and through cold plates joint to the battery pack and joint to the inverter.

For this analysis, mass and specific heat values shown in Table 8 have been considered. Heat transfer coefficients and heat transfer masses have not been considered as in a liquid cooling system they are of a lower order and require a level of detail of the components not available in this study.

Table 8. Considered thermal inertia, Cp.

Element	Composition	Cp (Jkg/K)
2 (Motor +gearbox)	Copper %23, Steel %63, housing %7, magnets %6	394-490
Inverter + Cold plate	Lumped mass	1000
Battery Pack (1)	Lumped mass	1000
(1) Energy density of 175 Wh/kg has been considered.		

Average mechanical power and thermal dissipation needs

The power of each element has been defined based on the estimated average electrical power of an EV model Hyunday Ioniq 5 at hard conditions (highway speed, heavy rain, 12-13ºC ambient). This estimated consumption is 30.9 kWh/100 km at a driving velocity of 120km/h [26] that provides an autonomy of 2.087 hours with a 77.4 kWh battery [27]. Therefore, the average electrical power is 37.08 kW.

Table 9. Thermal dissipation power.

Element	Average mechanical power (kW)	Efficiency	Average electrical power (kW)	Average thermal dissipation (kW)
Battery Pack	37	95%	37	1.9
Inverter	37	98.5%	35.1	0.5
Motor	37	98%	34.6	0.7

Therefore, the motor and the inverter must provide an average of 37 kW mechanical power. Considering each element efficiency, the average thermal dissipation requirement is calculated (see Table 9).

Cooling loops and additional considerations

The maximum operation temperatures of motor and inverter are much higher than ambient temperature. Hence, both elements could be in the same cooling loop.

The waste heat of motor and inverter can be used for passenger's cabin heating, for battery pack heating or otherwise, the exceeded waste heat will be dissipated to the exterior air.

Based on a radiator of 610 mm x 410 mm x 16 mm size (Ioniq models 2017-2020) and considering 2 mm tube thick, louvered fins and other specific geometry assumptions, the estimated heat transfer area in the air side of that radiator is 4.96 m^2 ; and at air speed of 3 m/sec, the estimated heat transfer coefficient in the air side is U= 62.9 W/m^{2}K.

The battery pack waste heat can be used for passenger's cabin heating, or it will be dissipated to the exterior air when the exterior air temperature is lower than 35ºC (< battery pack's maximum operation temperature). When the ambient temperature is higher than 35ºC, the battery pack will be cooled by an evaporator heat exchanger.

Usually, another additional evaporator of the vapor compression cycle (heat pump) is used to cool the passenger's cabin.

4.4.3 CASE STUDIES

In this study, two different cooling schemes have been analysed: one loop system with water-glycol (see Figure 71) and two loops system with oil and water-glycol (see Figure 74.). Although the second is more complex, it has the advantage of being able to cool the engines with dielectric oil and it is similar to that of the Hyundai Kona.

One Loop Systems Description.

Figure 71. shows the pre-design of an advanced cooling system for an electric vehicle that improves efficiency over a traditional system by carrying waste heat to the passenger cabin. This system has only a water-glycol circuit. It is a simpler system, but its increased performance is due to its ability to use waste heat from most components to heat the passenger compartment.
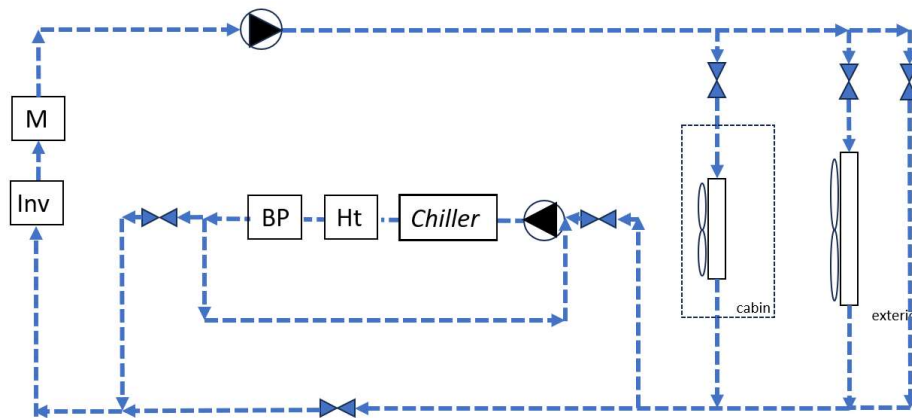
Figure 71. One loop system description

Figure 72. and Figure 73 show the main operating modes of the this system.

- Normal mode/Heating mode/By-pass mode: When the outside temperature is below 25 or 30 °C, the normal mode brings the heat from the engine, electronics and batteries to the outside radiator and is discharged to the outside air. In heating mode, the cab radiator is used. The by-pass of the external radiator makes possible to accelerate the heating of the battery by using the heat from the engines and power electronics.
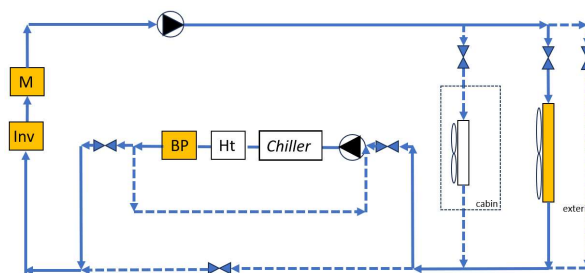
Figure 72. One loop system description: normal mode (coloured = active).

- Winter mode/hot mode: The battery does not dissipate heat to the outside, and the fluid recirculates over the battery itself. In winter mode, it activates the backup heater if necessary. In hot mode, on the other hand, the chiller is activated. The motors and electronics dissipate their waste heat to the outside air through the external radiator.
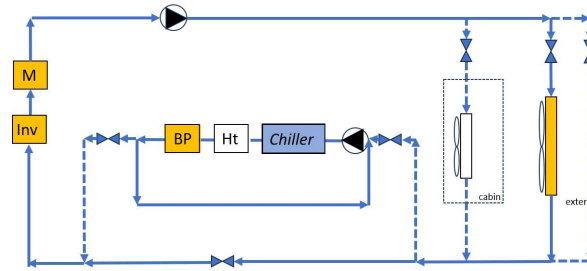
Figure 73. One loop system description: Hot mode (coloured = active)

Two Loops Systems Description.

Figure 74. shows the design of an advanced cooling system for an electric vehicle that improves efficiency over a traditional system. This is the thermal architecture that will be used in HEFT project. It is a complex system that aims to take advantage of the benefits of water as a heat transfer fluid and dielectric oil to cool critical electrical components. It is also capable of transporting all the waste heat to the passenger cabin.
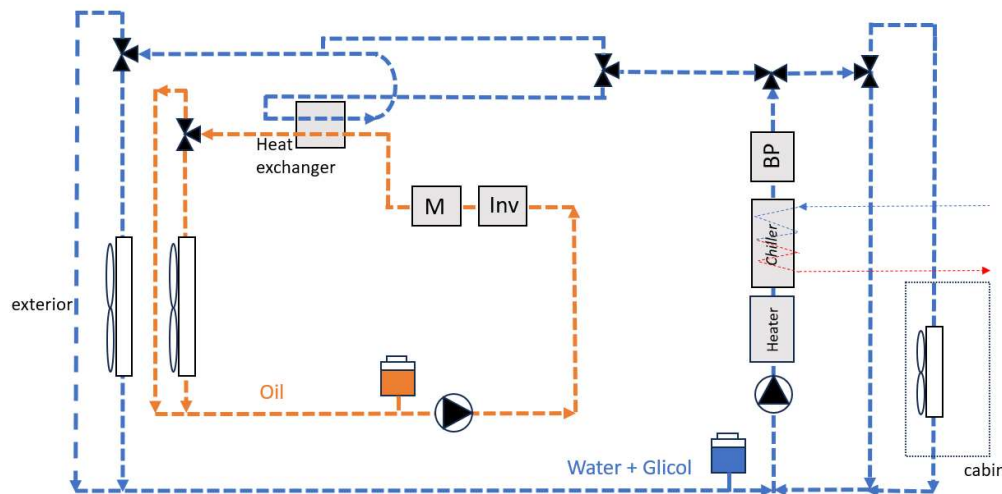
Figure 74.Two Loops Systems Description.

The system consists of two closed liquid cooling loops, one with oil and one with glycol water. The oil circuit collects heat from the engines and power electronics and dissipates it to the outside air through a high-temperature radiator. The water circuit cools and heats the batteries. It includes an auxiliary electrical resistance, to maintain the temperature of the batteries when the vehicle is stationary and connected to an external power supply. It also includes a cooler to cool the batteries when the outside temperature is higher than the battery temperature. The circuit allows the heat generated in the batteries to be dissipated to the outside air. It also allows it to be carried to the passenger cabin if heating is required. In the same way, thanks to the heat exchanger connecting the two circuits, the heat from the oil circuit can be recovered and dissipated. The heat exchanger also allows both radiators to be used during fast charging. Several 3-way valves allow the necessary circuits to be configured to supply fluid and heat to the desired component.

From Figure 76 to Figure 80, main operating modes of the thermal system are described. In an EV, the modes are switched dynamically as the temperatures of the various components, or the external conditions, change.

- Normal mode (see Figure 75): When the outside temperature is below 25 or 30 °C, the heat dissipated from the motors, power electronics and batteries, is discharged to the outside, via the two radiators. The heat exchanger, that links two coolant circuits, is not used.
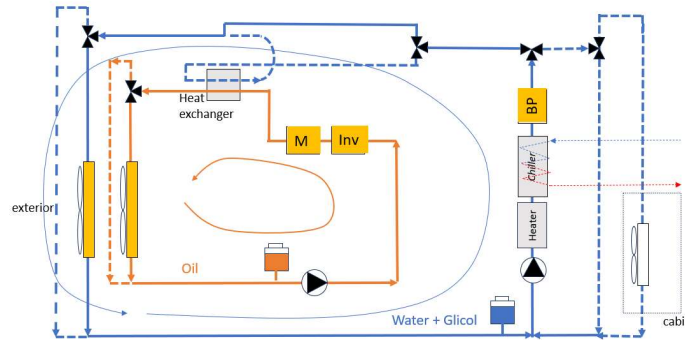
Figure 75.Two Loops Systems: Normal mode (coloured = active).

- Winter mode (see Figure 76): When the battery is below optimum temperature, no heat is dissipated from the batteries and, if necessary, the electric auxiliary heater is activated. The motors and electronics dissipate their heat to the outside air via the radiator.
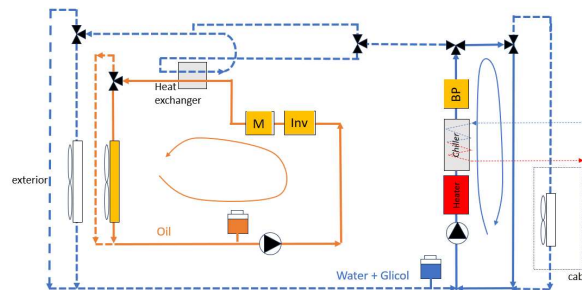
Figure 76.Two Loops Systems: Winter mode (coloured = active).

- Preheat mode (see Figure 77): With the vehicle stationary and connected to the mains, the heater is activated and the fluid is recirculated through the batteries itself to maintain its temperature above the minimum operating temperature (e.g. 6°C). The motors and electronics are switched off.
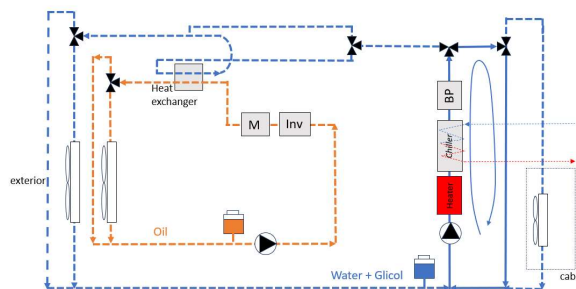
Figure 77.Two Loops Systems: Pre-heating mode (coloured = active).

- Hot mode (see Figure 78): Outdoor temperature above 35 ºC. Same as winter mode but the chiller is activated instead of the heater.
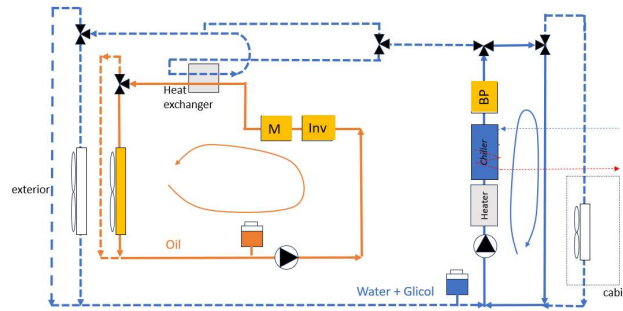
Figure 78. Two Loops Systems: hot mode (coloured = active).

- Cab heating mode (see Figure 79): All the heat (engines + power electronics + batteries) is conducted to the cab. The heat exchanger allows heat to be transferred from one circuit to another.
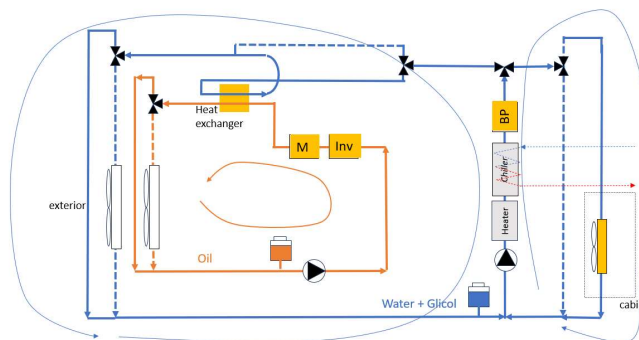
Figure 79. Two Loops Systems: Cab heating mode (coloured = active).

- Fast charge mode (see Figure 80): Thanks to the heat exchanger, the heat generated in the batteries can be dissipated to the outside via the two radiators (possibly also to the passenger cab).
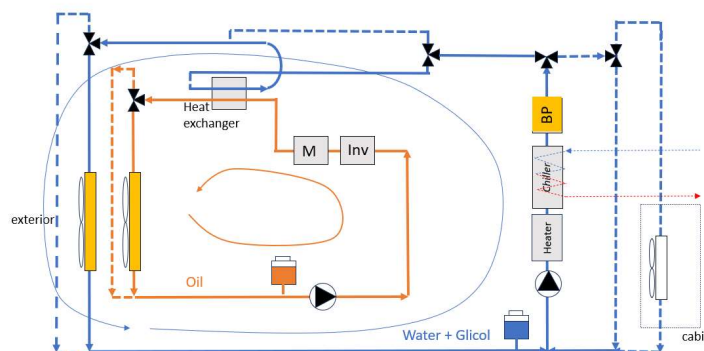
Figure 80. Two Loops Systems: Fast charge mode (coloured = active).

Modelica Simulation Model

A thermal simulation model has been developed using the modelling language Modelica. The model simplifies the components of the system, considering each of them as a grouped mass and, from its mass, its specific heat capacity and the energy exchanged with the environment, its average temperature is calculated. The model does not calculate the temperature dispersion within each component, nor its maximum temperature; however, it allows the simulation of the powertrain cooling system and the analysis of the various operating modes (winter mode, normal mode, etc.) in transient conditions, such as the start-up and initial heating of the battery pack.

Figure 81 shows the model corresponding to the One Loops System described above. The three main heat dissipation elements (motors, inverters and battery pack) are considered to have liquid cooling channels designed to minimise pressure loss and maximise heat dissipation. The pump and radiator fans operate in constant flow mode. PID type regulators control the battery temperature and the flow rates of the pumps.

Figure 81.One loop system modelica simulation model.

Figure 82 shows the model corresponding to the Two Loops System described also in the previous section. The three main heat dissipation elements (motors, inverters and battery pack) are considered to have liquid cooling channels designed to minimise pressure loss and maximise heat dissipation. The pump and radiator fans operate in constant flow mode. PID type regulators control the temperature of the cooling fluid at the entrance of the battery and the flow rates of the pumps.

Figure 82.Two Loops System Modelica simulation model.

Simulation results

Next figures show some of the results obtained with the developed models. These are only a sample of the results that can be obtained with these models. To achieve more accurate results, a very detailed description of each thermal system element is needed, which is not possible in this subtask, as no real hardware of the EV thermal system is going to be develop in this project.

Firstly, one loop circuit results have been analysed. Figure 83 shows the heating of the battery on a cold day (outside and starting temperature of 6°C) according to four different operating strategies. In one of them, the coolant circulates through the external radiator, in another one through the by-pass of the same radiator, and in a third one, it recirculates the coolant over the battery itself (winter mode, without activating the heater).

The fourth one is the same as the third one, i.e. the cooling fluid circulates over the battery in a closed loop, but unlike this one, now the control activates the heater (5kW) and the chiller (4 kW) as needed. It is observed that the battery reaches the setpoint temperature (30 ºC) before and stabilises there. On the other hand, the EV range decreases by 3%, and the SOC reaches zero after 6984 sec. Figure 84 shows the consumptions of the chiller and heater. Figure 85 shows the temperatures of the motor, the inverter and the battery in the temperature controlled closed loop mode.
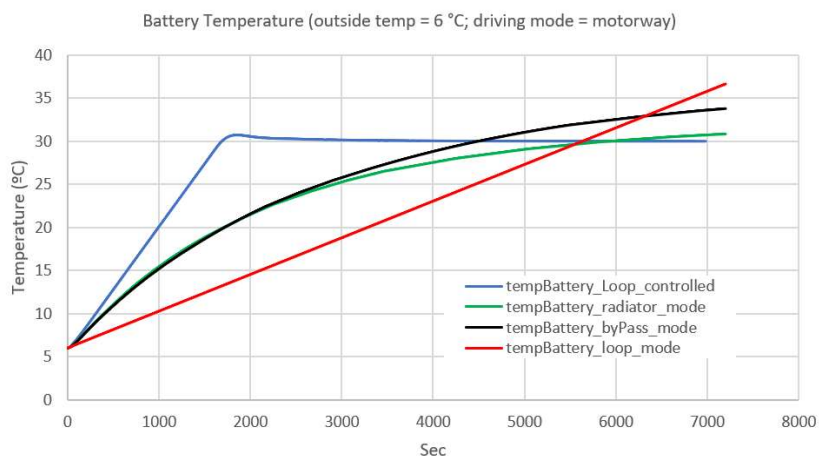
Figure 83 Heating of the battery on a cold day according to four different operating strategies. The battery runs out in 7200 seconds (6984 sec for temperature controlled closed loop mode).
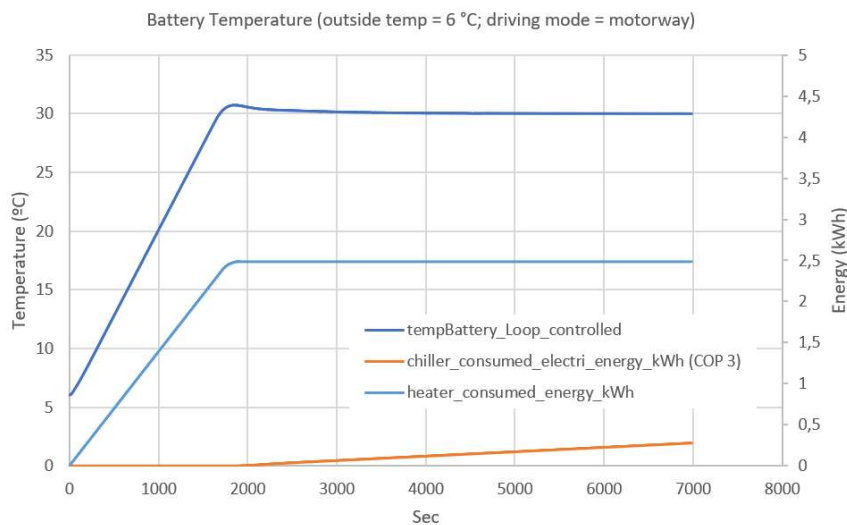
Figure 84 Battery temperature in controlled close loop mode. Cumulative consumption of heater and chiller.
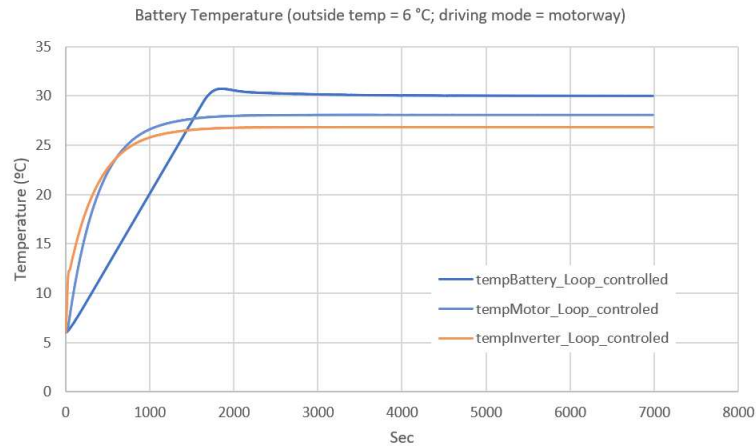
Figure 85 Battery, motor and inverted temperature in controlled close loop mode.

Figure 86 shows the temperatures of the motor, inverter and battery in warm mode, with an outside temperature of 45 °C, an initial temperature of 30 °C (garage) and driving on motorways, and Figure 87 the chiller consumptions (COP = 2 is considered to estimate the electric energy consumption).
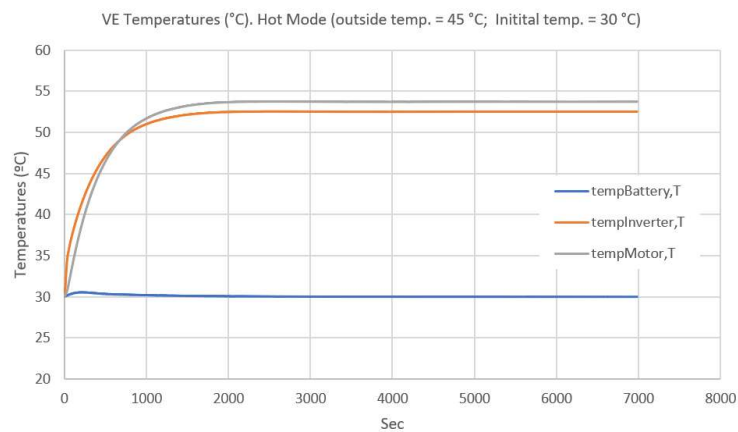
Figure 86 EV temperature in Hot Mode. Outside temperature: 45 °C, initial temperature: 30 °C.
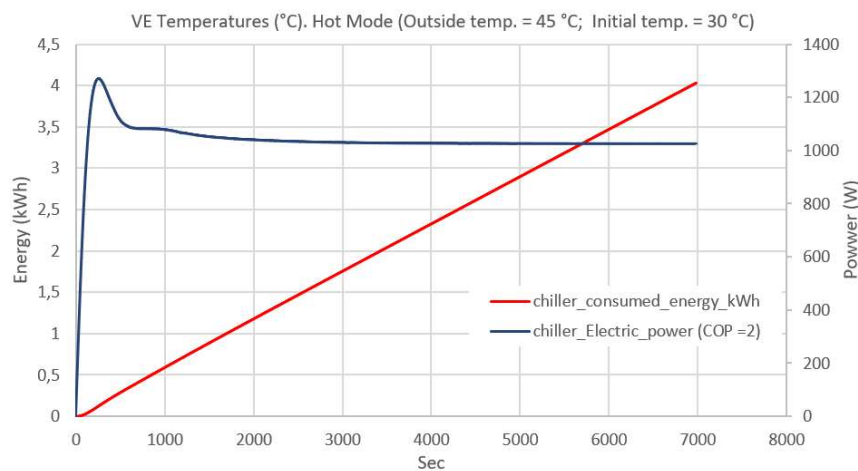
Figure 87 Chiller electric power (considered COP = 2) and accumulated energy consumption.

Secondly, **two loops circuit results** are analysed. Figure 88 shows the temperatures of the motor, inverter and battery in warm mode, with an outside temperature of 45 °C, an initial temperature of 30 °C (garage) and driving on motorways.
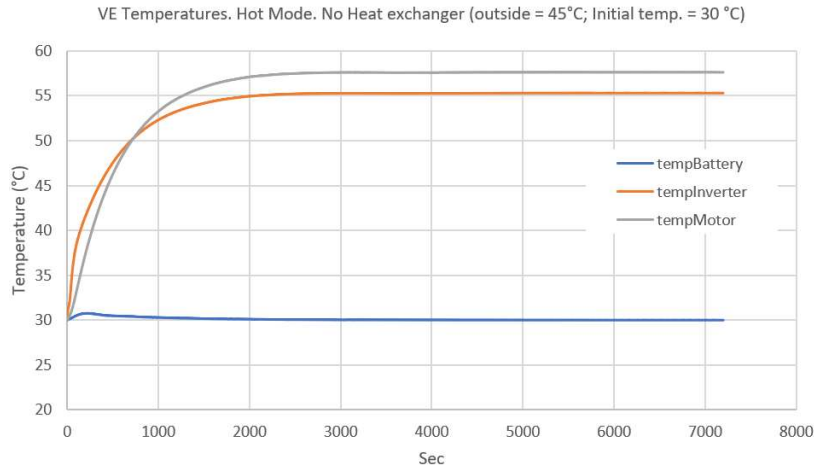
Figure 88 Battery, Inverter and Motor temperatures at Warm Mode.

Figure 89 shows the temperatures of the battery, inverter and motor in cold mode, with an outside temperature of 6 °C and a starting temperature of 20 °C (garage). Oil circuit dissipates the heat from the motor and inverter to the outside. However, the water-glycol circuit, after heating the battery with the 5 kW auxiliary heater, passes through the front radiator by-pass and dissipates the heat to the passenger compartment. Figure 90 shows the power and energy consumed (accumulated) by the heater.
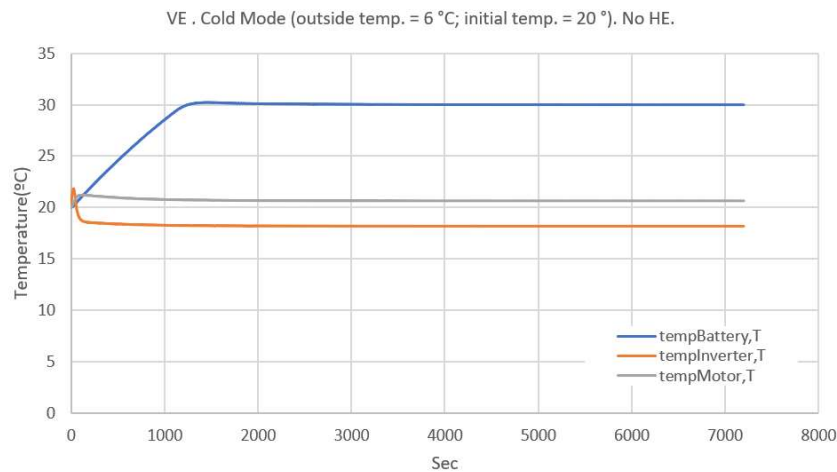
Figure 89 Battery, Inverter and Motor temperatures at Cold Mode and without heat exchanger.
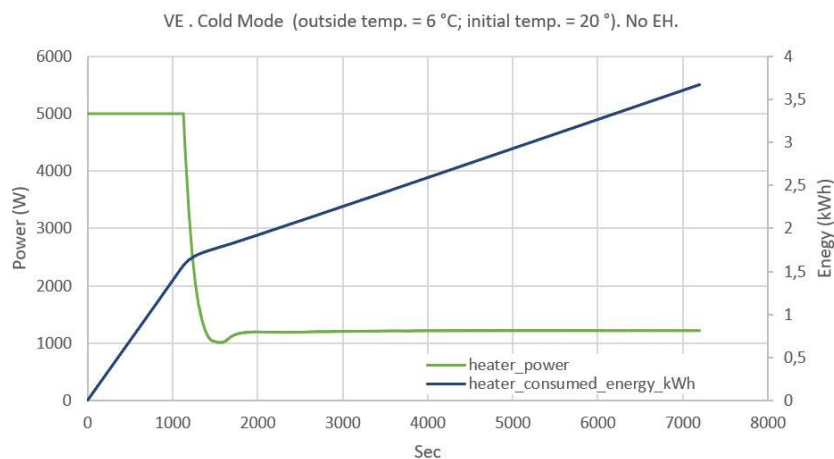
Figure 90 Auxiliary heater power and consumed energy at Cold Mode and without heat exchanger.

Figure 91 shows the heat (power) dissipated by the oil circuit to the outside air through the front radiator, and by the water-glycol circuit to the passenger cabin through the interior radiator. It is interesting to note that, once the battery is heated, the auxiliary heater consumes 1.2 kW, but 3.2 kW (generated by the auxiliary resistor and the battery) are introduced to passenger compartment heating. However, 1.4 kW (generated by motor and inverter) are lost through the front radiator, that is, 3.6 % of the energy stored in the battery pack. The EV range will decrease by the same percentage.
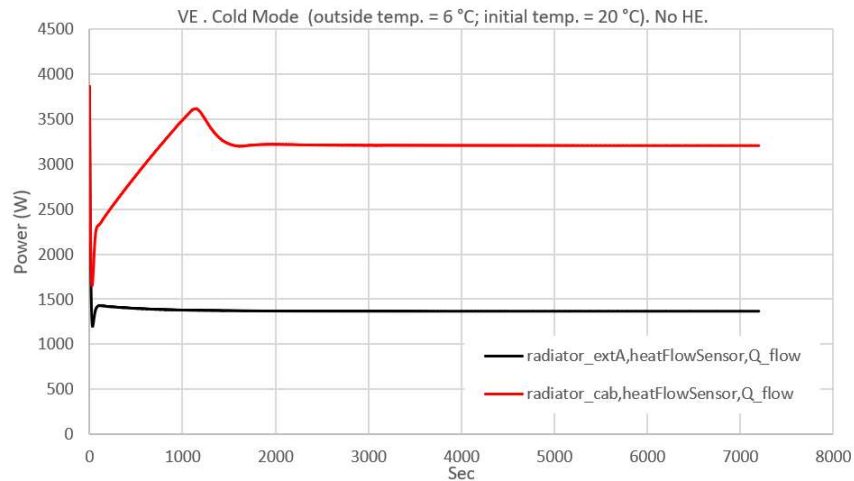
Figure 91 Heat power dissipated to outside air and to the cabin. Cold Mode and without heat exchanger.

4.4.4   CONCLUSIONS

Unlike a combustion engine vehicle, the propulsion components of an EV do not produce enough waste heat to adequately heat the passenger compartment, so auxiliary heaters are needed. A heat pump allows this heat to be collected and efficiently used to heat the passenger compartment. However, this requires a complex system of which the heat pump is only one part. The analysis of the technological situation in the EV market makes it clear that an advanced cooling system involves incorporating a heat pump into the cooling/heating system and harvesting waste heat from components with significant energy consumption. This improves efficiency and significantly increases the EV's range, especially in cold climates.

The worst thermophysical properties of the oil compared with the ethylene glycol water mixture (i.e. higher viscosity and lower thermal conductance) causes the need of higher heat exchanger and higher pump energy. However, its lubricant properties and low electric conductivity make it appropriate for motor cooling application. When motor is cooled by an oil instead of a mixture of water and ethylene glycol, usually is preferable to design a separate cooling loop (of oil) and link it with the rest coolant loop (ethylene glycol) by a heat exchanger, instead of using oil as a coolant in all the elements. In this work, the conceptual schemes of two powertrain cooling systems have been analysed and compared: a single loop system with water-glycol mixture and a two loops system with two cooling liquids (water-glycol mixture and oil).

Although the defined schemes of this work do not include the EV vapour compression air conditioning system, they include a heat exchanger to recover part of the heat to be used at the passenger compartment. In addition, the corresponding simulation models have been developed (in the modelling language Modelica), which allow the feasibility and interest of this heat recovery system to be analysed from a thermal point of view. It also allows the simulation of the powertrain cooling system and the analysis of the various operating modes (winter mode, normal mode, etc.) in transient conditions, such as the start-up and initial heating of the battery pack.

The work carried out makes it clear that when the priority is improving efficiency to maximising EV range, the EV thermal management must be designed from a complete EV perspective, taking into account all thermal loads of all elements, including passenger compartment, ambient

conditions and driving modes conditions of the EV, all together. The cooling system must be able to configure different refrigerant circuit connections to share as much as possible the heating and cooling alternatives to re-use waste heat at maximum. It is particularly important, especially in cold climates, to consider the passenger compartment climate control. Heating the passengers cabin using waste heat is crucial and the use of a heat pump becomes essential.

5 DELIVERY DEVIATIONS FROM THE INITIAL PLANNING

There has been a delay in the delivery of D3.1. Modular, high-efficient and cost-oriented 800V powertrain architecture

Contractual delivery: 2023-11-30

Deliverable Date: 2024-04-26

This delay is due to a mistake during the proposal writing, as Task 3.1 finished at the end of February (M15) but the deliverable deadline was in November (M12).

Administrative deviations:

First full version of this document (v1.0) has been uploaded to the TEAMS platform at the mid of February. Then, the document was shared between all WP3 partners to collect their comments and correction. After that, a new version (v2.0) was shared to be checked by the coordinator.

Delay effect on overall project planning: This report is only related to WP3 and it does not have any impact in Task 3.2 which is running. So, it does not generate any delay in the project.

6 CONCLUSIONS

In this deliverable firstly a state of the art about 800V EV was carried out, where it was concluded that 800V architecture is already a reality. There is a clear trend to move to higher voltage EV. There are also some new EU calls for 2024 dealing with this topic, "Integration and testing of next generation post-800V electric powertrains". Dedicated electric vehicle platforms are usually used and front and rear axles is the most common solution. PMSM motors and SiC based inverters are dominant at this moment, due to their best performances.

Regarding 800V **electrical architecture**, multiple powertrain configurations are possible, with axle drive being the most promising solution at present. The tendency is to have a primary axle drive (in the rear) and some EV also have a secondary axle drive (in the front). Using SiC based inverters drive efficiency is improved considerably. On the one hand, these devices have less losses, reducing inverter losses, and on the other hand, SiC devices higher switching frequency can be used by the control to reduce motor harmonics and those, motor losses. Modularity is achieved by the possibility to use different battery packs or OBC. The architecture is scalable to achieve different power levels using different motor lengths but same rotor diameter, using the same inverter and paralleling devices, using different gear ratios, etc. Finally, cost oriented solution can be achieved by using Si devices for the secondary axle drive, where less powerful systems are usually required.

Concerning 800V **thermal architecture**, there is a tendency to use oil cooling, not only for the motor but also for the inverter and even for the battery system. However, this is long term research and for HEFT drive oil cooling will be considered for the motor and, inverter and battery system will be cooled using water-glycol.

800V **mechanical architecture** and control architecture are quite similar to 400V architectures. No differences have been found.

On the other hand, a simulation model to analyze high dv/dt effects that generate SiC devices have been proposed in this study. The main conclusions are that the dv/dt are affected by common mode and differential mode perturbations. The main contribution is due to differential model perturbations (higher gain). However, the common model paths and their resonances cannot be neglected. In the time domain, the model developed makes possible the change the rise & fall time of the inverter's output waveforms, to evaluate the whole harmonic content of the variables. The influence of the main variables (wiring length and parasitic components) is evaluated in the AC domain, to see the frequency range affected by each parameter and it can be also evaluated in the time domain model, to see the frequency range affected by each parameter.

Moreover, it is important to consider the connection between voltage frequency harmonics obtained in simulation models and the frequency ranges and amplitudes defined in the standards. This is a crucial step in understanding the potential electromagnetic interference (EMI) issues and ensuring compliance with EMC standards. By correlating the voltage frequency harmonics from the simulation model with the frequency ranges and amplitudes outlined in EMC standards, it is possible to assess the potential impact of dv/dt on electromagnetic emissions and susceptibility. This understanding allows to anticipate any EMI problems and take appropriate measures to mitigate them, such as implementing filtering techniques or optimizing the motor drive system design.

From this charging time/extended range simulation study, it can be concluded that increasing voltage, as it is related with increased battery capacity, extends EV range. Moreover, 800V fast chargers (250kW) allow a considerably decrease in charging times.

Finally, advanced shared cooling system for the powertrain has been analysed and simulated. From this study can be concluded that when the priority is improving efficiency to maximising EV range, the EV thermal management must be designed from a complete EV perspective, taking into account all thermal loads of all elements, including passenger compartment, ambient

conditions and driving modes conditions of the EV, all together. The cooling system must be able to configure different refrigerant circuit connections to share as much as possible the heating and cooling alternatives to re-use waste heat at maximum. It is particularly important, especially in cold climates, to consider the passenger compartment climate control. Heating the passengers cabin using waste heat is crucial and the use of a heat pump become essential.

7 REFERENCES

[1] A Certain Move Towards WBG Semiconductors in Electric Vehicles (frost.com)Navdeep Saboo, November 28, 2022 (Last accessed: 1st March 2024).

[2] Accelerated Vehicle Electrification and Shift to 800V Architecture Spotlight Strong Growth Prospects for Wide-Bandgap (WBG) (frost.com), Aman Gupta, December 5, 2023 (Last accessed: 1st March 2024).

[3] Looking into E–GMP: A Balance of Function and Sensibility (hyundaimotorgroup.com) (Last accessed: 1st March 2024).

[4] An article to understand the high-voltage fast charging of Hyundai IONIQ 5 - iMedia (min.news) (Last accessed: 1st March 2024).

[5] PowerPoint Presentation (audi.com), Oliver Hoffman, Fermín Soneira Santos, July 7, 2021 (Last accessed: 1st March 2024).

[6] PAG_Taycan_Technology_PM_EN.pdf.PDF (porsche.com), The technology behind the new Porsche Taycan (Last accessed: 1st March 2024).

[7] Lucid Motors Unveils Lucid Air, the World's Most Powerful and Efficient Luxury Electric Sedan, September 9, 2020 (Last accessed: 1st March 2024).

[8] Funding & tenders (europa.eu), Integration and testing of next generation post-800V electric powertrains (2ZERO Partnership), HORIZON-CL5-2024-D5-01-02.

[9] (PDF) APEC2023-Christmann-Infineon-S01-Power electronics for Electric Vehicles-2023 03 18 (researchgate.net), Andre Christmann, Power Electronics in Electrified Powertrains, March 2023, APEC conference.

[10] Farnell España - distribuidor de componentes electrónicos

[11] Oil Cooling < Thermal Management Solutions < eMobility | Continental Industry (continental-industry.com) (Last accessed: 1st March 2024)

[12] Marelli News - Marelli presents new integrated Thermal Management Module for electric vehicles, improving efficiency, safety and driving range up to 20% Marelli (Last accessed: 1st March 2024).

[13] Flexible thermal unit – preintegrated thermal management module (bosch-mobility.com) (Last accessed: 1st March 2024).

[14] Details of the video asset GKN Automotive Our Technology January 2023 | GKN Automotive Asset library (assetbank-server.com) (Last accessed: 1st March 2024).

[15] Funding & tenders (europa.eu), Advanced battery system integration for next generation vehicles (2ZERO Partnership), HORIZON-CL5-2024-D5-01-03.

[16] EMC DESIGN TECHNIQUES FOR ELECTRIC VEHICLE POWERTRAIN MODULES. URL: https://incompliancemag.com/article/emc-design-techniques-for-electric-vehicle-powertrain-modules/

[17] Road vehicles - Electrical disturbances from conduction and coupling - Part 4: Electrical transient conduction along supply lines only. URL: https://www.iso.org/standard/72067.html

[18] Vehicles, boats, and internal combustion engine driven devices - Radio disturbance characteristics - Limits and methods of measurement for the protection of on-board receivers. URL: https://webstore.iec.ch/publication/64645

[19] Electrical disturbances from conduction and coupling. URL: https://webstore.iec.ch/publication/85594

[20] Wray, A.; Ebrahimi, K. Octovalve Thermal Management Control for Electric Vehicle. Energies 2022, 15, 6118. https://doi.org/10.3390/en15176118

[21] Biggest Winter Range Test Ever Reveals Best EVs For Cold Weather (insideevs.com) (Last accessed: 1st March 2024).

[22] Hyundai and Kia Turn Up EV Efficiency with New Heat Pump Technology (Last accessed: 1st March 2024).

[23] Tesla Model Y Heat Pump Details Infrequently Discussed By The Media (insideevs.com) (Last accessed: 1st March 2024).

[24] https://www.ebay.com/itm/144986348017 (Last accessed: 1st March 2024).

[25] Inversor de alta tensión | Inversor de tracción EV | Eaton (Last accessed: 1st March 2024).

[26] Hyundai Ioniq 5 Range Tested In The Worst Conditions (insideevs.com) (Last accessed: 1st March 2024).

[26] 2024 Hyundai IONIQ 5 Features & Specs | Hyundai USA (Last accessed: 1st March 2024).